The Influence of Impeller Designs on the Performance of a Vortex Pump

vorgelegt von
Master of Science
Angela Gerlach
geb. in Berlin

von der Fakultät V - Verkehrs- und Maschinensysteme
der Technischen Universität Berlin
zur Erlangung des akademischen Grades

Doktor der Ingenieurwissenschaften
- Dr.-Ing. -

genehmigte Dissertation

Promotionsausschuss:

Vorsitzender: Prof. Dr.-Ing. Roland Baar
Gutachter: Prof. Dr.-Ing. Paul Uwe Thamsen
Gutachter: Prof. M.Sc. Ph.D. Lasse Rosendahl

Tag der wissenschaftlichen Aussprache: 25.04.2018

Berlin 2018

Summary

Vortex pumps are particularly suitable for the transportation of solids-containing fluids. Hence, vortex pumps are applied to a wide range of operation domains, from wastewater transport to food processing. Characteristics of vortex pumps are their recessed, semi-open impeller and their enlarged gap between the impeller and the casing. These features strongly reduce the risk of clogging compared to conventional centrifugal pumps. Nevertheless, vortex pumps have been relatively inefficient. Improving the efficiency of vortex pumps therefore seems highly desirable. Yet, the operating principle of a vortex pump is poorly understood. As a consequence, it is unclear how exactly vortex pumps can be optimized. This dissertation therefore investigates to what extent the geometry of the impeller influences the characteristics and the operation principle of a vortex pump. Overall, it can be shown that the operation principle of vortex pumps resembles that of conventional centrifugal pumps with a semi-open impeller. Building on this insight, the dissertation proposes a method to optimize the impeller design of vortex pumps.

In more details, in a series of experimental studies this dissertation investigates the influence of individual design parameters of the impeller on the characteristics for clear water operation, on the flow field in the front chamber, and on the clogging behavior. Both, the clear water characteristics as well as the flow field in the front chamber clearly depend on the impeller design. Thus, various geometry parameters of the impeller under clear water operation are tested. The findings suggest that an impeller with highest head and highest efficiency also achieves the highest tangential and the highest radial flow velocities in the front chamber. Regardless of the impeller design, the tangential flow velocity always appears to be the main component in the flow as opposed to the radial velocity component. This means that for all the tested impellers the fluid predominantly rotates in the front chamber and it does not significantly contribute to the pumping process. An evaluation of the clogging behavior shows that an impeller with highest head and highest efficiency under clear water operation can pump a substantial proportion of solids. Such an impeller, however, is significantly less efficient under clogging conditions and it may accumulate solids near the hub. Hence, the common approach of optimizing a vortex pump by means of clear water tests could be misleading given that vortex pumps predominately operate under clogging conditions. That is, an impeller, which achieves optimal results under clear water conditions, may be less efficient for transporting solids-containing fluids. In order to avoid clogging impellers with a low head and a low efficiency under clear water operation could be altogether preferable.

Zusammenfassung

Vortexpumpen werden zu Förderung von feststoffhaltigen Fluiden eingesetzt, die beispielsweise in der Abwassertechnik und Lebensmitteltechnik auftreten. Das halboffene, zurückgesetzte Laufrad und der daraus resultierende große vordere Spalt verringern die Verstopfungsgefahr von Vortexpumpen im Vergleich zu konventionellen Kreiselpumpen. Der Wirkungsgrad von Vortexpumpen ist jedoch vergleichsweise gering. Eine konstruktive Anpassung zur Optimierungen des Wirkungsgrades von Vortexpumpen erscheint daher wünschenswert. Inwiefern eine solche Optimierung möglich ist, muss jedoch geklärt werden, da das Wirkprinzip von Vortexpumpen derzeit ungeklärt ist. Diese Dissertation untersucht daher den Einfluss der Laufradgeometrie auf die Fördercharakteristik und das Wirkprinzip von Vortexpumpen. Hierzu werden einzelne Geometrieparameter des Laufrades variiert und ihr Einfluss wird experimentell untersucht. Insgesamt kann gezeigt werden, dass das Wirkprinzip einer Vortexpumpe dem einer konventionellen Kreiselpumpe mit halb-offenem Laufrad ähnelt. Auf Basis dieser Erkenntnis wird ein Verfahren zur Optimierung der Laufradauslegung von Vortexpumpen vorgeschlagen.

Im Einzelnen umfasst diese Dissertation eine Reihe von Untersuchungen zum Einfluss von Geometrieparameter des Laufrades auf die Klarwasserkennlinie, auf das innere Strömungsfeld im vorderen Radseitenraum sowie auf das Verstopfungsverhalten von Vortexpumpen. Die Untersuchungen zeigen, dass sowohl die Klarwasserkennlinien wie auch die Strömungsgeschwindigkeiten im vorderen Radseitenraum deutlich von einzelnen Laufradparametern abhängen. Daher wird die Beeinflussung der Klarwasserkennlinien durch einzelne Geometrieparameter des Laufrades ausführlich dargestellt. Die Ergebnisse zeigen zudem, dass ein Laufrad mit höchster Förderhöhe und höchstem Wirkungsgrad auch die höchsten tangentialen und die höchsten radialen Strömungsgeschwindigkeiten im Radseitenraum erzielt. Unabhängig vom jeweilig untersuchten Laufrad erscheint die tangentiale Geschwindigkeitskomponente immer als die wesentliche Komponente in der Strömung im Gegensatz zu der radialen Geschwindigkeitskomponente. Das heißt, dass das Fluid für alle getesteten Laufräder vorwiegend im vorderen Radseitenraum rotiert und nicht wesentlich zum Transport beiträgt. Die Untersuchungen zum Verstopfungsverhalten zeigen, dass ein Laufrad mit höchster Förderhöhe und höchstem Wirkungsgrad unter Klarwasserbedingungen, zudem vergleichsweise viele Feststoffe pumpen kann. Für solch ein Laufrad reduziert sich der Wirkungsgrad beim Transport von feststoffhaltigen Fluiden jedoch deutlich und es treten vermehrt Verstopfungen im Nabenbereich auf. Da Vortexpumpen meist zur Förderung von feststoffhaltigen Fluiden eingesetzt werden, erscheint das konventionelle Verfahren zur Laufradoptimierung mittels Klarwassertests für eine Vortexpumpe daher ungeeignet. Zur Vermeidung von Verstopfungen kann daher ein Laufrad besser geeignet sein, welches unter Klarwasserbedingungen eine geringere Förderhöhe und einen geringen Wirkungsgrad erzielt.

Acknowledgment

There many people to whom I am pleased to acknowledge my cordial gratitude. I would like to thank my advisor Prof. Dr.-Ing. Paul Uwe Thamsen for his vital support and assistance. His encouragement made it possible to achieve the goal. I also appreciate Prof. Ph.D. Lasse Rosendahl from Aalborg University for serving as my second reviewer and Prof. Dr.-Ing. Roland Baar for chairing the thesis committee.

I am much obliged to the team of Grundfos Holding A/S, especially of Christian Brix Jacobsen, Flemming Lykholt-Ustrup, Svend Rasmussen, and Poul Johannes Henning, for their invaluable support of this work, for their insightful comments and for their kind encouragement — not to speak of the many challenging questions, which helped putting my research in the bigger picture.

I would also like to thank my colleagues, especially Dipl.-Ing. Stefan Gerlach, at the department of Fluid System Dynamics for their feedback, their cooperation and, of course, their friendship. I appreciated working with Dorian Perlitz, MSc. I am thankful for his stimulating discussions, the days and nights we were working together to meet deadlines, and the fun we had nonetheless.

I am also grateful to Prof. Ph.D. Henrik Sørensen, and his family, for accepting me so warmheartedly, for supporting me without any restrictions in the writing of this thesis, and for sharing a glimmer of hope for a post-dissertation normalcy.

Finally, I want to express my profound gratitude to my family for providing me with unfailing support and continuous encouragement throughout my years of study and through the process of research and, lastly, the writing of this thesis. This accomplishment would not have been possible without them. Thank you.

Contents

Chapter 1

Introduction

Vortex pumps are characterized by their semi-open impeller, which is set back in the casing. Therefore, an enlarged volute width emerges. This design feature allows vortex pumps to transport solid containing fluids at a reduced likelihood of clogging. The application areas of vortex pumps thus cover a wide range of fields, from wastewater transport to the food processing industry. However, the hydraulic efficiency of vortex pumps is comparatively low to that of conventional centrifugal pumps. In times of rapidly rising energy prizes and the much-needed adherence to energy saving goals improving vortex pumps becomes more desirable than ever. At the same time, such improvement must warrant the general ability of vortex pumps: to transport solid containing fluids. The most straightforward way of achieving higher efficiency levels is through the optimization of the design, for example, by improving the impeller.

Surprisingly little is currently known about how vortex pumps operate. Consequently, it is unknown how vortex pumps should be best designed to gain high heads and maximal efficiency. This is, for example, reflected in the fact that there are two different design types of vortex pumps basing on different assumptions of the underlying operation principle.

This dissertation evaluates the influence of impeller design on the performance of a vortex pump and thereby to gain further insights in the underlying operation principle. It summarizes the state of the art of the research on vortex pumps, describes different approaches to design vortex pumps and it reveals the assumed operation principles underlying these designs (Chapter 2). Through experimentally varying geometrical parameters and the designs of the impeller it tests and refines a method for calculating the characteristic curve of a vortex pump which allows comparing vortex pumps to conventional centrifugal pumps. The aim is to find the optimal design of vortex pump impeller given some predefined characteristics (Chapter 3 and 4).

The flow field in a vortex pump was measured for different impeller designs. Incorporating the flow field allows relating geometry parameters of the impeller to the resulting characteristic curves (Chapter 5).

Finally, experiments on the clogging behavior of a vortex pump with different impeller designs were conducted (Chapter 6). Rather surprisingly, no publicly available study has yet assessed the clogging behavior of a vortex pump — even though clogging operation is the typical operation condition of vortex pumps. The results give insights into the relations of impeller designs and the clogging behavior.

The dissertation concludes with a list of the influence of design parameters on the characteristics and a summary of the conducted clear water test, flow field measurements, and clogging tests (Chapter 7).

Chapter 2

State of the Art

This chapter summarizes the state of the art of research on vortex pumps. It begins by outlining the principle design approaches and the assumed operation principles at work. Based on the assumed operation principles and the insights from research design recommendations are derived and open research questions are discussed[1].

2.1   Design Principles of Vortex Pumps

As the name vortex pump implies, a recirculating flow, the vortex, develops in the front chamber gap between the impeller and the casing. So far, it is not clear whether and to what extent this vortex contributes to the fluid transport — or if it even disrupts the fluid transport. Rather, there are two different assumptions on how a vortex pump operates resulting in two different design types of vortex pumps. The following refers to them as the *covered design* and the *open design* (Figure 2.1).
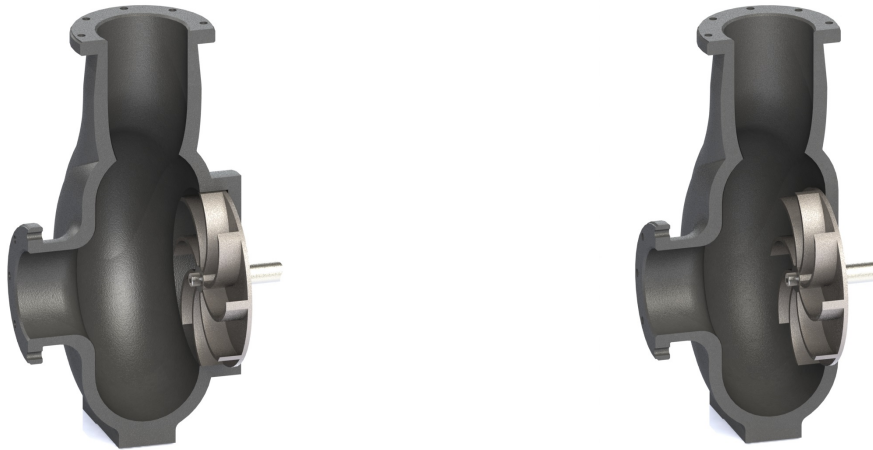

Figure 2.1: Examples of vortex pumps (from Gerlach et al. [1]): Vortex pump according to the covered design (left) and vortex pump according to the open design (right).

---

[1]A more thorough overview can be found in Gerlach et al. [1]

The covered design encloses the radial, outer circumference of the impeller with the casing (Figure 2.1 left). The covered design assumes that the vortex is mainly responsible for the fluid transport. The assumed operation principle is thus similar to a hydraulic coupling: the impeller induces the vortex in the front gap, and the vortex then promotes the fluid (e.g., Lubieniecki [2]; Grabow & Gneipel [3]). To create a stronger vortex and to strengthen the axial work transfer from the impeller to the front gap, the impeller is covered on its outer circumference. This covering aims at decreasing losses on the outer circumference of the impeller. Assuming that the vortex is mainly responsible for the fluid transport, the best design should strengthen the vortex formation and thereby result in highest heads and efficiency.

The open design lets the fluid freely outflow at the outer circumference of the impeller (Figure 2.1 right). The assumed operating principle is that of a conventional centrifugal pump: the fluid is directly pumped through the impeller itself — and not indirectly via the vortex. The vortex is merely the result of exchange losses from the pressure side to the suction side (e.g., Rütschi [4]). The large front gap and the missing front shroud thus facilitate the formation of these exchange losses, which explain the relatively low hydraulic efficiency of vortex pumps. Assuming that the vortex is a mere disruptive source for the fluid transport, the best design would allow a maximum free outflow from the impeller outlet and thereby result in highest heads and efficiency.

For both designs, the covered and the open design, the impeller itself is usually semi-open and without a suction mouth or a defined inlet diameter. The blades can be curved (Figure 2.2 left) or straight (Figure 2.2 right).

However, other impeller designs are in principle possible, largely depending on the principle vortex pump design. For example, the covered design is frequently associated with pan-like impellers (e.g., Ohba et al. [5]; Aoki [6]). Their shapes are either rectangular or round (Figure 2.3 left). In both cases, the design of the pan-like impellers aims at strengthening the vortex formation and thus the flow transport under the assumed working principle. The impeller of the open design has been frequently modified through the adding of winglets to the front edges of the blades (e.g., Zhu et al. [7, 8]; Sarvanne [9]; Figure 2.3 right).

Figure 2.2: Examples of impellers, which are typically used for vortex pumps: Impeller with curved blades (left) and impeller with straight blades (right).
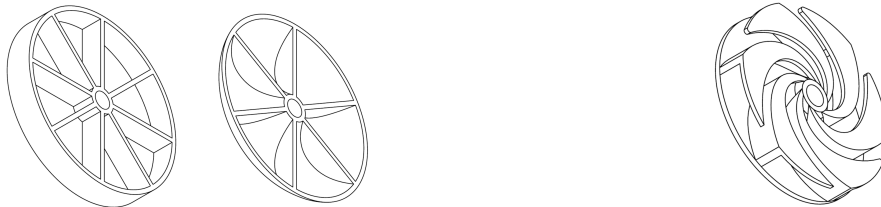

Figure 2.3: Examples of pan-like impellers, which are frequently used in covered designs (left) and examples of impeller with winglets, which is frequently used in open designs (right).
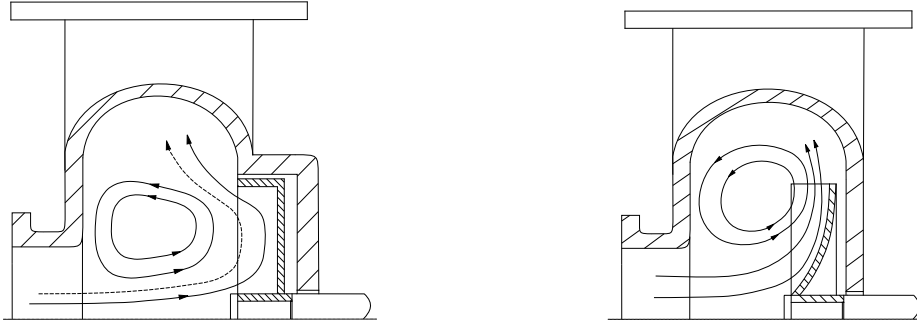
Figure 2.4: Flow in a vortex pump: Flow model for the covered design (adapted from Aoki [10]; left) and flow model for the open design (adapted from Hofmann [11]; right).

However, the use of pan-like impellers for the covered design and of winglets for the open design is not mandatory.

Regardless of the design type and the impeller a vortex develops in the casing. Figure 2.4 illustrates the flow in a covered design (left) and in an open design (right). In particular, Figure 2.4 left shows an adaptation of Aoki [10] who tested the covered design with a pan-like impeller of rectangular shape. He argued that the flow can be divided into two components: a through flow and a recirculation flow. The recirculation flow is the vortex, which forms in the front gap between the casing and the impeller. The through flow consists of the fluid which passes from the suction pipe via the impeller to the discharge. The covering of impeller leads to a deflection of the through flow at the impeller outlet. The fluid in this region is oriented in the direction of the vortex to strengthen it. Figure 2.4 right illustrates an adaptation of Hofmann [11] who tested with air different sizes of front gaps, including one configuration that was similar to a vortex pump. For the open design, the flow can be divided into a through flow and a recirculation flow too. The recirculation flow, the vortex, lies between the casing and the impeller in the large gap. The through flow leads from the suction pipe via the impeller to the discharge. However, since the open design allows a free outflow from the impeller, the through flow is less deflected when leaving the impeller and orientates to the discharge.

Some authors developed models on the flow in a vortex pump and approaches for design processes (e.g., Ohba et al. [5, 12]; Aoki [13]; Wang [14]; Schivley & Dussourd [15]; for a theoretical approach on the solid transport, see Grabow & Gneipel [3]). However, all these studies are limited to covered designs only. The resulting models are difficult to construct and often need to be specifically adapted to the targeted pump.

Several authors have measured the velocity and pressure in the front chamber of vortex pumps (e.g., Rütschi [4]; Ohba et al. [5, 16]; Sha & Hu [17]; Li & Feng [18]; Guan et al. [19]; Schivley & Dussourd [15]; Aoki [10]; Wu et al. [20]).

Figure 2.5 left depicts the measured velocity in the front gap between impeller and casing of vortex pump of Schivley & Dussourd [15]. The authors assessed the velocity profiles for different flow rates and different configurations to formulate a theoretical derivation for improving the design. Similar curves of tangential velocity in the front gap of a vortex pump resulted from other authors (e.g., Ohba et al. [5]). The graphic illustrates the tangential velocity component over the radius for three different flow rate i.e. flow coefficients φ. It is noteworthy, that the course of tangential velocity resembles that of a theoretical vortex, such as the Hamel-Oseen vortex (also called Lamb-Oseen vortex). The Hamel-Oseen vortex model expresses vortex motion for laminar, linear viscous, incompressible fluids while the flow is circular and time dependent (Saffman [21]). The mathematical description applies to cylindrical coordinates. The Hamel-Oseen vortex model
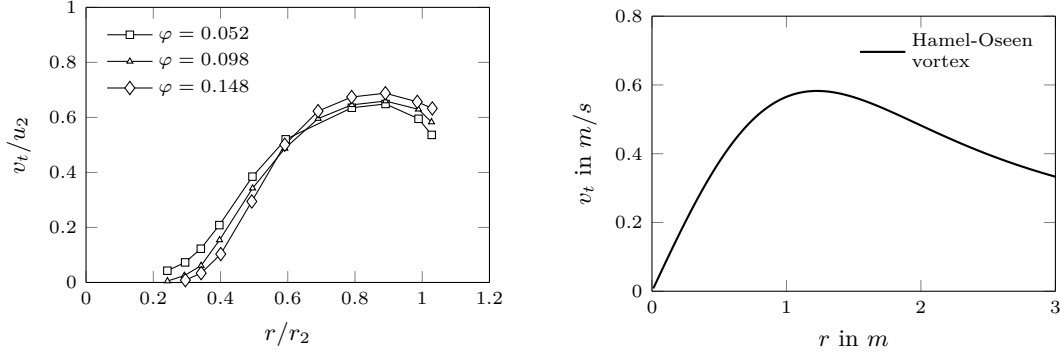
Figure 2.5: Measured normalized tangential velocity over normalized radius for a flow rate of zero (adapted from Schivley & Dussourd [15]; left) and example of the tangential velocity over radius for the theoretical Hamel-Oseen vortex (adapted form Gerlach et al. [22]; right).

divides the the vortex into two parts: A property of fluid in solid body rotation for small radii and a property of a potential vortex for larger radii. Fluids, which rotate in vortices at a small radius, are behaving similarly to a solid body. The tangential velocity is therefore proportional to the radius. From a defined radius, the fluid motion can be described as a potential vortex, whose properties are known from potential theory.

The mathematical description of tangential velocity v_t of the Hamel-Oseen vortex model is defined as (Formula 2.1):

$$v_t = \frac{\Gamma}{2 \cdot \pi \cdot r} \cdot (1 - e^{-\frac{r^2}{4 \cdot \nu \cdot T}}) \tag{2.1}$$

with Γ as the circulation, r as the radius, ν as kinematic viscosity, and T as time.

Figure 2.5 right illustrates the tangential velocities over radius for the theoretical Hamel-Oseen vortex calculated by Formula 2.1. For the sake of illustration, time T was set to $0.3\ s$, viscosity ν to $1\ m^2/s$ and circulation Γ to 2π (adapted form Gerlach et al. [22]).

The course of tangential velocity measured by Schivley & Dussourd (Figure 2.5 left), like the course of the theoretical Hamel-Oseen vortex (Figure 2.5 right), shows the linear increase of the velocity for small radii up to a maximum from which the velocity decreases again with increasing radius. The resemblance of the courses suggests that the Hamel-Oseen vortex model might adequately account for the observed behavior of the vortex in a vortex pump. When optimizing the design process of a vortex pumps this could be a starting point for a design approach. Nonetheless, it would be desirable to verify the fit between the model predictions and the observed behavior via more sophisticated analyses. For this purpose, the vorticity ω should also be considered. The vorticity can be described as the tendency of a fluid element to rotate and describes the local spinning motion (Morrison [23]). It is an useful tool to differentiate between a solid body rotation and a potential vortex as the vorticity for solid body rotation is *not* equal to zero and for a potential vortex the vorticity is equal to zero. The vorticity for a Hamel-Oseen vortex can also be calculated and peaks at a radius of zero in the area of solid body rotation. For the area of potential vortex motion of a Hamel-Oseen vortex is the vorticity equal to zero (Daily & Harleman [24]).

An own study therefore numerical simulated the flow in a vortex pump and compared it to the predictions of the Hamel-Oseen vortex model (Gerlach et al. [22]). The courses of tangential velocity and vorticity of the theoretical Hamel-Oseen vortex were compared to the numerically calculated flow field of a vortex pump (Gerlach et al. [22]). Overall, the results suggested that the

Hamel-Oseen vortex model provided only an accurate description for the tangential velocity and for the vorticity under strong part load conditions. For all other flow rates the tangential velocity of the simulations fitted to the theoretical Hamel-Oseen vortex too, but not the vorticity courses. However, because the simulated model violated boundary conditions of the theoretical vortex model, it is little surprising that some deviation from the Hamel-Oseen vortex model occurred. It should be examined by measurement data to determine the course of the vorticity in a vortex pump. To the best of the author's knowledge, so far no study calculated the vorticity in the flow field of the vortex pump by measured data and it thus remains overall an open question to what extend the flow field in a vortex pump truly resembles that of a theoretical vortex model.

The two different views of operation principles and design principles imply different design recommendations for the impeller and casing in order to reach high heads and efficiency. If the vortex is primarily responsible for the fluid transport and the covered design is correct, an impeller design should be preferred which supports and strengthen the vortex formation. Then, for example, a pan-like impeller would always be preferable, regardless of the pump's further design (covered or open design). If it is true that the impeller is primarily responsible for the fluid transport and the vortex is a disturbing side effect, the impeller should have a large impeller width, the side gap should be small, and design guides of conventional centrifugal pumps apply, for example, by the influence of blade angle, etc.

2.2   Design Recommendations

Despite the lack of clear design criteria and design procedures for vortex pumps some general design recommendations can be derived from the multitude of existing studies. To provide such quantitative synthesis a meta-analysis has been conducted which integrated experimental studies (for details see Gerlach et al. [1]). The meta-analysis identified a total of 18 relevant primary articles with 53 parameter manipulations. Figure 2.6 provides an overview on all these parameters and Table 2.1 lists the primary articles, which manipulated parameters of the impeller; Table 2.2 lists articles, which manipulated parameters of the casing and rotational speed.
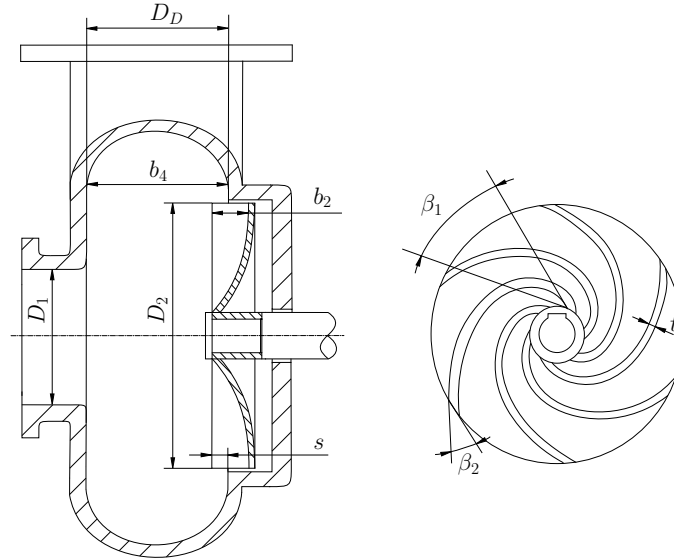

Figure 2.6: Design parameters of a vortex pump (adapted from Gerlach et al. [1]).

Table 2.1: Meta-analytically assessed parameters for the impeller of a vortex pump and their respective sources (adapted from Gerlach et al. [1]).

Assessed Parameter	Prefix	Article(s)
Impeller diameter	D_2	Lubieniecki [2]; Rütschi [4]; Ohba et al. [5]; Guan et al. [19] (Guan et al. [25]); Wang [14]; Zheng et al. [26]; Sha et al. [27]; Sha et al. [28]; Sha et al. [29]
Impeller width	b_2	Rütschi [4]; Ohba et al. [5]; Aoki [6]; Guan et al. [19] (Guan et al. [25]); Wang [14]; Zheng et al. [26]; Sha et al. [27]; Sha et al. [28]; Sha et al. [29]
Blade number	z	Rütschi [4]; Aoki [6]; Guan et al. [19] (Guan et al. [25])
Blade outlet angle	β_2	Aoki [6]; Guan et al. [19] (Guan et al. [25]); Sha et al. [27]; Sha et al. [29]
Blade inlet angle	β_1	Guan et al. [19] (Guan et al. [25])
Blade thickness	t	Guan et al. [19] (Guan et al. [25])
Winglets	-	Zheng et al. [26]; Jiang et al. [30] (Zhu et al. [8]); Gerlach et al. [31]

Note: Articles in parenthesis used the same experimental results as the aforementioned articles did.

Table 2.2: Meta-analytically assessed parameters for the casing and rotational speed of a vortex pump and their respective sources (adapted from Gerlach et al. [1]).

Assessed Parameter	Prefix	Article(s)
Volute width	b_4	Ohba et al. [5]; Zheng et al. [26] (Cheng et al. [32]); Sha et al. [27]; Sha et al. [28]; Sha et al. [29]
Covering	s	Rütschi [4]; Sha & Hou [17]
Suction pipe diameter	D_S	Ohba et al.[5]; Guan et al. [19] (Guan et al. [25]); Zheng et al. [26]; Sha et al. [27]
Pressure pipe diameter	D_D	Zheng et al. [26]
Geometry of suction pipe inlet	-	Rütschi [4]
Geometry of casing	-	Zheng et al. [26]
Rotational speed	n	Li & Feng [18]; Sha & Bai [33] (Wu et al. [20])

Note: Articles in parenthesis used the same experimental results as the aforementioned articles did.

The meta-analysis required the reporting of common dependent variables, including the head H, the pressure coefficient ψ, and the efficiency η at the Best Efficiency Point (hereafter referred to as *BEP*). Hence, several studies were excluded because of their internal scaling (e.g., Schivley & Dussourd [15]; Aoki [34]; and Ohba et al. [12]). Also, numerical simulations without an experimental validation were excluded (e.g., Zhu et al. [7]; Wang et al. [35, 36]; Cervinka [37]; Steinmann et al. [38]).

Figure 2.7 shows an example how variations in the impeller diameter D_2 affected the head H and efficiency η in one of the primary studies (Sha et al. [29]) To integrate each primary study, the highest efficiency point for each impeller diameter was first read off from the given diagram(s) in the original article to define the BEP. All BEP values were ultimately combined into a single graph and plotted against their respective impeller diameter (Figure 2.7 left). The
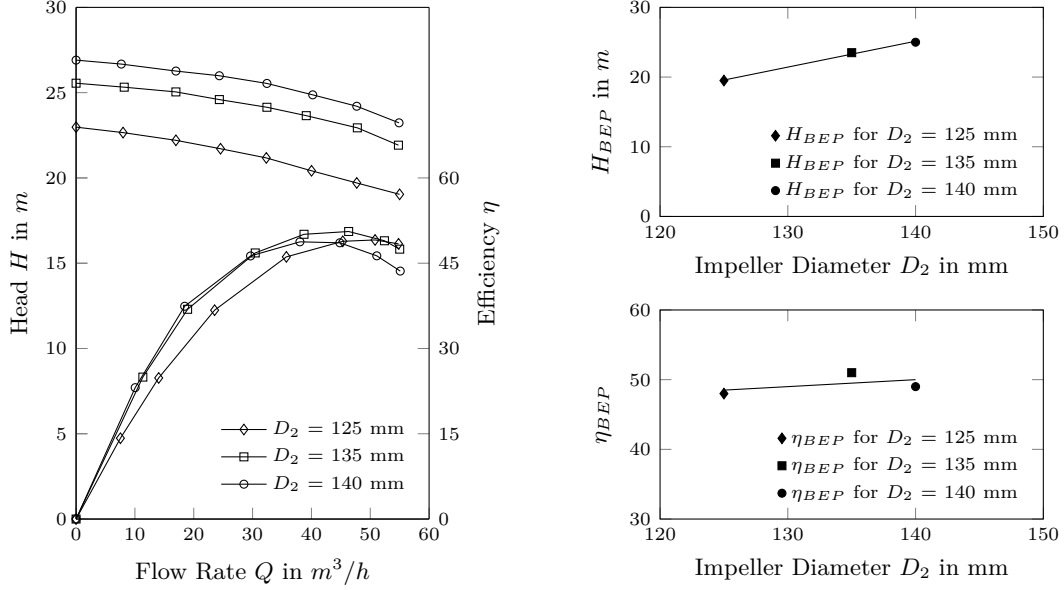
Figure 2.7: Illustration of a meta-analytical integration of a primary study (adapted from Sha et al. [29]). The examples show the head and efficiency curves for different impeller diameters. The original values (left) were limited to the head at the BEP (top right) and the efficiency at the BEP (bottom right) over the impeller diameter.

top right panel of Figure 2.7 exemplifies this procedure on behalf of the head of BEP, H_{BEP}, over impeller diameter, D_2. The bottom right panel of Figure 2.7 shows the efficiency of BEP, η_{BEP}, over impeller diameter, D_2. Finally, a linear trend line was fitted to reveal the trend between all BEPs per primary study. These steps were repeated for all primary studies, which manipulated the respective parameter. Thus, overall trends of individual design parameters on head and efficiency can be compared and design recommendation can be deduced.

The derived design recommendations for the vortex pump impeller and casing can be summarized as follows (for an overview, see Table 2.3 and Table 2.4).

Larger impeller diameters D_2, larger impeller widths b_2 and higher blade numbers z lead to higher heads and greater efficiency and are therefore recommended. The blade outlet angle β_2 should be as large as possible and blades should be straight or forward curved ($\geq 90°$). The

Table 2.3: Design recommendations for the impeller of a vortex pump (adapted from Gerlach et al. [1]).

Parameter	Prefix	Recommendation
Impeller diameter	D_2	as large as possible
Impeller width	b_2	as large as possible
Blade number	z	as large as possible
Blade outlet angle	β_2	as large as possible
Blade inlet angle	β_1	as small as possible
Blade thickness	t	as small as possible
Winglets	-	should be used

Table 2.4: Design recommendations for the casing and rotational speeds of a vortex pump (adapted from Gerlach et al. [1]).

Parameter	Prefix	Recommendation
Volute width	b_4	as small as possible
Covering	s	open design preferable
Suction pipe diameter	D_S	results contradicting
Pressure pipe diameter	D_D	as small as possible
Geometry of suction pipe inlet	-	straight preferable over an inlet with a constriction and an inlet with a large radius of curvature
Geometry of casing	-	ring casing preferable over a spiral casing and a half spiral casing
Rotational speed	n	as large as possible

blade outlet angle recommendation stands in contrary to design recommendations of conventional centrifugal pumps with front shrouded impellers, for which the highest efficiency is obtained for blade outlet angles between 17° and 40° (Pfleiderer [39]). Yet, high values of blade outlet angles — up to straight or forward curved blades — are also recommended for centrifugal pumps with semi-open impellers, which have smaller front gaps than vortex pumps (Gülich [40]). Gülich [40], for example, argued that more blades and greater blade outlet angles are preferable for conventional centrifugal pumps with semi-open impellers because the velocity of fluid in the gap has a high tangential component whose energy contributes to the flow deflection. For small blade angles, however, the gap flow has a radially inwardly directed component, which is opposite to the main flow. The effect of increasing the blade outlet angle suggests a similarity of vortex pumps to centrifugal pumps with semi-open impellers and it is of interest whether further design aspects could be adopted to vortex pumps. In the case of centrifugal pumps with semi-open impellers occur losses due to the missing front shroud. The losses are considered by empirical factors when designing centrifugal pumps with semi-open impellers (e.g., Hofmann [11]; Pfleiderer [39]; Ganter [41]; Ni [42]). However, for vortex pumps are the gap sizes up to 100 times the gap sizes of a centrifugal pumps with semi-open impellers. Thus, empirical factors are missing and further the design methods due to not solvable equations not applicable to vortex pumps.

Other recommendations of the meta-analysis are a small blade inlet angle β_1, small blades thickness t, and the use of winglets. The volute width b_4 should be small and the impeller should *not* be covered (open design).

The influence of the suction pipe diameter D_S could not be unambiguously identified. Some studies showed diverging trends or even no influence. The pressure pipe diameter D_D should be small and the suction pipe inlet geometry straight in order to achieve higher heads and more efficiency. A casing in the shape of a ring — as opposed to a spiral casing and a half spiral casing — seems preferable. Higher rotational speed is associated with an increase in heads and efficiency.

The meta-analysis distinguished between the design types of the vortex pump. Interestingly, the covered design was applied in 32 of the 53 studies. In 13 articles the design was unspecified. Although the open design is used for commercially available vortex pumps (e.g., Gerlach et al. [43]), the meta-analysis suggested that open designs are relatively little represented by the publicly available literature on vortex pumps.

There are several limitations to the meta-analysis. The gradients of trend lines differ be-

tween the studies. This indicates that unknown parameters co-founded the resulting heads and efficiency. Overall, the meta-analysis did not take interaction effects of parameters into account. Instead only linear trends were assumed. Some of the considered articles, however, varied two or more parameter at the same time, which allows drawing possible conclusions on interaction effects of geometric parameters (e.g., Lubieniecki [2]; Rütschi [4]; Ohba et al. [5]; Wang [14]; Li & Feng [18]; Guan et al. [19]; Sha et al. [29]). These studies were analyzed on interaction effects; however, explicit recommendation from these multi-parameter investigations can be hardly derived due to missing data and/or limited parameter variations. For a large number of studies the details of the implementation are unclear. Another limitation of the meta-analysis was that all primary studies used clean water only. However, clogging is the typical operation condition of vortex pumps. It follows that the design recommendations apply exclusively to clean water operation. It therefore remains an open question how the design recommendations relate to clogging.

2.3 Interim Summary

This chapter summarized the state of the art of research on vortex pumps. The goal was to provide a comprehensive overview on the publicly available literature, their central assumptions, and their design recommendation. In brief, the literature review suggests that the operational principle of a vortex pump is not fully understood, and that two differing assumptions about the underlying working principle co-exist. Covered designs assume that a vortex pump mainly transport fluids via the vortex in the front chamber. Open designs describe vortex pumps as 'poorly designed' conventional centrifugal pump whose operational principle is similar to that of a conventional centrifugal pump. At the moment, it is ambiguous which of the underlying operation principle is at work. Hence, it is unclear which of the design types should be prioritized in order to achieve high heads and great efficiency.

A meta-analysis evaluated the influence of some design parameters on the characteristics of vortex pumps. From the results several design recommendations could be derived. These recommendations, however, have to be seen in the lights of the limitations of the meta-analysis. In particular, an adequate study with only one specific vortex pump configuration is missing thus far. Such study would be highly desirable to evaluate precisely the influence of a variety of different geometry parameters. Moreover, the meta-analysis suggests the absence of experimental studies on the clogging behavior of vortex pumps. This is rather surprising given that clogging is the typical operation conditions of vortex pumps. How clogging relates to the geometric parameters and the flow field thus remain to be worked out. Consequently, an experimental investigation with clogging seems highly desirable. Before Chapter 6 addresses the clogging behavior of vortex pumps via an experimental study, Chapter 3 provides a more systematic analysis of the parameters under clean water operation.

Chapter 3

Impeller Designs and their Characteristic Curves

This chapter analyzes the influence of different impeller geometry parameters on characteristic curves under clear water operation. To this end, test of parameters, such as variations in the impeller diameter and the blade number, were complemented with previously untested modifications, such as variations in winglets and splitter blades. The chapter provides new insights on the strengths of individual design parameters and it constitutes the empirical basis for investigations on a design approach for vortex pumps, on their flow field, and their clogging behavior.

This chapter is organized as follows: First, the test setup and the vortex pump under investigation are described, followed by the test results and a comparison of the characteristic curves of the impellers with different geometry parameters[1].

3.1 Methods

3.1.1 Test Setup

The experiments were conducted on a test rig that was built according to ISO 9906. The test rig is schematically illustrated in Figure 3.1. A tank with adjustable system pressure maintained the fluid via a suction pipe to the vortex pump. A pressure pipe re-connected the pump to the tank. The flow rate was adjusted with a throttle valve in the pressure pipe. A frequency converter allowed varying the rotational speed of the pump. Measures included temperature, volume flow, suction pressure and the pressure difference between the suction and the pressure side of the pump. The flow rate was measured by means of a magnetic flow meter.

Figure 3.2 illustrates the vortex pump under investigation. Figure 3.3 depicts the casing design from the front (left panel) and as a cross section (right panel). The vortex pump had an open design with a concentric casing. The suction pipe diameter and the pressure pipe diameter were both 80 mm. The ball passage had a width of 78 mm. The casing was milled from aluminium and black anodised. The casing allowed visual access to the side chamber through acrylic windows. The entire front side of the casing was an acrylic window and there were four side windows distributed over the circumference of casing. The design was chosen to allow for Particle Image Velocimetry measurements (cf. Chapter 5).

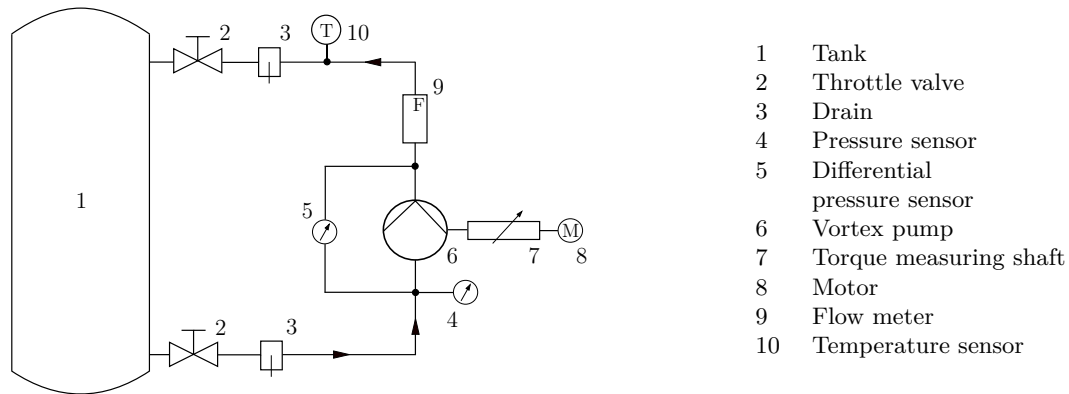[1]Parts of these studies were presented in Gerlach et al. [31] and [43]

1	Tank
2	Throttle valve
3	Drain
4	Pressure sensor
5	Differential pressure sensor
6	Vortex pump
7	Torque measuring shaft
8	Motor
9	Flow meter
10	Temperature sensor

Figure 3.1: Schematic illustration of the test rig.

1	Front window
2	Impeller
3	Side windows
4	Rails
5	Torque measuring shaft
6	Motor
7	Casing
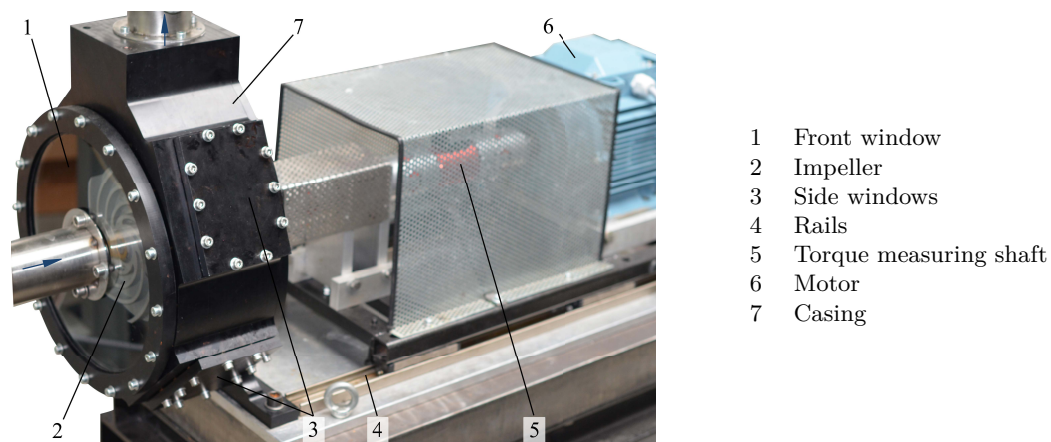
Figure 3.2: Vortex pump under investigation.

The casing had a shape, which resembled commercially available vortex pumps. However, constructive simplifications were necessary to enable the windows and a cost-efficient manufacturing. A torque-measuring shaft allowed metering torque and rotational speed. The drive train and the motor were mounted on rails to keep the drive train aligned when replacing the impeller. The performance curves in terms of head, flow rate, torque, rotational speed, and efficiency were measured.
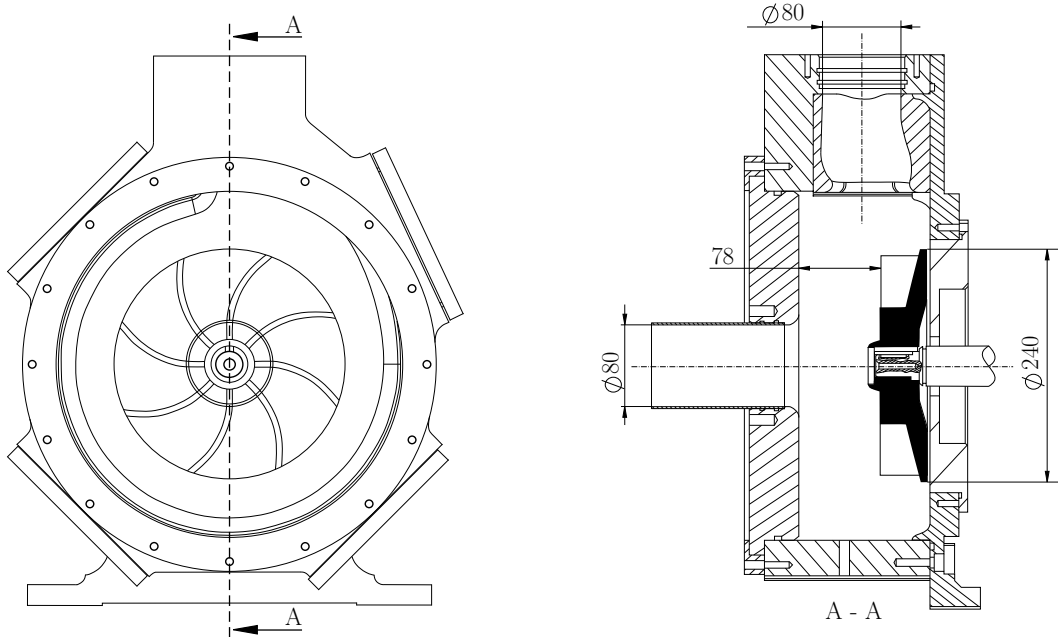
Figure 3.3: Front view of used vortex pump (left) and cross section view (right).

The influences of the following parameters was tested (cf. also Figure 2.6 on page 6):

- Blade number z
- Blade outlet angle β_2
- Impeller diameter D_2
- Impeller width b_2
- Impeller suction inlet diameter D_S
- Winglets
  - Adding winglets
  - Length of winglets
  - Orientation of winglets
- Pan-like impeller
- Adding splitter blades
- Vortex-influencing designs
  - Vortex-strengthening design
  - Vortex-weakening design
- Rotational speed n

Table 3.1 illustrates the impellers in respect to the parameter studies. It lists the assessed design parameters with a sketch of tested impellers and an indication of parameter modification by arrows.

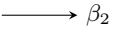13

Table 3.1: Impellers of the assessed parameters.
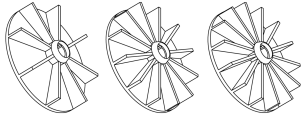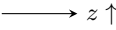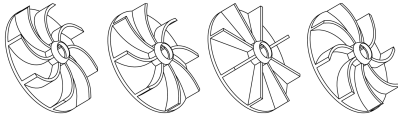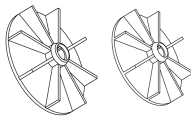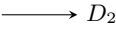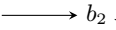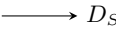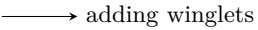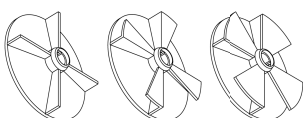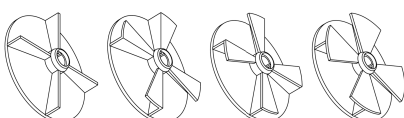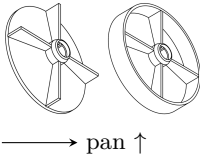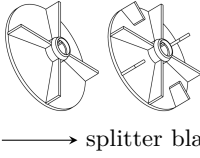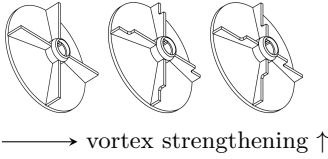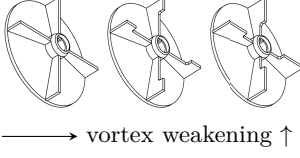
Assessed Parameter	Prefix	Sketch
Blade number	z	$\longrightarrow z \uparrow$
Blade outlet angle	β_2	$\longrightarrow \beta_2 \uparrow$
Impeller diameter	D_2	$\longrightarrow D_2 \downarrow$
Impeller width	b_2	$\longrightarrow b_2 \downarrow$
Impeller suction diameter	D_S	$\longrightarrow D_S \uparrow$
Adding winglets	-	$\longrightarrow$ adding winglets $\uparrow$
Length of winglets	-	$\longrightarrow$ length of winglet $\uparrow$
Orientation of winglets	-	$\longrightarrow$ orientation of winglets

Table 3.1: (continued).

Assessed Parameter	Prefix	Sketch
Pan-like impeller	-	
		⟶ pan ↑
Splitter blades	-	
		⟶ splitter blades ↑
Vortex-strengthening design	-	
		⟶ vortex strengthening ↑
Vortex-weakening design	-	
		⟶ vortex weakening ↑

The parameter study included the testing of typical variations in parameters, such as variation in the impeller diameter, the blade number or the blade outlet angle. Moreover, alternative impeller designs were assessed, for example, such as added winglets or added splitter blades. Appendix A lists the impellers and their specific geometries related to their parameter study.

Manufacturing the impellers required different production processes. An aluminum sintering process produced the impellers to assess the typical variations in parameters, such as blade number and blade outlet angle. The impellers with winglets and splitter blades consisted of turned and milled parts. Noteworthy the different production process resulted in a different surface roughness, which might have influenced the characteristic curves. Investigations on the influence of the surface roughness of impellers in vortex pumps suggest that rougher surfaces decrease efficiency and increase the head — similar to conventional centrifugal pumps (Gerlach et al. [31]). To isolate the effects of the parameters only impellers of the similar production processes are compared.

3.1.2 Presentation of the Data

The core dependent variables are the flow coefficient, the pressure coefficient, the power coefficient and efficiency. The flow coefficient corresponds to a dimensionless description of the flow rate, the pressure coefficient correspond to a dimensionless description of head, and the power coefficient to a dimensionless description of power.

Different definitions for the flow coefficient exist (e.g. Pfleiderer [39]). Here, the most common definition for radial impellers is used (Siegloch [44]). The flow coefficient φ is described as (Formula 3.1):

$$\varphi = \frac{v_\varphi}{u_2} \tag{3.1}$$

with v_φ as a fictive velocity and u_2 as the circumferential speed of the impeller.

For a flow that is equally distributed over a circular impeller area of the diameter D_2 the following calculation can be made: $v_\varphi = 4 \cdot Q / \pi \cdot D_2^2$ and $u_2 = \pi \cdot D_2 \cdot n$ (Formula 3.2):

$$\varphi = \frac{4 \cdot Q}{\pi^2 \cdot D_2^3 \cdot n} \tag{3.2}$$

with Q as the flow rate, D_2 as the impeller diameter, and as n the rotational speed.

The pressure coefficient ψ is defined as the ratio of head and the kinetic energy of the circumferential speed at the impeller outlet (Formula 3.3):

$$\psi = \frac{g \cdot H}{u_2^2 / 2} \tag{3.3}$$

with g as the gravitational acceleration, H as the head, and u_2 as the circumferential speed at the impeller outlet.

The pressure coefficient can be calculated using the above definition of u_2 (Formula 3.4):

$$\psi = \frac{2 \cdot g \cdot H}{\pi^2 \cdot n^2 \cdot D_2^2} \tag{3.4}$$

with g as the gravitational acceleration, H as the head, n as the rotational speed, and D_2 as the outer diameter of the impeller.

The power coefficient λ is defined as (Formula 3.5):

$$\lambda = \frac{\varphi \cdot \psi}{\eta} \tag{3.5}$$

with φ as the flow coefficient, ψ as the pressure coefficient, and η as efficiency. Hence, the power coefficient for an efficiency value of zero does not exist by definition.

The efficiency was calculated as the ratio of the hydraulic power to the power at the shaft (Formula 3.6):

$$\eta = \frac{P_{hyd}}{P_{shaft}} \tag{3.6}$$

with P_{hyd} as the hydraulic power, and P_{shaft} as the power at the shaft.

The efficiency can be expressed as (Formula 3.7):

$$\eta = \frac{H \cdot g \cdot Q \cdot \rho}{M \cdot 2 \cdot \pi \cdot n} \tag{3.7}$$

with the hydraulic power calculated as the product of the head H, the gravitational acceleration g, the flow rate Q, the density ρ (depending on the measured temperature) and the power at the shaft calculated as the product of the torque M and the angular velocity ω (with $\omega = 2 \cdot \pi \cdot n$).

3.2 Results on the Influence of Parameters

3.2.1 Blade Number

The nature of the study allowed isolating the influence of single design parameters on the characteristics. Variation in the number of blades z was evaluated by comparing an impeller with 8 straight blades to an impeller with 12 straight blades to an impeller with 14 straight blades (Figure 3.4). All impellers had a diameter of 240 mm and a blade depth of 40.3 mm. Figure 3.5 shows the pressure coefficient (left panel), the power coefficient (middle panel) and the efficiency (right panel) over the flow coefficient. The pressure coefficient and the power coefficient slightly increase with blade number increasing. However, the positive effect of changing the blade number from 12 to 14 straight blades on the pressure coefficient is marginal and the effect diminishes entirely in over load operation. The efficiency is highest for the impeller with 12 straight blades (47.3%) followed by the impeller with 14 straight blades (47.2%). The 8 bladed impeller reached lowest values of efficiency with a value of 46.6%. The resulting values of flow coefficient for BEP operation were similar for all three impellers.

Overall, the pressure coefficient increase with blade number increasing. In terms of efficiency a design with 12 blades was preferable over other blade numbers.

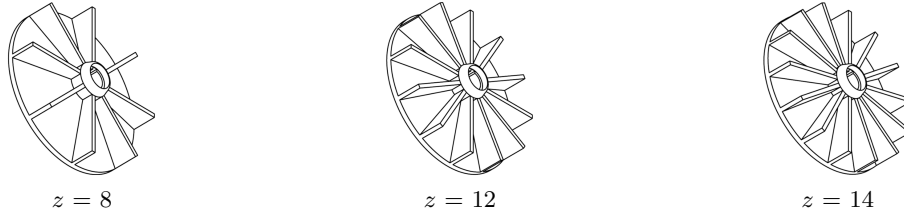$z = 8$ $\qquad\qquad$ $z = 12$ $\qquad\qquad$ $z = 14$

Figure 3.4: Impellers used to test the influence of the number of blades: Impeller with 8 straight blades (left), impeller with 12 straight blades (middle), and impeller with 14 straight blades (right).
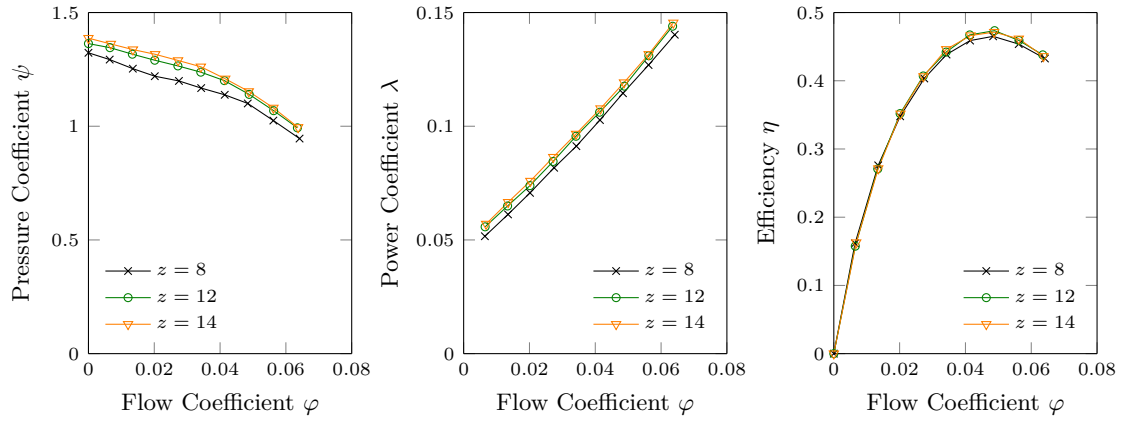

Figure 3.5: Influence of the blade number on the pressure coefficient (left), on the power coefficient (middle) and on efficiency (right).

3.2.2 Blade Outlet Angle

The effect of blade outlet angle β_2 was assessed via four different impellers with an outlet angle of $40°$, $60°$, $90°$ and $130°$. As illustrated in Figure 3.6 all impellers had 8 blades and an inlet angle of $90°$. The diameter was 240 mm. Figure 3.7 shows the influence of blade outlet angle on the characteristic curves.

The results suggest that the pressure coefficient, the power coefficient, and the efficiency increase with blade outlet angle increasing. In other words, the impellers with straight and forward curved blades (i.e., blade outlet angles of $90°$ and $130°$) were superior to the impellers with backward curved blades (i.e., blade outlet angles of $40°$ and $60°$) in terms of their pressure coefficients and their efficiency. The straight-bladed impeller reached the highest value of efficiency. However, the power consumption increased significantly with blade outlet angle increasing. This trade-off between higher pressure coefficients and efficiency against higher power consumption has to be considered for finding the optimal motor size.

Increasing the blade outlet angle flattened the slope of the pressure coefficient curve. This behavior is known from conventional centrifugal pumps (e.g. Pfleiderer [39]). Further, increasing the blade outlet angle shifted the highest efficiency point to higher values of the flow coefficient.

Overall, increasing the blade outlet angle improved the characteristics in terms of higher pressure coefficients and efficiency. In terms of efficiency a design with straight blades is preferable over other blade outlet angles.

$\beta_2 = 40°$ $\beta_2 = 60°$ $\beta_2 = 90°$ $\beta_2 = 130°$
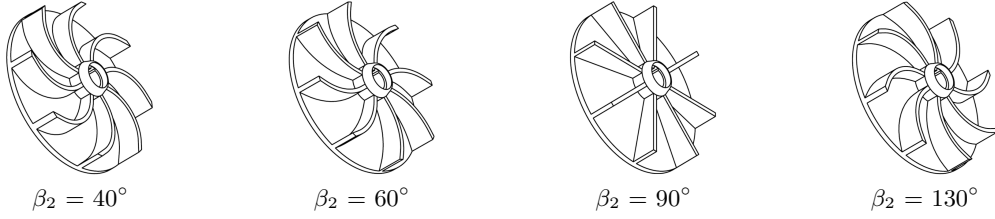
Figure 3.6: Impellers used to test the influence of blade outlet angle: Impeller with a blade outlet angle of $40°$(far left), $60°$(middle-left), $90°$(middle-right), and $130°$(far right).
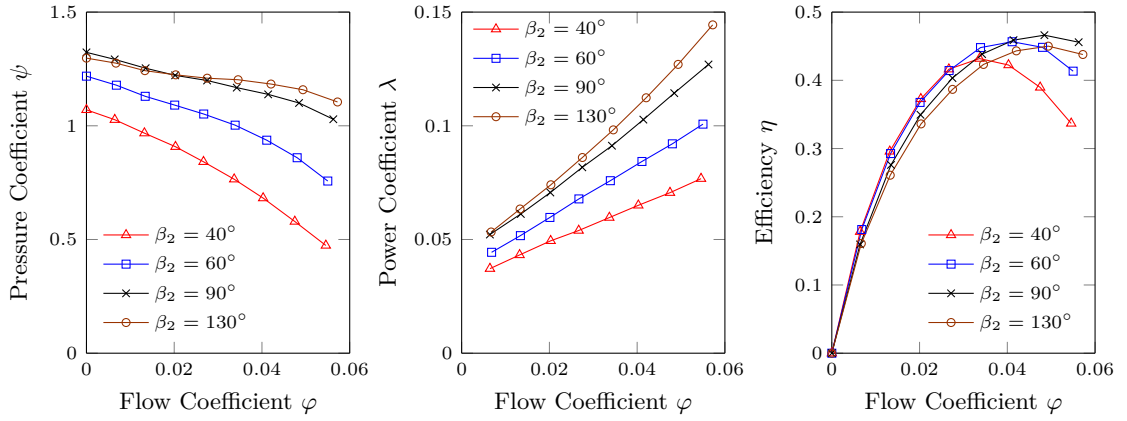

Figure 3.7: Influence of the blade outlet angle β_2 for backward curved blades on the pressure coefficient (left), on the power coefficient (middle), and on the efficiency (right).

3.2.3   Impeller Diameter

To evaluate the influence of the diameter the impeller with 8 straight blades was gradually trimmed. That is, the initial diameter of 240 mm was reduced first to 220 mm and then again to 210 mm. Figure 3.8 shows the impellers of these tests and Figure 3.9 shows the associated characteristic curves. Trimming slightly decreased the pressure coefficients, power coefficients, and efficiency. Decreasing the diameter also shifted the highest efficiency point to greater values of the flow coefficients (corresponding to a shift of highest efficiency to smaller values of flow rates).

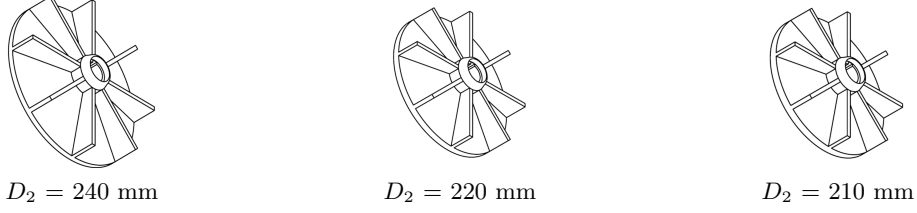$D_2 = 240$ mm $D_2 = 220$ mm $D_2 = 210$ mm

Figure 3.8: Impellers used to test the influence of the impeller diameter: Impeller with a diameter of 240 mm (left), 220 mm (middle), and 210 mm (right).
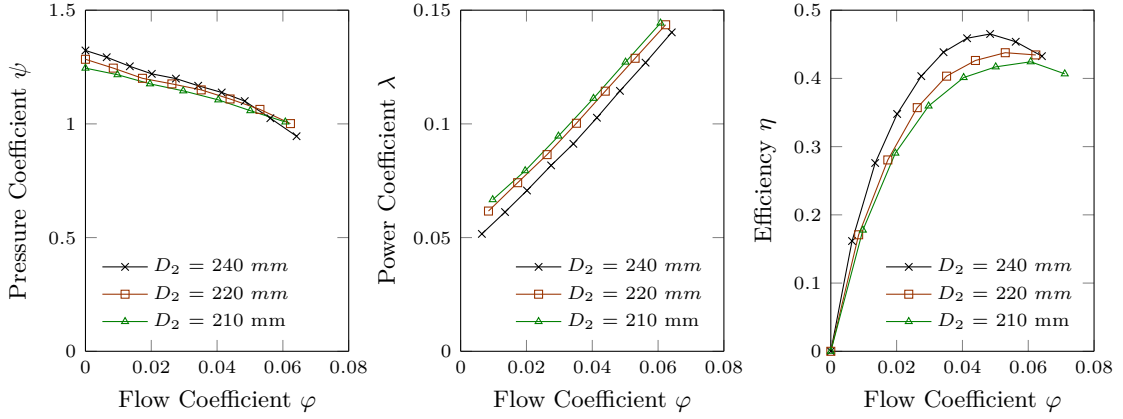
Figure 3.9: Influence of the impeller diameter D_2 for an impeller with 8 straight blades on the pressure coefficient (left), on the power coefficient (middle) and on the efficiency (right).

For conventional centrifugal pumps Pfleiderer [39] (and also Yedidiah [45]) suggested approximating the flow rate and the head for a trimmed impeller from the flow rate and the head of an untrimmed impeller as described in Formula 3.8 and Formula 3.9, respectively:

$$\frac{Q_t}{Q_f} \approx \frac{D_{2,t}}{D_{2,f}} \tag{3.8}$$

$$\frac{H_t}{H_f} \approx \left(\frac{D_{2,t}}{D_{2,f}} \right)^2 \tag{3.9}$$

with Q_t as the flow rate of the trimmed impeller, Q_f as the flow rate of the impeller with full diameter, $D_{2,t}$ as the diameter of the trimmed impeller, $D_{2,f}$ as the diameter of the impeller

with full diameter, H_t as the head of the trimmed impeller, and H_f as the head of the impeller with full diameter.

It was tested whether the relationship described by Formula 3.8 and Formula 3.9 generalize to vortex pumps. To this end, the flow rate and head for the diameters of 220 mm and 210 mm were converted by means of Formula 3.8 and Formula 3.9 to a diameter of 240 mm. The calculated characteristics were then compared to the measured curve of the initial diameter of 240 mm. The throttle curves of different diameters normalized to the BEP data of the untrimmed impeller (240 mm) are depicted in Figure 3.10 left. The middle panel of Figure 3.10 compares the measured curve of 240 mm to the calculated curve of 240 mm, derived from the measured values of 220 mm. The right panel of Figure 3.10 does the same for the values of 210 mm. Figure 3.10 middle suggests that the calculated and the measured curve are in good agreement. Only at part load operation the calculated characteristics move slightly below the measured curve. The calculated curve derived from the measured values of 210 mm lies altogether below the measured curve suggesting a mismatch between the trimmed impeller and the casing volute (Figure 3.10 right). Pfleiderer [39] argues that the flow rate at the highest efficiency decreases when the impeller diameter decreases. This is because of a lower absolute fluid velocity at the impeller outlet while the casing remains of the same size and becomes oversized. Yedidiah [45] argues similar that trimming the impeller can cause mismatches between the geometry of the trimmed impeller, the blade geometry and the casing volute. These mismatches can distort the relations between the calculated and tested curves for trimmed impellers. As a result, the relations suggested in Formula Formula 3.8 and Formula 3.9 become limited in terms of agreement between calculated and tested curves.

The comparisons suggested that the relation of the flow rate, the head and the diameter of conventional centrifugal pumps with trimmed impellers can be generalized to vortex pumps. Overall, increasing the impeller diameter is preferable as it increases the pressure coefficient and the efficiency.
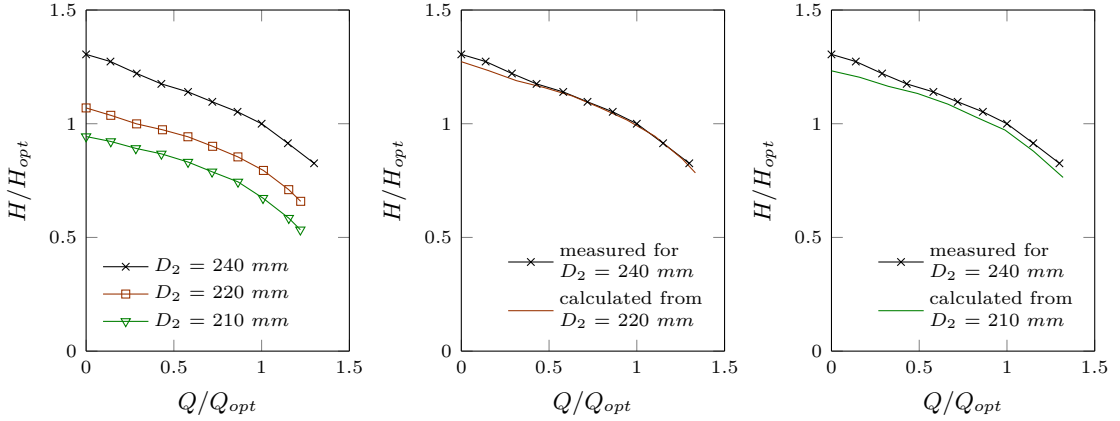

Figure 3.10: Influence of the impeller diameter D_2 for an impeller with 8 straight blades on the normalized H-Q-curve (left), calculated curve from a diameter of 220 mm (middle), and from a calculated curve of a diameter of 210 mm (right).

3.2.4 Impeller Width

To evaluate the influence of the impeller width b_2 an impeller with 4 curved blades was trimmed in steps of 3 mm: from the original width of 40.3 mm over 37.3 mm to 34.3 mm (Figure 3.11). Noteworthy, trimming the impeller width is associated with an increased volute width b_4. Hence, to isolate the influence of the impeller width b_2, the volute width b_4 should be kept constant which was not possible in the tests due to the design of used vortex pump. Nonetheless, a simple trimming of the impeller width can still provide valuable insights. As shown in Figure 3.12 decreasing the impeller width decreases the pressure coefficient, the power coefficient and the efficiency. When decreasing the impeller width the BEP values shifted to lower values of the flow coefficient.

Overall, the effect of trimming the impeller width was relatively strong compared to the other tested parameters (cf. blade numbers or impeller diameter) and increasing the impeller width is preferable as it increases the pressure coefficient and the efficiency.

$b_2 = 40.3$ mm $\qquad$ $b_2 = 37.3$ mm $\qquad$ $b_2 = 34.3$ mm
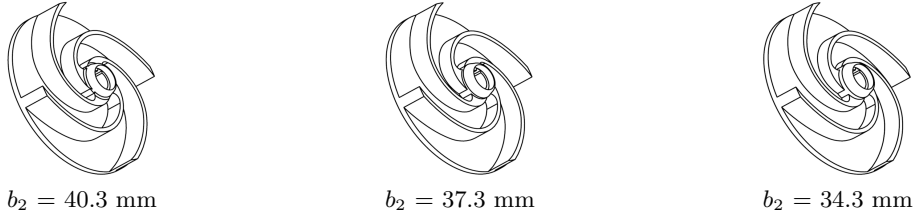
Figure 3.11: Impellers used to test the influence of impeller width: Impeller with a width of 40.3 mm (left), 37.3 mm (middle), and 34.3 mm (right).

Figure 3.12: Influence of the impeller width b_2 on the pressure coefficient (left), on the power coefficient (middle), and on the efficiency (right).

3.2.5 Impeller Suction Inlet Diameter

To evaluate the influence of impeller suction inlet diameter D_S the suction inlet diameter was trimmed. The original impeller had 4 curved blades, a diameter of 240 mm and no inlet diameter (Figure 3.13 left). The original impeller was compared to an impeller with an inlet diameter with $D_2/D_S = 3$ (Figure 3.13 middle) and to an impeller with an inlet diameter of $D_2/D_S = 2$ (Figure 3.13 right). For all three impellers, the hub remained constant.

no inlet $D_2/D_S = 3$ $D_2/D_S = 2$

Figure 3.13: Impellers used to test the influence of the suction inlet diameter: Impeller without suction inlet diameter (left), impeller with a suction inlet of $D_2/D_S = 3$ (middle), and impeller with a suction inlet of $D_2/D_S = 2$ (right).

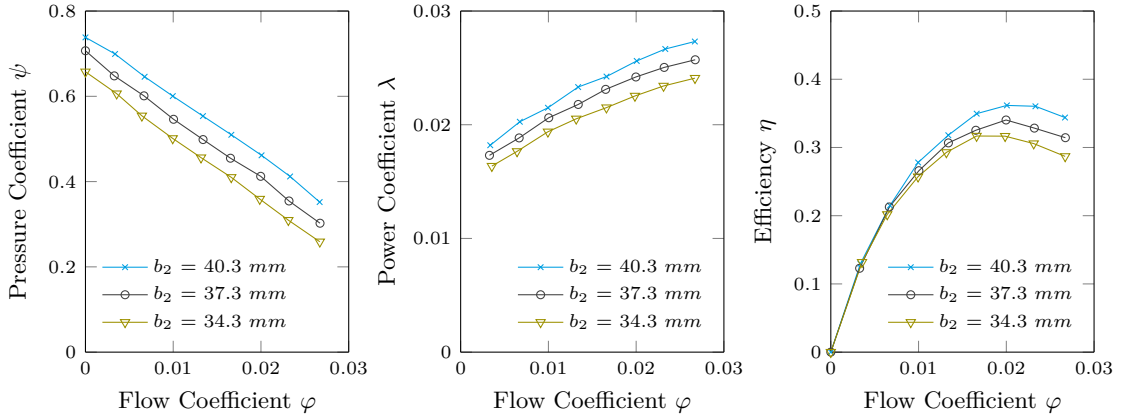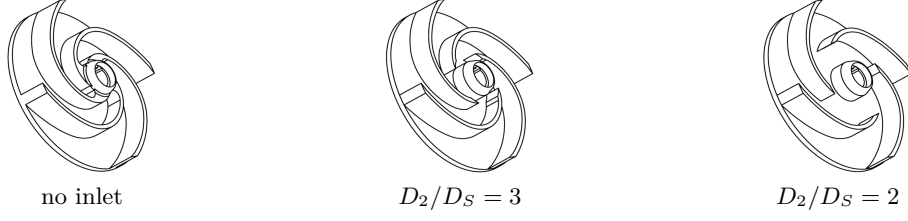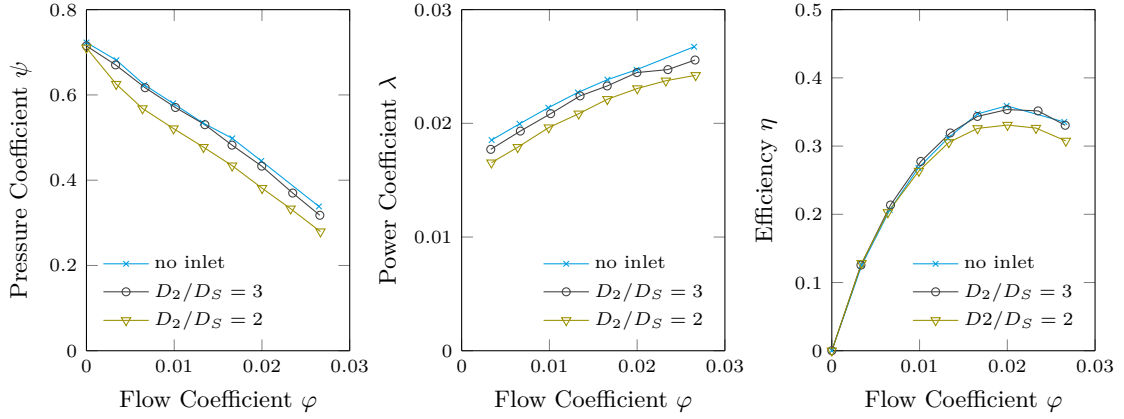Figure 3.14: Influence of the impeller suction inlet diameter D_S on the pressure coefficient (left), on the power coefficient (middle) and on the efficiency (right).

Figure 3.14 illustrates the pressure coefficient, the power coefficient and efficiency at different flow coefficients as a result of changing the inlet diameter. Compared to an impeller without inlet, introducing a suction inlet diameter of $D_2/D_S = 3$ slightly decreased the pressure coefficient, the power coefficient and efficiency. Further, introducing a suction inlet diameter of $D_2/D_S = 2$ strongly decreased the pressure coefficient, the power coefficient and efficiency.

Interestingly, all impellers with different suction inlet diameters had similar values of pressure coefficient at operation under shut-off conditions ($\varphi = 0$) (Figure 3.14 left). The author Rütschi [4] argues that unlike in conventional centrifugal pumps shock losses in vortex pumps are marginal because of the enhanced distance between the impeller and the suction pipe. Shock losses for conventional centrifugal pumps lead to a decrease of pressure coefficient at part load operation and operation at shut-off conditions due to an 'misguided' inflow to the impeller inlet. Hence, modifying the impeller inlet geometry for conventional centrifugal pumps changes the values of pressure coefficient. In vortex pumps, impellers with different inlet diameters reach similar values of pressure coefficient at operation under shut-off conditions. This is because the large distance between the impeller and the suction pipe limits the guidance of inflow to the impeller and parts of fluid can propagate in the side chamber without entering the impeller. Hence, it can be assumed that shock losses in vortex pumps are indeed marginal.

Overall, in terms of pressure coefficient and efficiency a design with no suction inlet diameter is preferable over designs with suction inlet diameters.

3.2.6 Winglets

The effect of winglets was evaluated by comparing an impeller with 4 curved blades without winglets to an impeller with winglets (Figure 3.15; from Sarvanne [9]). The impellers had similar blade curvatures ($\beta_2 = 19°$, $\beta_1 = 44°$) and similar diameters (240 mm). Figure 3.16 illustrates their characteristics. Adding winglets led to a clear increase in pressure coefficient, power coefficient and efficiency. Moreover, the course of the pressure coefficient became steeper with winglets (Figure 3.16 left).

4 curved blades   4 curved winglets

Figure 3.15: Impellers used to test the influence of adding winglets: Impeller with 4 curved blades (left) and impeller with 4 curved winglets (right).
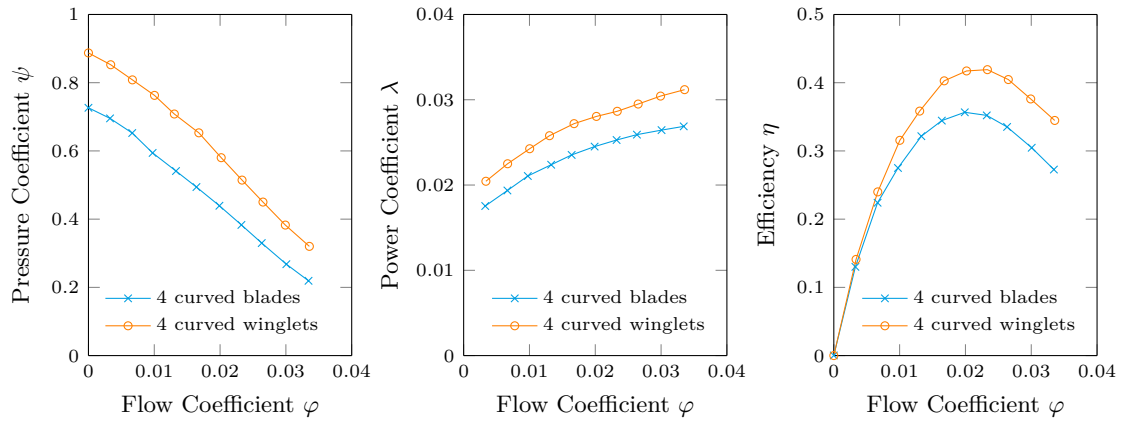

Figure 3.16: Influence of winglets for curved blades on the pressure coefficient (left), on the power coefficient (middle), and on the efficiency (right).

To gain further insights on the favorable design of winglets additional tests on the length and the orientation were performed. First, to test the effect of winglet length an impeller with 4 straight blades was considered.

Figure 3.17 depicts the tested impellers that were used to study the influence of winglets length: An impeller without winglets was compared to a similar impeller with 1/4 winglet length and to a similar impeller with 1/2 winglet length (note: 1/4 winglet length means that 1/4 of the impeller channel were covered from the front chamber; 1/2 winglet length means that a 1/2 of the impeller channels were covered from the front chamber). Figure 3.18 shows the influence of winglet length on the characteristics. The 1/4 winglet length increased the pressure coefficient and efficiency compared to the impeller without winglets. The impeller with 1/2 length of winglets reached higher values of pressure coefficients in part load operation than the impeller without winglets, however, it was less efficient. As with curved blades, adding winglets

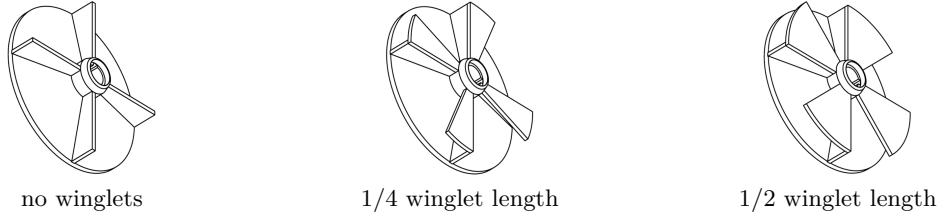no winglets   1/4 winglet length   1/2 winglet length

Figure 3.17: Impellers used for testing the length of the winglets: Impeller with 4 blades (left), impeller with 1/4 winglet length (middle), and impeller with 1/2 winglet length (right).
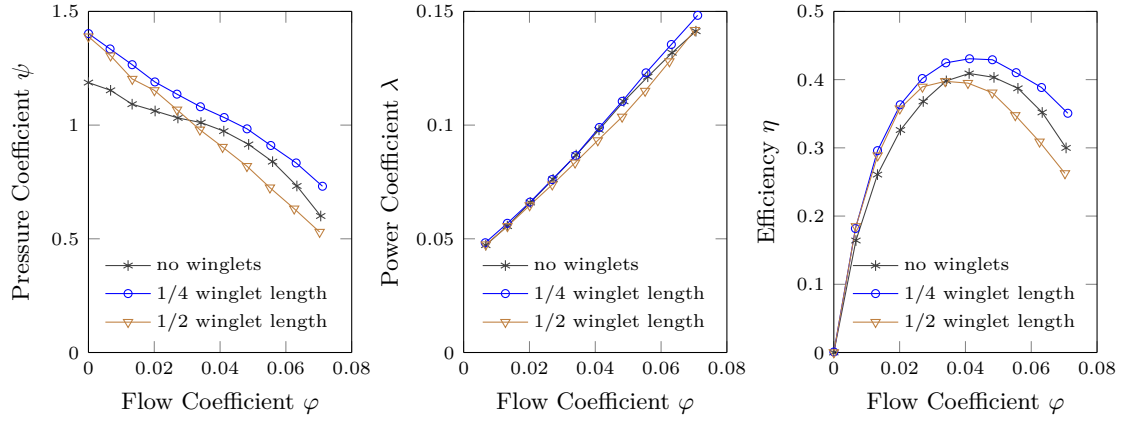

Figure 3.18: Influence of winglet length on the pressure coefficient (left), on the power coefficient (middle) and on the efficiency (right).

to straight blades makes the slope of the pressure coefficient curve steeper. The power coefficients were comparable for all impellers with highest values for the impeller with a winglet length of 1/4. Overall, the results suggest an upper limit for the favorable influence of winglet length. Best results were obtained for a winglet length of 1/4.

To evaluate the influence of the orientation of winglets four different impellers were tested: An impeller without winglets, an impeller with winglets only on the suction side of the blades, an impeller with winglets only on the pressure side of the blades, and an impeller with winglets on both sides of the blades (Figure 3.19). All impellers had 4 straight blades and, based on the previous findings, a winglets length of 1/4.

no winglets   suction side   pressure side   both sides
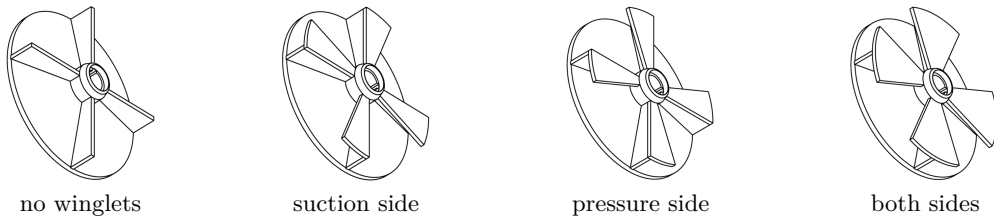
Figure 3.19: Impellers used for testing the orientation of the winglets: Impeller without winglets (far left), impeller with winglets on the blade suction side (middle-left), impeller with winglets on the blade pressure side (middle-right), and impeller with winglets on both sides of blade (far right).
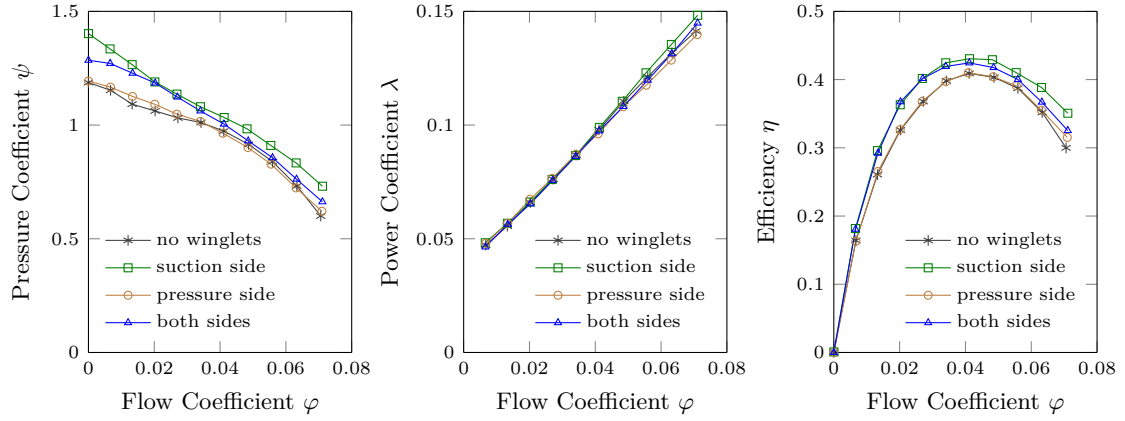
Figure 3.20: Influence of winglets orientation on the pressure coefficient (left), on the power coefficient (middle) and on the efficiency (right).

Figure 3.20 shows the resulting characteristics. The impeller with winglets only on the suction side reached the greatest pressure coefficients and highest efficiency. The impeller with winglets only on the pressure side was associated with the lowest pressure coefficients and the least efficiency. The impeller with winglets on both sides approached pressure coefficients and efficiency that were comparable to the impeller without winglets. The power coefficient was comparable for all impellers. If anything somewhat higher values for the impeller with winglets on the suction side for overload operation were observed.

Conventional centrifugal pumps with semi-open impellers are known to form a flow from the pressure side of the blade to the suction side of the blade. This flow is due to the pressure difference between the blade sides (e.g., Pfleiderer [39]). A similar behavior should be expected for vortex pumps. Winglets on the suction side close off the blade channel areas with low pressure from areas with higher pressure (at the blade pressure side and the side chamber). As a result, the low pressure is maintained at the suction side of the blade. Hence, the overall pump process improves if winglets are added on the suction side of blades. In contrast, winglets on the pressure side close off high pressure area of the channel. The low pressure area of the blade suction side is, however, still exposed to the side chamber. A flow from the side chamber to the suction side of blade is therefore possible and the pump process does not improve when the winglets are on the pressure side of blade. Thus, adding winglets to the pressure side are associated with similar characteristics as designs without winglets. Yet, adding winglets to both sides of the blade result in too much area of the blade channels being covered. As a result the pumping process is disturbed (similar to increasing the winglet length to 1/2 of the front side). Thus, a design with winglets on the suction side of blades seems preferable over other winglet positions.

Overall, adding winglets improved the characteristics in terms of higher pressure coefficients and efficiency for impeller designs with backward curved blades and straight blades. In terms of pressure coefficient and efficiency a design with a winglet length of 1/4 and winglets on the suction side of blades is preferable over other winglet lengths and positions.

3.2.7   Splitter Blades

To evaluate the influence of splitter blades three impellers were compared: an impeller with 4 straight blades only, an impeller with both 4 straight blades and 4 splitter blades, and an impeller with 8 straight blades (Figure 3.21). The ratio of the impeller diameter to the inlet diameter of the splitter blades was 1.7. Figure 3.22 depicts the pressure coefficients, power coefficient and efficiency of the impellers. Adding splitter blades noticeably increased the pressure coefficient and the efficiency. Compared to the impeller with splitter blades, the impeller with 8 blades reached even higher values of pressure coefficients and efficiency than the other two impellers did. The Power coefficients of the impeller with splitter blades and the impeller with 8 blades were similar and superior to the impeller with 4 blades.

The effect of adding splitter blades for a vortex pump impeller is comparable to the effect of adding splitter blades to conventional centrifugal pumps: Adding splitter blades leads to higher pressure coefficients. Adding splitter blades is comparable to increasing the blades number and thus decreasing the slip factor (e.g, Pfleiderer [39]). The study on the impeller suction inlet diameter (Chapter3.2.5) explain the slight lower pressure coefficient and efficiency for the impeller with 4 additional splitter blades compared to the 8 bladed impeller: The design with splitter blades is similar to a design with suction inlet diameter (less blades at the inlet of impeller) and thus lower pressure coefficient and efficiency result compared to the 8 bladed impeller.

Overall, splitter blades are preferable as they increase the pressure coefficient and the efficiency.

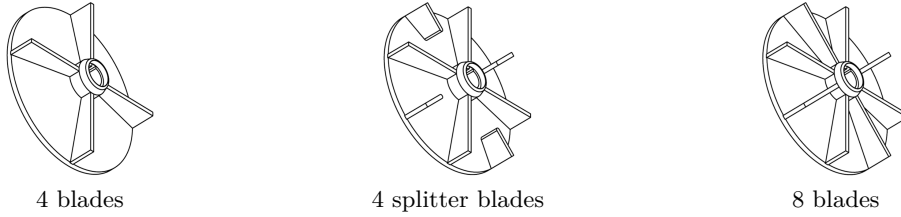4 blades   4 splitter blades   8 blades

Figure 3.21: Impeller used to test the influence of splitter blades: Impeller with 4 straight blades (left), impeller with additional 4 splitter blades (middle), and impeller with 8 straight blades (right).
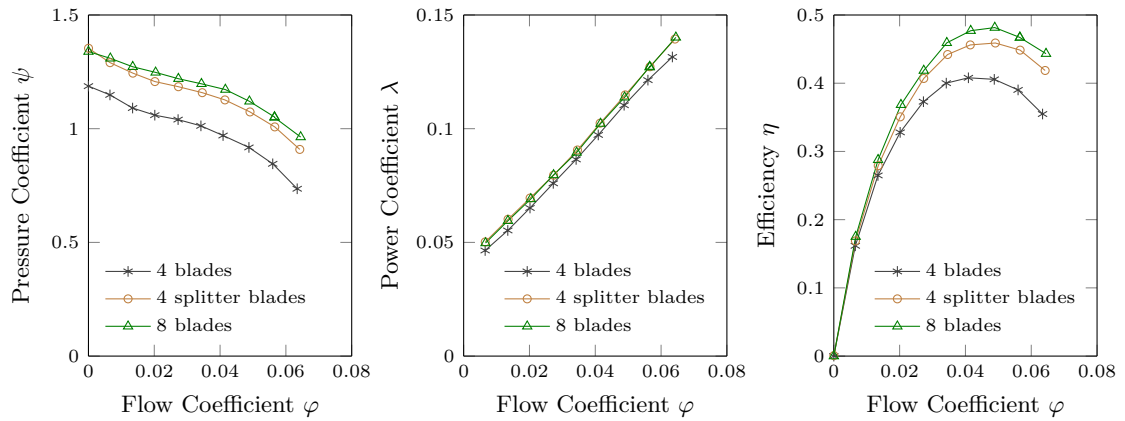

Figure 3.22: Influence of splitter blades on the pressure coefficient (left), on the power coefficient (middle) and on the efficiency (right).

3.2.8   Pan-Like Impeller

To analyze the work transfer in vortex pumps a semi-open impeller was compared to a pan-like impeller (Figure 3.23). The semi-open impeller allows a free outflow from the impeller (Figure 3.23 left panel). The pan-like impeller covers the outlet of impeller with the intention to strengthen the axial work transfer from the impeller to the front gap and to create a stronger vortex formation (Figure 3.23 right panel). All components were structurally equivalent for the two tests. As outlined in Chapter 2 pan-like impellers are frequently used in the covered design of vortex pump. Noteworthy, the here-considered vortex pump was an open design. This is because changing the designs — from open to covered design — would mean changing geometry parameters, which this study aims to keep constant, such as volute width.

Figure 3.24 shows the pressure coefficient, power coefficient and efficiency over flow coefficient for the semi-open impeller and the pan-like impeller. The pressure coefficient, the power coefficient and the efficiency, were higher for the semi-open impeller.

In addition, the two designs reached their BEP at different flow coefficients: The BEP of the semi-open impeller occurred at a higher flow coefficient than the BEP of the pan-like impeller did. Thus, the semi-open impeller had a greater operating range than the pan-like impeller had.

It can be concluded that the outer ring of the pan-like impeller causes hydraulic losses. These are reflected in a sharper drop in pressure coefficient in overload operation for the pan-like impeller design.

Overall, in terms of pressure coefficient and efficiency a semi-open impeller design is preferable over a pan-like impeller design.

semi-open impeller   pan-like impeller

Figure 3.23: Semi-open impeller with free outflow (left) and pan-like impeller (right).
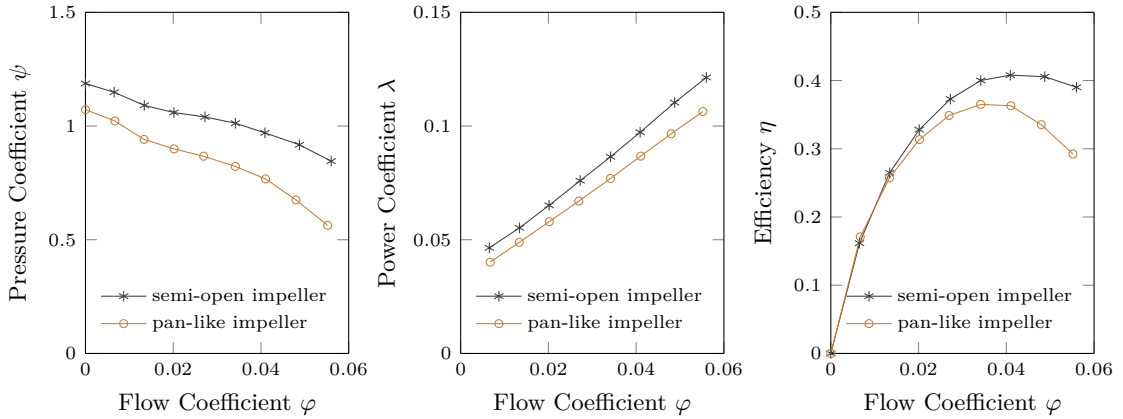

Figure 3.24: Influence of a pan-like impeller design on the pressure coefficient (left), on the power coefficient (middle), and on the efficiency (right).

3.2.9 Vortex-Influencing Designs

A study tested modifications of the impeller design to strengthen the formation of a vortex. In particular, the blades were partly set back in the region of the vortex zone. As a result, the vortex should be able to freely propagate (Figure 3.25). Two modifications of the impeller with 4 blades were tested (Figure 3.26). The modifications differed as to how far the blades were set back in radial direction. The modification will be referred to VS-No1 ('Vortex Strengthening Number 1') and VS-No2 ('Vortex Strengthening Number 2') where the blades of VS-No2 are set back further in radial direction than the blades of VS-No1. The depth in axial direction was the same for both impellers. All impellers had the same basic blade depth.
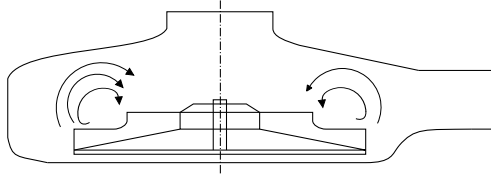

Figure 3.25: Schematic illustration for an impeller design to strengthen the vortex formation.
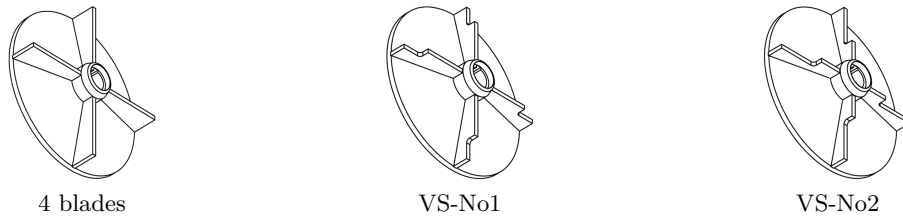

| 4 blades | VS-No1 | VS-No2 |

Figure 3.26: Impeller designs to strengthen the vortex formation: Impeller with 4 blades (left), impeller modification VS-No1 with blades set back in radial direction (middle), and impeller modification VS-No2 with blades set back further in radial direction (right).

The assumed vortex zone was derived from streamline pictures based on a numerical study (Gerlach et al. [22]), which included a simulation of a comparable vortex pump, including the impeller (in terms of diameter, blade number, and depth), and the casing (in terms of pipe diameter and ball passage).

The simulations of Gerlach et al. [22] suggest that the size of the vortex depends on the operation point. Testing and comparing two modifications allowed analyzing the vortex over the whole operation range, from part load to overload operation. Setting back the blades to strengthening the vortex formation means to increase the side chamber width partly. Thus, two modifications were used too, to rule out the effect of an enlarged side chamber width on the characteristics.

Figure 3.27 depicts the characteristics for the three impellers. The results suggest that the vortex-strengthening modifications yielded lower pressure coefficients and lower efficiency than the impeller with 4 blades. The more material was removed in radial direction the more the pressure coefficient and efficiency decreased, and the BEP shifted to smaller flow coefficients. Thus, it can be concluded that setting back the blades to strengthen the vortex formation causes pressure coefficient losses and efficiency losses.
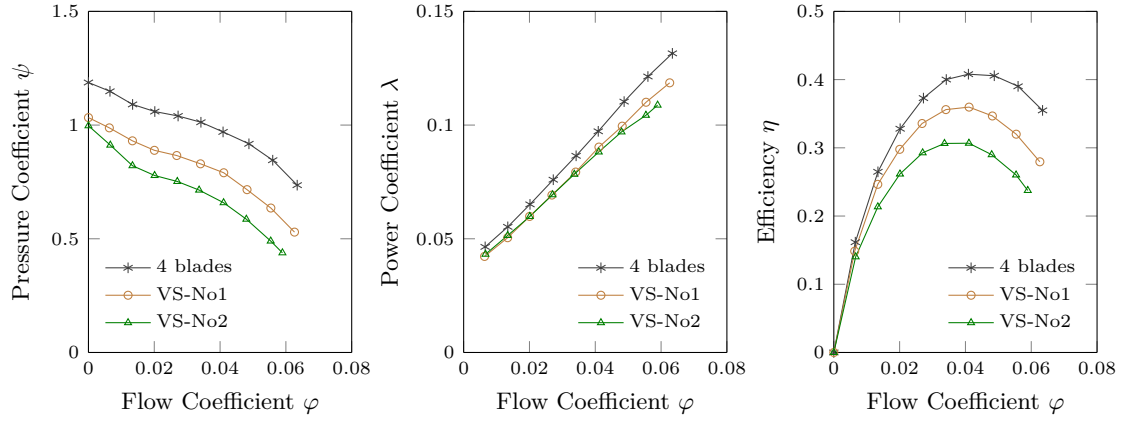
Figure 3.27: : Influence of the vortex-strengthening impellers on the pressure coefficient (left), on the power coefficient (middle), and on the efficiency (right).

An additional study aimed at weakening the formation of the vortex by means of adding material to the blades at the vortex zone (Figure 3.28). To this end two modifications of the impeller with 4 straight blades were tested (Figure 3.29): VW-No1 ('Vortex Weakening Number 1') and VW-No2 ('Vortex Weakening Number 2'). Because these modifications added material to the blades at the exact same radial positions as the vortex-strengthening designs the vortex-weakening impellers VW-No1 and VW-No2 can be seen as 'counterparts' of VS-No1 and VS-No2, respectively. The axial depth of the retracted area was the same for VW-No1 and VW-No2. The basic blade depth of VW-No1 and VW-No2 corresponded to that of the impeller with 4 straight blades. All impellers had the same diameter and the same blade number. Again, the vortex zone was defined through streamline pictures from a numerical study (Gerlach et al. [22]).
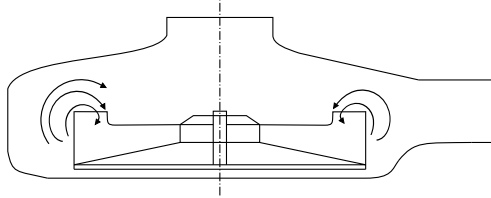

Figure 3.28: Schematic illustration for an impeller design to weaken the vortex formation.
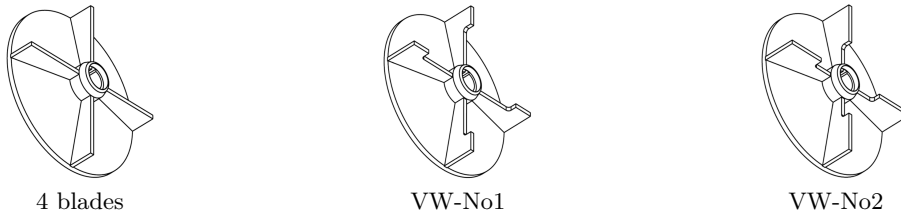

Figure 3.29: Impeller designs to weaken the vortex formation: Impeller with 4 blades (left), impeller modification VW-No1 with pulled-out blades in radial direction (middle), impeller modification VW-No2 with even further pulled-out blades in radial direction (right).
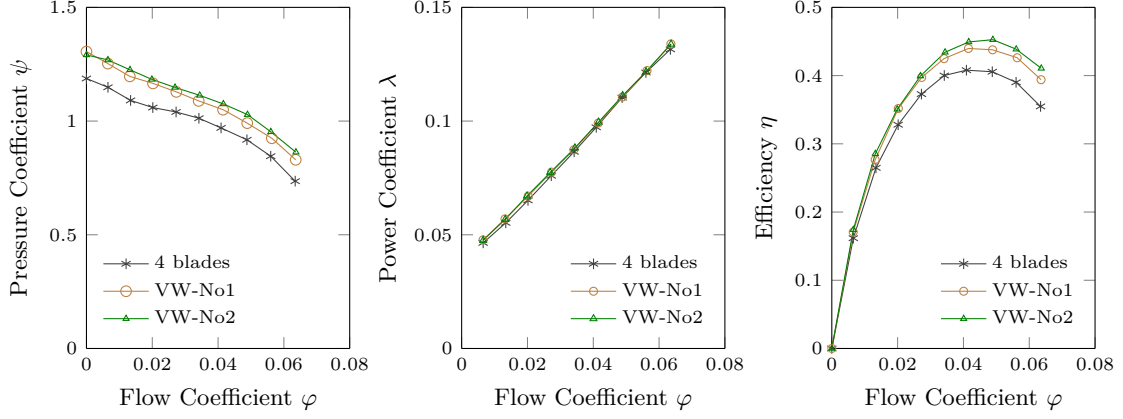
Figure 3.30: Influence of the vortex-weakening impellers on the pressure coefficient (left), on the power coefficient (middle), and on the efficiency (right).

Figure 3.30 shows the characteristics for the vortex-weakening impellers compared to the impeller with 4 straight blades. Both designs, which should weaken the vortex formation, reached higher pressure coefficients and higher efficiency than the impeller with 4 straight blades did. This was true for the entire operation range. The more vortex-weakening design (VW-No2) reached somewhat higher values of pressure coefficient and efficiency than the less vortex-weakening design (VW-No1) did although the differences were marginal.

Taken together, the studies on the vortex-strengthening and the vortex-weakening designs suggest that the outer edge of the impeller plays a key role in reaching high pressure coefficients and high efficiency.

Overall, the results suggest that the less the vortex formation is supported the better the characteristic curves become.

3.2.10   Rotational Speed

Finally, a series of tests analyzed the influence of rotational speed on the characteristics using different impeller designs. Figure 3.31 exemplifies the characteristics with an impeller with 4 curved winglets (the impeller is depicted in Figure 3.15, right panel). Three rotational speeds were tested: 50 Hz (corresponding to 1465 1/min), 35 Hz (1030 1/min), and 25 Hz (730 1/min). The results suggest that the pressure coefficient was independent of the rotational speed, however, the power coefficient increases with decreasing rotational speed and the efficiency decreases with decreasing rotational speed (Figure 3.31). Similar results were obtained for other impeller designs.

For conventional centrifugal pumps the head and the flow rate depend on the rotational speed and the pressure coefficient independent of the rotational speed (eg., Pfleiderer [39]; Yedidiah [45]). Formula 3.10 describes the change in the flow rate as a function of a change in the rotational speed:

$$Q_2 = Q_1 \cdot \frac{n_2}{n_1} \tag{3.10}$$

with the initial flow rate Q_1 at the initial rotational speed n_1, and the new flow rate Q_2 for the new rotational speed n_2.
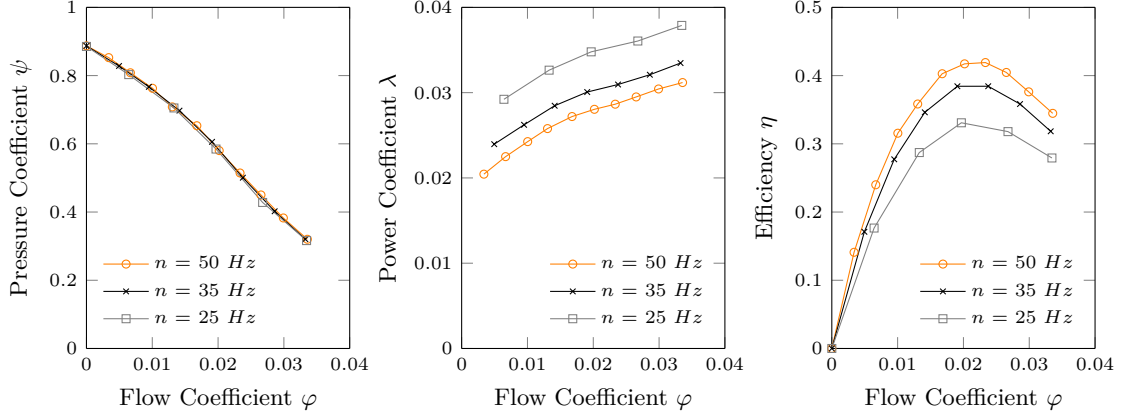
Figure 3.31: Influence of the rotational speed on the pressure coefficient (left), on the power coefficient (middle), and on the efficiency (right) for an impeller with 4 curved winglets.

Formula 3.11 describes the change in head as a function of a change in the rotational speed:

$$H_2 = H_1 \cdot \left(\frac{n_2}{n_1}\right)^2 \tag{3.11}$$

with the initial head H_1 at the initial rotational speed n_1, and the new head H_2 for the new rotational speed n_2.

To test if the suggested relationships of conventional centrifugal pumps also generalize to vortex pumps the flow rate and head for the rotational speeds of 35 Hz and 25 Hz were converted by means of Formula 3.10 and Formula 3.11 to a rotational speed of 50 Hz. The calculated characteristics were then compared to the measured curve at a rotational speed of 50 Hz. The left panel of Figure 3.32 shows the throttle curves of different speeds normalized to the BEP at a speed of 50 Hz. The results suggest that the head decreases with rotational speed decreasing.
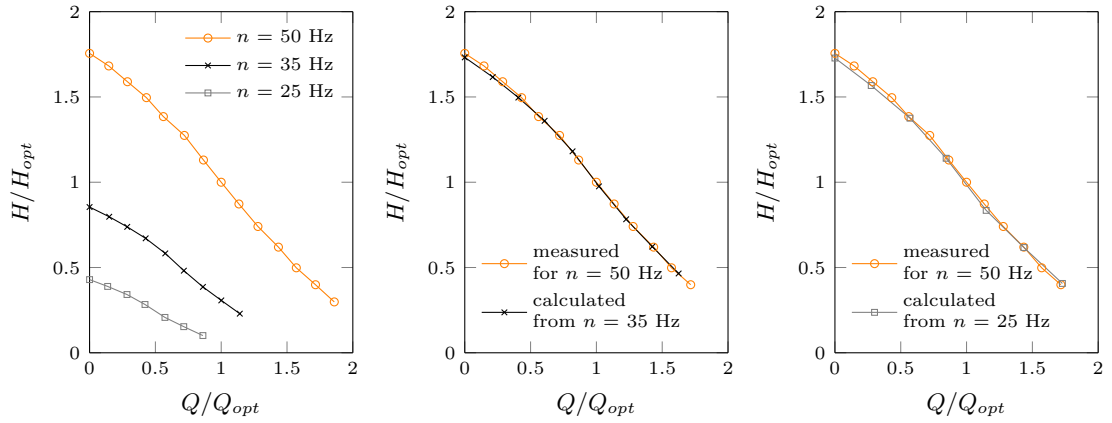
Figure 3.32: Influence of the the rotational speed n on the normalized throttle curve (left), the calculated throttle curve derived from the measured values of 35 Hz (middle), and the calculated throttle curve derived from the measured values of 25 Hz (right; all impellers had 4 curved blades and winglets straight blades).

The middle panel of Figure 3.32 compares the *measured* curve of 50 Hz to the *calculated* curve of 50 Hz, derived from the measured values of 35 Hz. The right panel of Figure 3.32 does the same for the measured values of 25 Hz. Both calculated curves are in good agreement with the measured curve suggesting that relation of rotational speed to flow rate and head, as known from conventional centrifugal pumps, can be generalized to vortex pumps.

Overall, increasing the rotational speed is preferable as it increase the efficiency.

3.3 Comparison of Impellers

To identify the optimal impeller design this section sums up the insights, which have been gained so far. The goal is to identify the most promising impeller design in terms of highest pressure coefficient and efficiency. Figure 3.33 depicts the pressure coefficient (top left), the power coefficient (top right) and efficiency (bottom right) for different flow coefficients of the most influencing parameter changes in the impeller designs: Increasing the outlet angle and adding winglets. Hence, five impellers are compared from the study on the influence of blade outlet angle (cf. Figure 3.6) and the study of adding winglets (cf. Figure 3.15): An impeller with 8 blades and a blade outlet angle of $40°$; an impeller with 8 blades and a blade outlet angle of $90°$; an impeller with 8 blades and a blade outlet angle of $130°$; an impeller with 4 curved blades and $19°$ outlet angle; and an impellers with 4 curved winglets and $19°$ outlet angle. All impellers had a diameter of 240 mm and had equal blade depth.
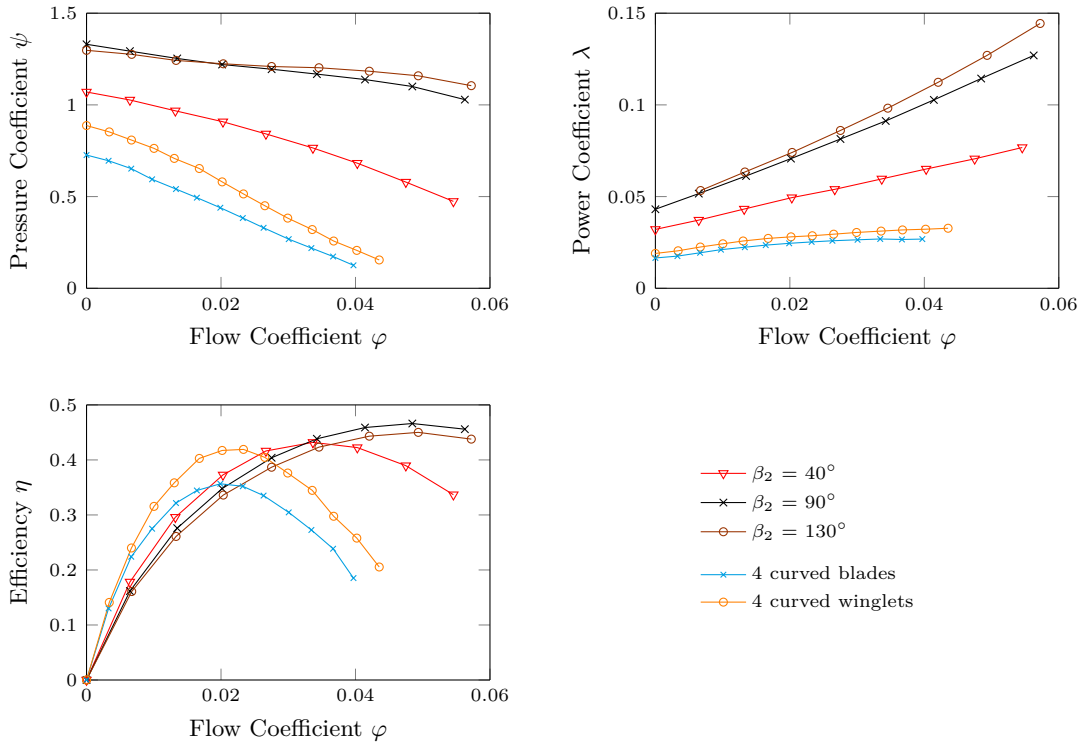

Figure 3.33: Influence of the changes in the parameters of impeller designs on the pressure coefficient (top left), on the power coefficient (top right) and on the efficiency (bottom left).

Figure 3.33 shows that the blade design significantly influences the characteristics, both in in the gradient of the pressure coefficient curve, the possible maxima, and in the position of the BEP. Interestingly, the impeller with 4 curved winglets and the impeller with 8 blades and an outlet angle of 40° reached an approximately equally high value of efficiency. However, the impeller with the 40° outlet angle had it at a higher flow coefficient and its pressure coefficient and power coefficient were significantly higher compared to the impeller with 4 curved winglets. In contrast, the impeller with 4 curved blades achieved lowest pressure coefficient and the lowest efficiency. Hence, the impeller with 4 curved blades seems inferior to all other designs. Overall, the relatively simple design of the impeller with 8 straight blades reached the highest pressure coefficients and the greatest efficiency — however, it also consumed most power.

In a next step, the design of the impeller with 8 straight blades was compared to the impeller with 4 curved winglets. To this end, the diameter of the impeller with 8 straight blades was trimmed to 175 mm. In this way, the head curves of the impeller with 8 straight blades intersected at the BEP of the impeller with 4 curved winglets. Figure 3.34 shows a scaled comparison of the two impellers.

Figure 3.35 shows the resulting characteristics, normalized to the BEP values of the impeller with 4 curved winglets. Compared to the impeller with 4 curved winglets, the impeller with 8 straight blades had a flatter course of the head and it is somewhat less efficient. Both impellers reach similar values of flow rate at their BEP. The impeller with 8 straight blades consumes less power in part load operation but more in overload operation. Overall, the design with 8

4 curved winglets
8 straight blades

Figure 3.34: Impeller with winglets and a diameter of 240 mm (left) and impeller with 8 straight blades and a diameter of 175 mm (right).
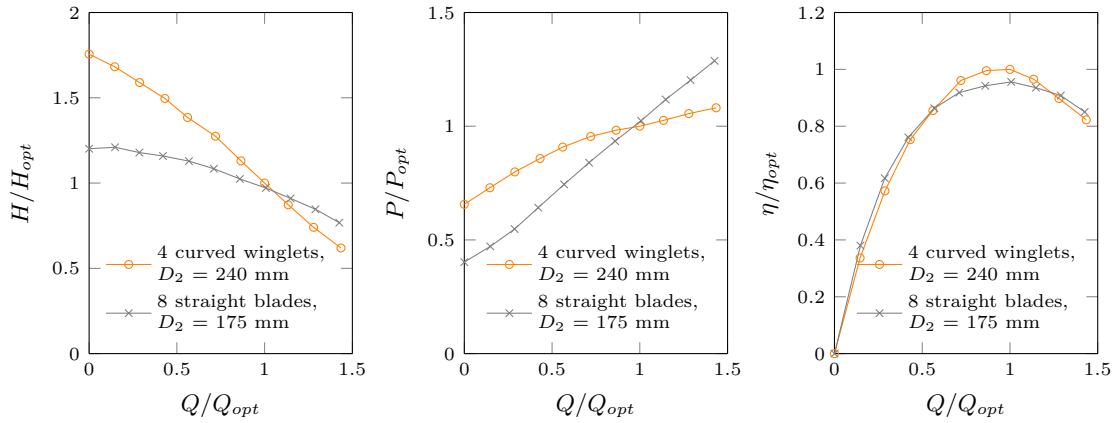

Figure 3.35: Comparison of an impeller with 4 curved winglets of diameter 240 mm to an impeller of 8 straight blades and diameter of 175 mm on the head (left), on the power consumption (middle) and on the efficiency (right).

straight blades and a reduced diameter had different characteristic of pressure coefficient and power coefficient compared to impeller with 4 curved winglets, but its design is simpler.

Taken together, the comparisons of the impeller characteristics, as shown in Figure 3.33 and Figure 3.35, point at an important trade-off when designing impellers for vortex pump: If the goal is to maximize efficiency straight, even forward curved, blades seem preferable. However, straight and forward curved blades yield a flat characteristic curve and consume much power. If the goal is to obtain a steep characteristic of pressure coefficient the blade outlet angle should be small ($< 90°$). Smaller blade outlet angles require less power but they are also less efficient. Adding winglets can be a powerful tool to improve the characteristic of an impeller in terms of achieving more pressure and greater efficiency without consuming much more power. At the same time, the characteristic curve becomes steeper. However, adding winglets could have a negative impact on the clogging behavior.

3.4   Codier Diagram

It is of interest whether the tested impellers of the vortex pump can be represented via the Cordier diagram as this is unknown yet. The Cordier diagram is a widely used tool for determining the optimal design of diverse fluid flow machines such as conventional centrifugal pumps, water turbines and fans. If impellers of the vortex pump can be represented via the Cordier diagram, this could be used for the design process of vortex pump impellers and further indicates that a vortex pump operation principle is similar to a conventional centrifugal pump.

The Cordier diagram plots the dimensionless speed number σ over the dimensionless diameter number δ. Close-to-optimal values of well-established fluid flow machines, such as centrifugal pumps, fans and turbines, lie on or close to the Cordier line. Thus the Cordier line represents the data of speed number and diameter number of existing machines with high efficiency.

The speed number σ is defined as (Formula 3.12):

$$\sigma = \frac{\varphi^{1/2}}{\psi^{3/4}} \tag{3.12}$$

with φ as the flow coefficient and ψ as the pressure coefficient.

The diameter number is defined as (Formula 3.13):

$$\delta = \frac{\psi^{1/4}}{\varphi^{1/2}} \tag{3.13}$$

with φ as the flow coefficient and ψ as the pressure coefficient.

At the beginning of a design process, the Cordier diagram is used to determine the principle design of the machine in terms of radial, diagonal or axial design. The speed number is calculated and the Cordier diagram used to define the diameter number to meet the best design of a fluid flow machine in terms of efficiency.

It has not yet been tested to what extend vortex pumps are on the Cordier line and thus represent good design practices. Figure 3.36 plot selected impellers of the same diameters (240 mm), but different in characteristics and efficiency on the Cordier diagram (adapted from Cordier [46]). It can be seen that all the selected impellers cluster at the Cordier line. Yet, impellers with higher efficiency tend to be closer to the Cordier line (e.g., the impeller with 8 straight blades) than impeller designs with less efficiency (e.g., the impeller with 8 blades and outlet angle of 40°). This tendency suggests that the Cordier diagram can be used for vortex pumps and to identify the optimal impeller design of a vortex pump.
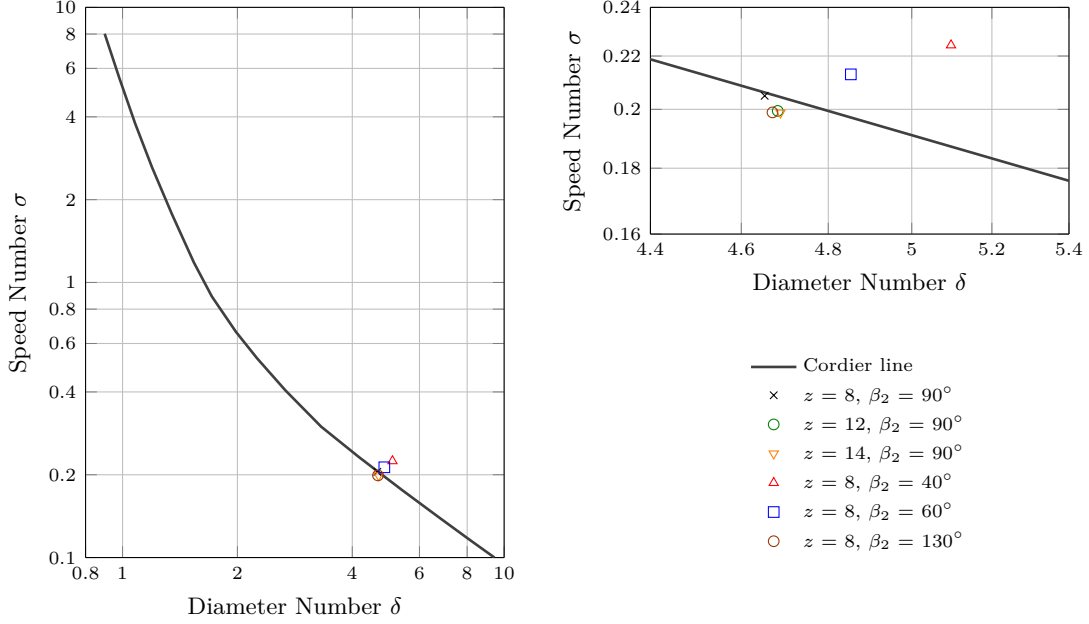
Figure 3.36: Cordier digram (adapted from Cordier [46]) with selected impellers of the tests (left) and zoomed illustration of the Cordier diagram with selected impellers of the tests (top right).

3.5 Interim Summery

This chapter analyzed the influence of different impeller designs of a vortex pump on its characteristic curves. To this end, a vortex pump with an open design (see Chapter 2.1) and a simplified casing was built. All tests were restricted to clear water operation.

In several tests typical variations in parameters, such as variation in the impeller diameter, the blade number or the blade outlet angle, and alternative impeller designs, such as added winglets or added splitter blades were tested and the resulting characteristics measured. Overall, it could be shown that the blade outlet angle β_2 had one of the greatest influence on the characteristics: Impellers with straight blades ($= 90°$) or forward curved blades ($> 90°$) were superior to backward curved blades ($< 90°$) in terms of pressure coefficients and efficiency. Yet, high blade outlet angles ($\geq 90°$) also led to significantly greater power consumption. In these tests, a blade outlet angle of $90°$ reached highest efficiency. For impellers of conventional centrifugal pumps a backward curved blade with an outlet angle between $20°$ and $40°$ is recommended if the goal is to reach highest efficiency [39]. However, for conventional centrifugal pumps with semi-open impellers it is recommended to choose high blade outlet angles, even forward curved blades ($\geq 90°$), to reach high efficiency — although their gap clearances are smaller than that of vortex pumps.

Increasing the blade outlet angle also flattened the curve of the pressure coefficient. The relation between blade outlet angle and pressure coefficient as the blade outlet angle influences the slope of pressure coefficient curve is also known from of conventional centrifugal pumps [39]. This indicates that the operation principle of a vortex pump is similar to a conventional centrifugal pump, more precisely a conventional centrifugal pump with semi-open impeller.

The studies in this chapter furthermore suggested that the outer radius of the impeller strongly affected the characteristics. The impact of the outer radius was demonstrated by multiple tests, including tests that varied the inlet diameter, that added splitter blades, and that

designs to strengthen or to weaken the vortex formation.

Overall, the challenge to design optimal vortex pump impellers seems the trade-off between reaching high efficiency at low power consumption. Increasing the blade number, increasing the blade outlet angle, and increasing the impeller diameter increases the pressure coefficient and the efficiency. Further, adding winglets and adding splitter blades improves the characteristics in terms of higher pressure coefficients and efficiencies. A semi-open impeller design is preferable over a pan-like impeller design and the results suggest that the less the vortex formation is supported the higher are the pressure coefficients and efficiencies.

Chapter 4

A Design Approach for Vortex Pump Impellers

In 1968, the Swiss author Rütschi [4] assessed how various geometry parameters influenced the performance of a vortex pump. He thereby suggested that the characteristic curves of vortex pumps could be calculated. These calculations extended the work by Pfleiderer [39] on conventional centrifugal pumps and a radial impeller. Rütschi thereby adapted the slip factor, the hydraulic efficiency, and neglected shock losses. Overall, Rütschi's calculations have been shown to provide a good fit to the measures of an impeller with straight blades [4]. However, it is unclear to what degree the approach is suitable for impellers with non-straight blades.

To this end, this chapter tests if Rütschi's approach can be used to predict the throttle curve of a vortex pump with impellers that are dissimilarly designed to those of Rütschi [4]. A positive answer would suggest that Pfleiderer's [39] design approach to conventional centrifugal pump impellers is generalizable to various vortex pump impellers. This would allow designing vortex pump impellers thereby.

Therefore, this chapter presents the approach by Pfleiderer and its extension by Rütschi to calculate the throttle curve for a vortex pump impeller. The approach is tested for different impeller designs with curved blades, and to gain further insights on the influence of impeller design parameters. Based on the results, a design approach for vortex pump impellers is presented and proved by designing an impeller with pre-defined throttle curve.

4.1 Calculating the Throttle Curve

4.1.1 The Approach by Pfleiderer and its Extension by Rütschi

To calculate the throttle curve Pfleiderer [39] first calculated the head of an impeller with an *infinite* number of blades, $H_{th,\infty,x}$ (Formula 4.1):

$$H_{th,\infty,x} = \frac{u_2}{2} \cdot \frac{u_2 \cdot \cot(\beta_2) \cdot Q_x}{\pi \cdot D_2 \cdot b_2} \tag{4.1}$$

with u_2 as the circumferential speed at the outer diameter, β_2 as the blade outlet angle, Q_x as the flow rate, D_2 as the impeller diameter, and b_2 as the impeller width.

To incorporate the deflected flow on the impeller blades, the head of a conventional centrifugal

pump with an impeller of *finite* number of blade $H_{th,x}$ can be calculated to (Formula 4.2):

$$H_{th,x} = \frac{1}{1+p} \cdot \frac{u_2}{g} \cdot \frac{u_2 - Q_x \cdot \cot(\beta_2)}{\pi \cdot D_2 \cdot b_2} \qquad (4.2)$$

with u_2 as the circumferential speed at the outer diameter, Q_x the flow rate, β_2 as the blade outlet angle, D_2 as the impeller diameter, b_2 as the impeller width, and p as the slip factor. The slip factor p accounts for losses, such as the losses from a reduced deflection at the end of the blades. For a radial impeller the slip factor can be calculated as (Formula 4.3):

$$p = 2 \cdot \frac{\psi'}{z} \cdot \frac{1}{1 - (r_1/r_2)^2} \qquad (4.3)$$

with ψ' as experienced based factor which depends on the impeller design and type of guide device, z as the blade number, r_1 as the radius of the impeller inlet, and r_2 as the radius of the impeller outlet.

The value ψ' for a radial impeller adapted Pfleiderer as (Formula 4.4).

$$\psi' = \kappa \cdot \frac{1 + \beta_2}{60°} \qquad (4.4)$$

with κ as experienced based factor depending on the design of guide device respectively casing, and β_2 as the blade outlet angle. For example, Pfleiderer recommended κ to be between 0.65 to 0.85 for a spiral casing and between 0.85 to 1.0 for a smooth ring casing.

To incorporate hydraulic losses, the friction parabola $Z_{h,x}$ must be determined. The friction parabola has its low point in the origin of the flow rate and increases with the flow rate. The friction parabola $Z_{h,x}$ can be calculated as (Formula 4.5):

$$Z_{h,x} = (1 - \eta_{hyd}) \cdot H_{th,x} \cdot \left(\frac{Q_x}{Q_{sf}}\right)^2 \qquad (4.5)$$

with η_{hyd} as the hydraulic efficiency, $H_{th,x}$ as the calculated head for an impeller with finite number of blades, Q_x as the flow rate, and Q_{sf} as the flow rate without shock losses.

Further, shock losses are accounted for by the parabola $Z_{s,x}$ which peaks at shock-free flow (i.e., the design point). The shock losses can be calculated as (Formula 4.6):

$$Z_{s,x} = \frac{\psi'}{2 \cdot g} \cdot \left(1 - \frac{Q_x}{Q_{sf}}\right)^2 \cdot \left(u_1^2 + \left(\frac{u_2}{1+p}\right)^2\right) \qquad (4.6)$$

with ψ' as experienced based factor (cf. Formula 4.4), Q_x as the the flow rate, Q_{sf} as the flow without shock losses, u_1 as the circumferential speed at the inner diameter, u_2 as the circumferential speed at the outer diameter, and p as the slip factor (cf. Formula 4.3).

The characteristic curve is the result of subtracting the friction parabola $Z_{h,x}$ and the parabola of shock losses $Z_{s,x}$ from the head of a centrifugal pump with an impeller of finite number of blade $H_{th,x}$ (Formula 4.7):

$$H_x = H_{th,x} - Z_{h,x} - Z_{s,x} \qquad (4.7)$$

with $H_{th,x}$ as the head for an impeller with finite number of blades $H_{th,x}$, $Z_{h,x}$ as the friction parabola, and $Z_{s,x}$ as the parabola of shock losses.

Rütschi [4] extended Pfleiderer's approach. He argued that the head of a vortex pump impeller with an *infinite* number of blades $H_{th,\infty,x}$ is identical to the head of a conventional centrifugal pump with an *infinite* number of blades (cf. Formula 4.1). The head of a vortex pump impeller

with a *finite* number of $H_{th,x}$ blades, however, can be calculated by means of Formula 4.2 when changing the slip factor p to (Formula 4.8):

$$p = 2 \cdot \frac{\psi'}{\sqrt{z}} \cdot \frac{1}{1 - (r_1/r_2)^2} \cdot k \tag{4.8}$$

with ψ' as experienced based factor, z as the number of blades, r_1 the radius of the impeller inlet and r_2 as the radius of the impeller outlet, and k as factor introduced by Rütschi. He recommended values of k between 0.28 and 0.30.

In other words, Rütschi argued that the slip factor for vortex pumps can be transformed into the slip factor of conventional centrifugal pumps by multiplying p with $\sqrt{z}/(k \cdot z)$.

The factor ψ' for vortex pumps is defined by Rütschi as (Formula 4.9):

$$\psi' = 0.6 \cdot \left(\frac{1 + \beta_2}{60°} \right) \tag{4.9}$$

with β_2 as the blade outlet angle. It is worth emphasizing that Rütschi thus defines the value of κ for vortex pumps with 0.6 similarly to Pfleiderer for bladed casings of conventional pumps.

Rütschi calculated the friction parabola $Z_{h,x}$ for vortex pumps similarly to that of conventional centrifugal pumps (cf. Formula 4.5). However, he also argued that the hydraulic efficiency of a vortex pump is only about 1/3 of the efficiency of conventional centrifugal pumps with a small gap clearance. It follows that the calculated hydraulic efficiency of vortex pump should be about 2/3 higher compared with the actual observations.

Furthermore, Rütschi claimed that shock losses in vortex pumps are marginal, due to the great distance between the impeller and the suction pipe. He also argued that the influence of the suction mouth is negligible in vortex pump impellers so that the blades can be pulled to the hub without a defined suction mouth. Accordingly, the parabola of shock losses $Z_{s,x}$ are ignored in the calculations for vortex pumps.

Overall, the characteristic curve of a vortex pump is thus the head for an impeller with a finite number of blades $H_{th,x}$ differentiated only by the friction losses $Z_{h,x}$ (Formula 4.10):

$$H_x = H_{th,x} - Z_{h,x} \tag{4.10}$$

4.2 Calculated Throttles Curves of a Vortex Pump

4.2.1 Methods

In his seminal investigation Rütschi also demonstrated a good fit of the calculated throttle curve to two measured throttle curves [4]. So far, it nonetheless remains unclear whether his approach can be generalized to impellers with different designs. To test the generalizability of Rütschi [4], the influences of the blade number, of the blade outlet angle, and of the impeller diameter on the throttle curves were measured and compared with the calculated throttle curves. The measurements were conducted with the test rig and vortex pump described in Chapter 3.

The influence of blade number z was evaluated by testing an impeller with either 8 straight blades, 12 straight blades or 14 straight blades. All impellers had a diameter of 240 mm. The influence of blade outlet angle β_2 was tested via blade outlet angles of 40°, 60°, 90°, and 130°. These impellers had again a diameter of 240 mm. The influence of impeller diameter D_2 — either 220 mm or 240 mm — was tested on behalf of two impellers for each diameter, one impeller had 8 straight blades, the other impeller had 12 straight blades.

4.2.2 Results

Figure 4.1 shows the calculated and the measured throttle curve for an impeller with 8 straight blades (left panel) and 12 straight blades (right panel). Due to the simplified design of the casing all calculations assumed that κ was equal to 1. Following Rütschi k was set to 0.3 for the calculations for the blade numbers. Figure 4.1. suggests a relative good fit between the calculated and the measured curves. The good fit seemed robust, that is irrespective of the number of blades. A limitation so far was that the calculations were developed for impellers with straight blades and the throttle curves were compared with impellers with straight bladed impellers.

To test the robustness of the calculations the influence of blade outlet angle was assessed. The blade outlet angle varied between 40° (Figure 4.2, left panel), 60° (right panel), 90° (Figure 4.3, left panel), and 130°. (Figure 4.4, right panel). All impellers differed only in their outlet angle. Otherwise, they were similar (e.g., in respect to impeller diameter, blade depth, blade number and tested rotational speed, etc.). Similar to the previous calculations $\kappa = 1$ was assumed. For k the values 0.7 (for blade outlet angle 40°), 0.5 (for 60°), 0.3 (for 90°), and 0.25 (for 130°) were assumed. Again, the calculated and the measured curves had a good fit. However, the k values differ from the proposed range of Rütschi (i.e., $k = 0.28 \ldots 0.30$). This suggests that the adaptation of slip factor by Rütschi is only an approximation and once again, as in the case of
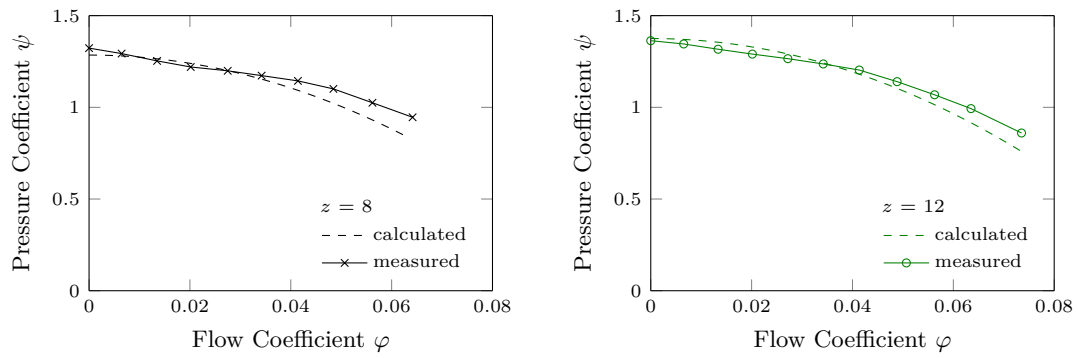

Figure 4.1: Comparison of the calculated with the measured throttle curves for impellers with 8 straight blades (left) and with 12 straight blades (right).
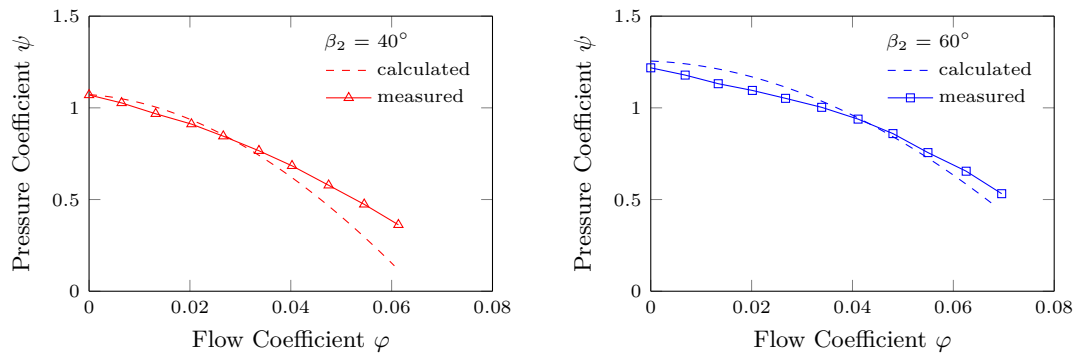

Figure 4.2: Comparison of the calculated with the measured throttle curve for impellers with a blade outlet angle of 40° (left) and with 60° (right).
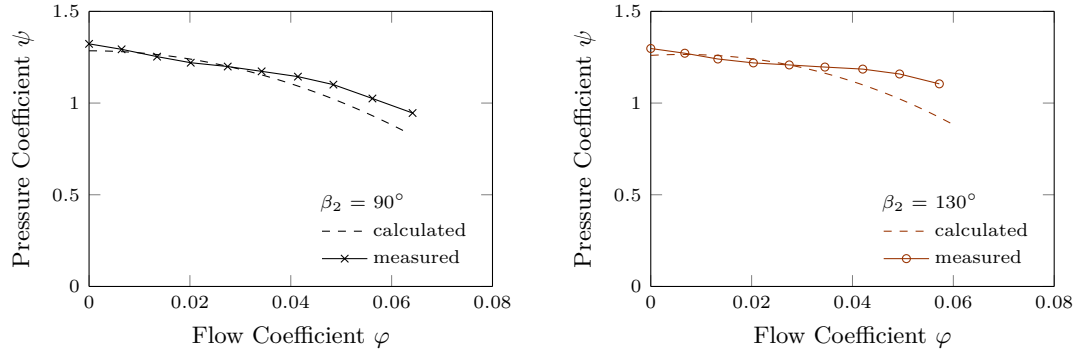
Figure 4.3: Comparison of the calculated with the measured throttle curves for impellers with a blade outlet angle of 90° (left) and with 130° (right).

conventional centrifugal pumps, experienced based factors are necessary for vortex pumps too.

Figure 4.4 depicts the calculated and the measured throttle curves for an impeller with 8 straight blades and a diameter of either 240 mm (left panel) or 220 mm (right panel). Again values of $\kappa = 1$ and $k = 0.3$ were assumed. The measured curved and the calculated curves had an overall good fit, irrespective of the diameter. Only the hydraulic losses at the 220 mm diameter were somewhat overestimated by the calculations (cf. Figure 4.4, right panel). Potentially, the trimming of the impeller itself caused this slight misfit: As a result of the trimming, the smaller impeller did not perfectly match the casing. Such mismatches are known to lead to efficiency losses in conventional centrifugal pumps (Yedidiah [45]). Comparable good fits were obtained for the diameters of 240 mm and 220 mm and an impeller with 12 straight blades (Figure 4.5) and similar assumptions (i.e., $\kappa = 1$; $k = 0.3$). Overall, the calculated throttle curves seemed to fit good the measured throttle curves independent of the impeller diameter.
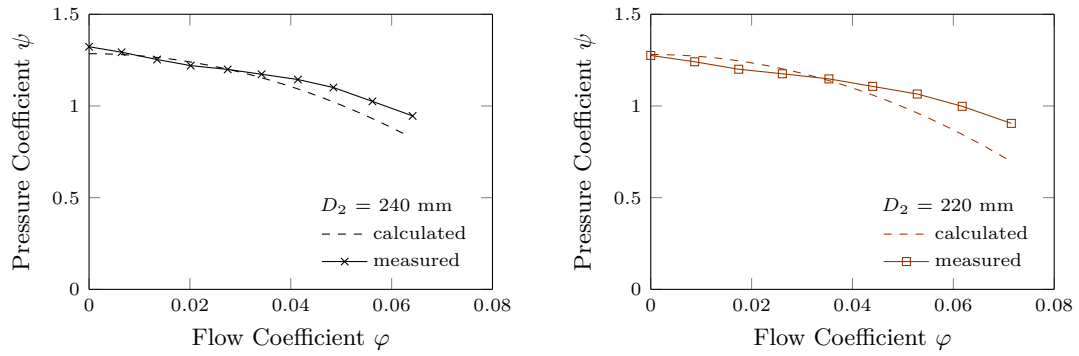

Figure 4.4: Comparison of the calculated with the measured throttle curves for an impeller with 8 straight blades and a diameter of 240 mm (left) and a diameter of 220 mm (right).
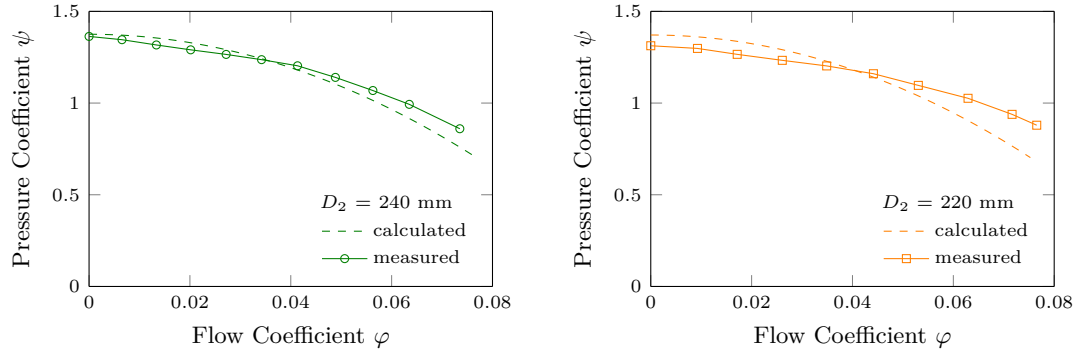
Figure 4.5: Comparison of the calculated with the measured throttle curves for an impeller with 12 straight blades and a diameter of 240 mm (left) and a diameter of 220 mm (right).

Table 4.1: Summary of the tested parameters on k and p for calculating the throttle curve.

Assessed Parameter	Compared Values	Defined Geometries	Factor k	Slip Factor p
Blade number z	$z = 8$ $z = 12$ $z = 14$	$D_2 = 240$ mm, $\beta_1=\beta_2= 90°$	0.3	0.557 0.454 0.421
Blade outlet angle β_2	$\beta_2= 40°$ $\beta_2= 60°$ $\beta_2= 90°$ $\beta_2= 130°$	z = 8, $D_2 = 240$ mm, $\beta_1=90°$	0.7 0.4 0.3 0.25	0.866 0.594 0.557 0.587
Impeller diameter D_2	$D_2 = 240$ mm $D_2 = 220$ mm	z = 8, $\beta_1=\beta_2= 90°$	0.3	0.557 0.562
	$D_2 = 240$ mm $D_2 = 220$ mm	z = 12, $\beta_1=\beta_2= 90°$	0.3	0.454 0.459

Table 4.1 lists the values of factor k and the resulting slip factors p on behalf of the assessed parameters, including their tested values, and their associated geometries. In sum, the results suggest the blade outlet angle is the most influential factor for k and therefore also for p.

4.3   A New Design Approach for Vortex Pumps

Overall the calculations by Rütschi provided a sufficient approximation to the actual throttle curves of vortex pumps under different parameter configurations. The exception was the blade outlet angle. On the basis of these insights a design approach for a vortex pump impellers was developed. To this end, a program code in Matlab was generated whose goal was to design a radial impeller with one-dimensional curved blades. This based on the design of radial impellers proposed by Pfleiderer by means of adapting the slip factor, the hydraulic efficiency, and neglecting shock losses as proposed by Rütschi.

It is worth noting already that the design method of Pfleiderer and its adaptation by Rütschi leads to several open question when it comes to designing vortex pumps. In contrast to conventional centrifugal pumps vortex pumps, for example, lack a front shroud; the definition of

the suction mouth is challenging but needed for the calculations; and some empirical factors must be ultimately chosen by the designer. Moreover, the enlarged side chamber gap of vortex pumps, which potentially causes hydraulic efficiency losses and the overall lower efficiency of vortex pumps must be taken into account (by adapting the slip factor). The gained knowledge from the previous tests proves to be informative here in terms of choosing the factor k depending on the blade outlet angle (cf. Table 4.1). Furthermore, calculating the radial impeller of conventional centrifugal pumps requires specifying the diameter of the impeller suction inlet. Tests on the influence of this parameter (Chapter 3.2.5) showed that the diameter can influence the head and the efficiency, however, such influence is negligible for small suction inlet diameters ($D_2/D_S = 2...3$). All further calculations therefore assumed a suction inlet diameter in the calculations, which was for the final design closed (i.e., the blades were pulled to the hub in the CAD-Model).

The Matlab code was calibrated to obtain the empirical factors for the subsequent calculations. To this end, an impeller of a defined geometry and a known throttle curve were calculated with the Matlab code until the geometry and throttle curve of this known impeller fitted the calculations.

Figure 4.6 illustrates the flow chart of the design process. First, the desired values of head H, flow rate Q, and rotational speed n must be defined by the user. Subsequently, the suction side of the impeller is calculated (according to the method of Pfleiderer). Then, the impeller pressure side is calculated (according to Rütschi's adaptations) and supplemented by the measured values for k which depend on the blade outlet angle. In a next step, it is tested whether the data of speed number and diameter number of the resulting vortex pump impeller lie on the Cordier line (cf. Chapter 3.3). If the values do not lie around the Cordier line insufficiently high values of efficiency are reached and the head H and the flow rate Q must be adjusted by the user. The design process is then repeated. If the impeller passes the test the program continues by calculating the throttle curve. Subsequent, it is assessed whether the calculated curve fits the desired throttle curve. If not, geometry values must be adapted by correcting the blade outlet angle β_2 and the impeller diameter D_2. If the calculated curve fits the desired throttle curve, the blade geometry is calculated pointwise and a CAD-model of the impeller is produced.

To ensure that the program yields valid results an impeller was designed and then tested against its predicted throttle curve. The desired characteristic curve should be steep and comparatively high efficiency should be achieved. The 4-bladed impeller with winglets (Figure 4.7, right panel) has a steep throttle curve and a comparatively high efficiency. As suggested in Chapter 3.2.6 the high efficiency is due to the winglets. It would be desirable, however, to obtain similar characteristic curves with a simpler design (without winglets).

The prior investigation on the blade outlet angle suggested that a high outlet angle up to straight or forward curved leads to high efficiency (cf. Chapter 3.2.2). However, high outlet angles were also associated with a flat throttle curve and increased power consumption (cf. Chapter 3.2.2). Thus, a compromise between a high blade outlet angle, blade number, and impeller diameter seems desirable to obtain a steep throttle curve at an acceptable efficiency. To this end, the blade outlet angle was set to 30° so that a desirable steep throttle curve could be achieved. Because factor k was unknown for a 30° angle the value was extrapolated and set to 0.9. The program suggested that an impeller with a diameter of 250 mm and 6 blades would be the best fit to the Cordier line. A hub diameter of 52 mm was chosen to achieve similar hub geometry as for the previously tested impellers. The calculations assumed a suction inlet diameter of 108 mm, which was closed in the CAD model by pulling the blades onto the hub. The inflow angle β_0 was 20°. The resulting impeller was trimmed to a diameter of 235 mm to fit the throttle curve of the BEP of the impeller with 4 curved winglets. The resulting impeller is illustrated in the right panel of Figure 4.7.
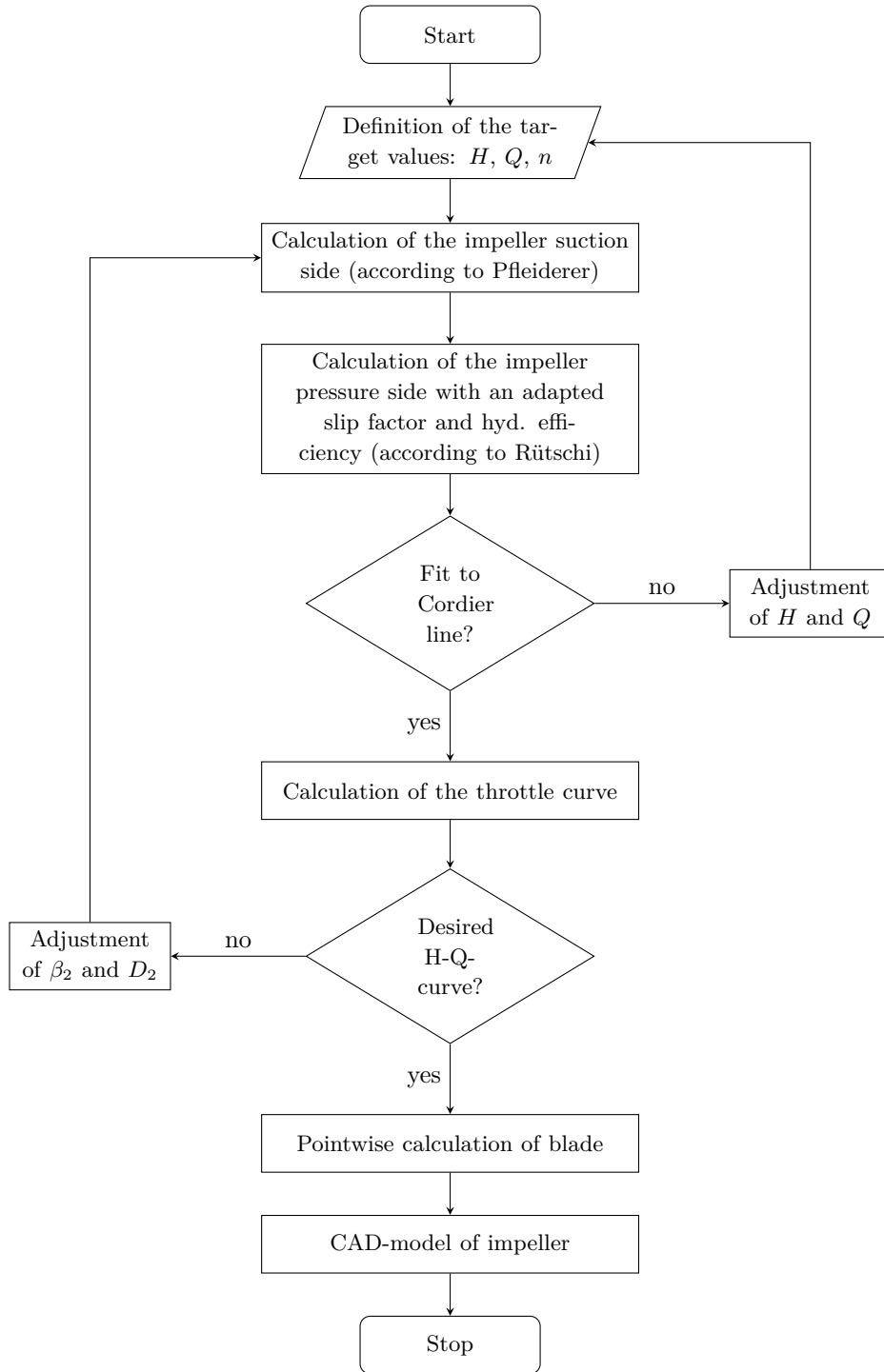
Figure 4.6: Flow chart for the design process of a vortex pump impeller.

4 curved winglets   New impeller

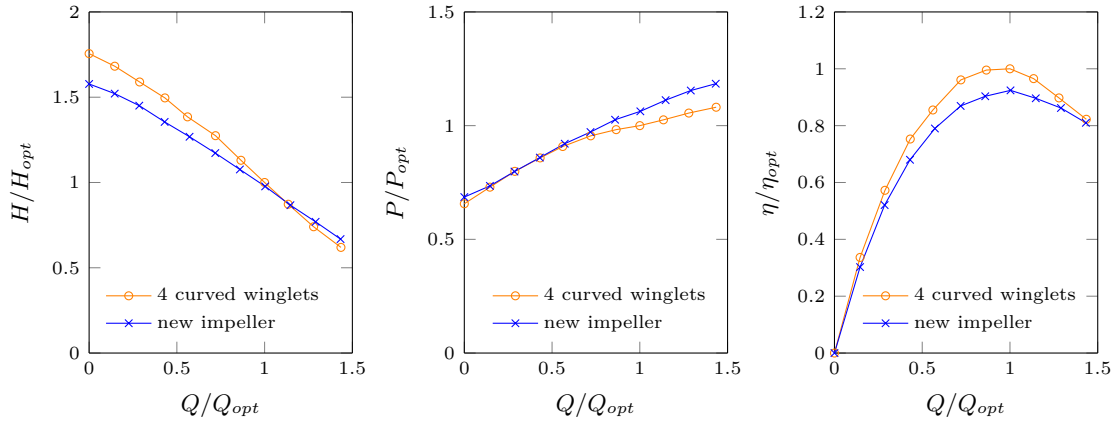Figure 4.7: Impeller with 4 curved winglets (left) and new impeller (right).

Figure 4.8: Characteristic curves of the impeller with 4 curved winglets compared with the new designed impeller with 6 blades: pressure coefficient (left), power coefficient (middle), and efficiency (right).

Figure 4.8 plots the characteristic curves of the impeller with 4 curved winglets and compares them to the newly designed impeller with 6 blades. For the sake of illustration, head, power consumption, efficiency, and flow rate of the impeller with 6 blades were normalized to the BEP values of the impeller with the 4 curved winglets. The throttle curves of both impellers were similar, although the throttle curve of the impeller with 6 blades was somewhat flatter than the throttle curve of the impeller with 4 curved winglets (Figure 4.8, left panel). The power consumption of the impellers at part load operation were comparable, however, the impeller with 6 blades consumed more power at overload operation (Figure 4.8, middle panel). The efficiency of the impeller with 4 curved was somewhat higher ($\eta_{BEP} = 42\%$) compared to the impeller with 6 blades ($\eta_{BEP} = 39\%$; Figure 4.8, right panel). Both impellers reached their BEP at comparable values of flow rate. Overall, the design of a new vortex pump impeller with a steep throttle curve and an acceptable efficiency was thus successful and the design method therefore validated.

4.4 Interim Summery

This chapter introduced, generalized and validated the approach of Rütschi [4] for calculating the throttle curve of a vortex pump. Rütschi's approach builds on Pfleiderer's [39] calculations for conventional centrifugal pumps with a radial impeller by means of adjusting the slip factor, the hydraulic efficiency and neglecting shock losses. Rütschi validated his method on impellers with straight blades. This chapter extended Rütschi's calculations by introducing new measurements

and calculations to assess how different impeller design parameters influence the fit of measured and calculated throttle curve. Variations in the blade number, the blade outlet angle, the impeller diameter were analyzed. It could be confirmed that Rütschi's approach was generalizable to vortex pumps impellers with curved blades. To this end, a new factor k was introduced by Rütschi into the slip factor calculations. The factor k could be adjusted to the specific impeller design. Overall, the blade outlet angle strongly influenced k. The extended approach was then used to design an impeller with a targeted, steep throttle curve as well as acceptable efficiency. The introduced measurements and calculations provide useful information for calculating the throttle curve of a vortex pump as well as for designing curved bladed impellers.

The fact that these calculations were ultimately derived from calculations for conventional centrifugal pumps suggests that the operational principles of both vortex pumps and conventional centrifugal pumps are largely similar. Nonetheless, it remains unclear why the approach of Rütschi provides a good match between the calculated and the measured throttle curves and the interpretation of the factor k remains ambiguous. Further research is needed to asses how other parameters, such as the blade inlet angle, would influence the fit between the calculations and the actual measurements. Also an improved approach to handle the suction mouth should become an integral part of such advanced calculations. A key advantage of the here-extended approach for designing a vortex pump impellers is its simplicity, which might find acceptances among the designers of centrifugal pumps.

Chapter 5

Flow Field in a Vortex Pump

This chapter investigates the relation between the impeller design and the flow field in a vortex pump. To this end, a series of Particle Image Velocimetry (PIV) measurements were conducted to assess the flow field of different impeller designs. Variations in the impeller designs include the blade number, the blade outlet angle, the adding of winglets, and the operation point.

5.1 Methods

5.1.1 Test Setup

PIV measurements are an optical method to visualize the flow field in fluids by velocity vectors. To this end, a fluid is premixed with particles, called seeding material. A high speed camera then takes a series of images of the fluid in short time intervals ($>$ 100 ns). In this way, individual particles can be traced and the speed and the direction of particles can be estimated. As a result, PIV allows calculating the velocity vectors of the flow field in a fluid.

For the following tests Figure 5.1 schematically illustrates the PIV test setup that was used to investigate the flow in a vortex pump with different impeller designs. Table 5.1 lists some of the specifications of the specific PIV equipment.
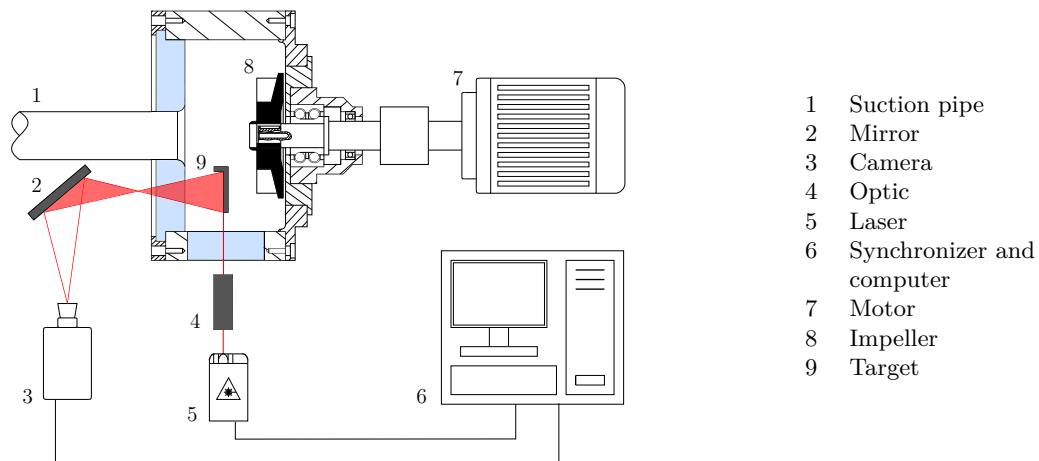

1	Suction pipe
2	Mirror
3	Camera
4	Optic
5	Laser
6	Synchronizer and computer
7	Motor
8	Impeller
9	Target

Figure 5.1: Schematic illustration of the PIV setup.

Table 5.1: PIV equipment used for the measurements.

Equipment	Product Description of Respective Manufacturer
Laser	Solo PIV. Nd: YAG Laser Systems, Co. New Wave Research
Optic	LS Mini Light Sheet Optics, Co. Intelligent Laser Applications GmbH
Camera	sensicam qu double shutter cooled digital 12bit CCD camera system, Co. Intelligent Laser Application GmbH
Seeding material	Iriodin 100 Silver Pearl 1.04670.1000

Obtaining precise images of the particles in a defined plane requires good illumination. Hence, a double pulse laser was used, which could be focused on a sufficiently thin light section. To focus the laser a light-section optical system was used referred to as optics. Due to spatial limitations a mirror was placed in front of the camera so that the images were perpendicular to the illuminated plane. A synchronizer ensured that the images recorded by the camera, the light pulse, and the intensity of the laser were exactly tuned. The camera was calibrated before the test began. To focus the camera a defined geometry, called target, was precisely placed in the plane. This procedure ensured that the images were sufficiently sharp to trace individual particles for calculating the velocity vectors. After focusing the camera the target was removed.

The commercial software PIVView2C processed the raw images. The software traces the particles to evaluate their movement. The flow field was calculated by means of image filters and correlation calculations. A window size of 32 px to 32 px sampled the images with an overlap of 50% of the window size. The correlation mode was set to the standard Fast Fourier Transformation correlation and filtering was set to Nyquist frequency. A multi-grid interrogation and a Whittaker reconstruction fitted sub-pixel peaks. Particles whose presumably movement exceeded a displacement difference of 5 px were defined as outliers and subsequently removed from the calculations.

The left panel of Figure 5.2 depicts the position of the measured plane in the vortex pump. The plane was positioned in between the front of the casing and the impeller. The right panel of Figure 5.2 exemplifies the measured flow field for an impeller with an outlet angle of 60°.
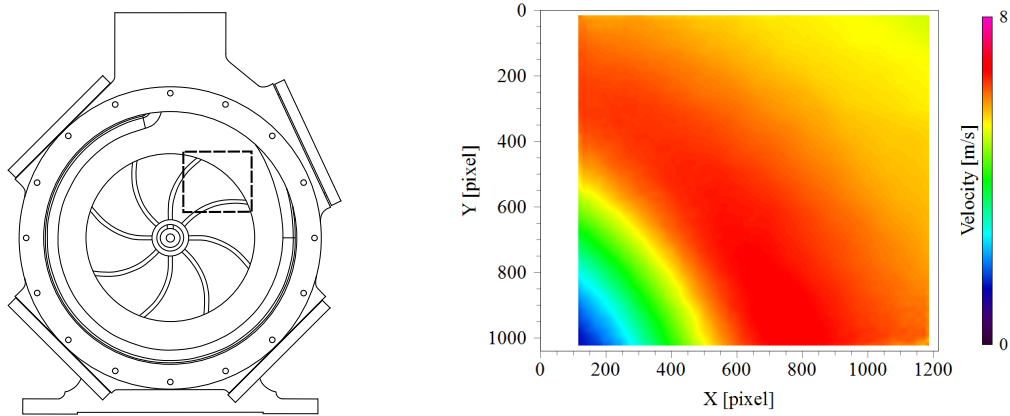

Figure 5.2: Schematic illustration of the position of the measured plane in the vortex pump (left), and an example of the post-processed PIV image of the flow field (right; example taken from the impeller with a 60° outlet angle).

5.1.2 Parameters under Investigation

The assessed parameters were: the blade number, the blade outlet angle, and the adding of winglets. Furthermore, the influence of the operation point on the flow field was studied by comparing the flow field at the BEP operation ($\varphi = $ BEP) to the flow field at shut-off conditions ($\varphi = 0$). Table 5.2 lists the assessed parameters, the tested values, and the geometries of the respective impellers. Appendix Table C1 provides more details on the operation data underlying the tests.

Table 5.2: Summary of the assessed parameters for measuring the flow fields in a vortex pump.

Assessed Parameter	Compared Values	Defined Geometries
Blade number z	$z = 8$ $z = 12$	$D_2 = 200$ mm, $\beta_1 = \beta_2 = 90°$
Blade outlet angle β_2	$\beta_2 = 40°$ $\beta_2 = 60°$ $\beta_2 = 130°$	z = 8, $D_2 = 240$ mm, $\beta_1 = 90°$
Adding winglets	without winglets with winglets	z = 4, $D_2 = 240$ mm, $\beta_1 = 44°$, $\beta_2 = 19°$
Operation point	operation at BEP operation at shut-off conditions	all of the above defined geometries

To compare the different impellers a radius at the center of the impeller was defined for all measurements. This radius is always presented as the dimensionless variable r/r_2 by dividing the radius r by the outer radius r_2 of the respective impeller. Thus, the radius of the impeller is defined as $r/r_2 = 1$. The velocity vectors were divided into two components: The tangential velocity and the radial velocity. The tangential velocity component v_t is normalized to the circumferential velocity u_2 of the respective impeller resulting in the dimensionless value v_t/u_2. Similarly, the radial velocity component v_r is normalized to the circumferential velocity u_2 of the respective impeller proceeding the dimensionless value v_r/u_2.

Additionally, the vorticity ω was calculated with the software PIVView2C. The vorticity helps to describe the motion of the vortex and it is a useful tool for comparing a measured flow to a theoretical vortex models (cf. Chapter 2.1). Unlike the other measures, the vorticity ω was not normalized.

5.2 Results

5.2.1 Blade Number

To investigate the influence of the blade number on the flow field an impeller with 8 straight blades was compared to an impeller with 12 straight blades. In all other regards, the impellers were similar. Furthermore, both impellers were studied with regard to their BEP operation and their operation at shut-off conditions. The top left panel of Figure 5.3 shows the normalized tangential velocity over the radius for both impellers at BEP and at shut-off conditions. For small radii the tangential velocity increased with the radius increasing. Once a maximum was reached a transition took place and the tangential velocity decreases with increasing radius. For BEP operation, both impellers reached their maximum value at a comparable value of the radius, at around 0.8 and therefore in the inner region of the impeller. The peaks for the tangential
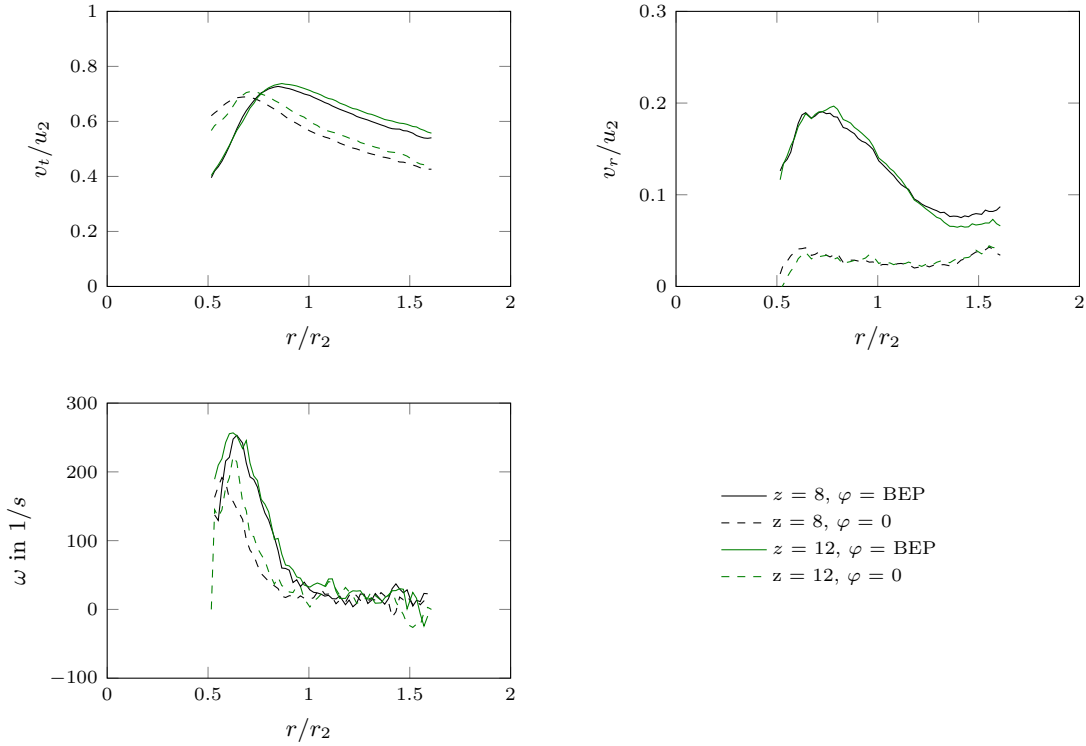
Figure 5.3: Influence of the blade number on the tangential velocity (top left), the radial velocity (top right), and the vorticity (bottom left) for BEP operation ($\varphi = \text{BEP}$) and for operation at shut-off conditions ($\varphi = 0$).

velocity at shut-off operation were overall lower and occurred at smaller normalized radii than they did for BEP operation. Overall, the impeller with 12 straight blades reached somewhat higher values of tangential velocity than the impeller with 8 straight blades did. This was true for both operation conditions.

The top right panel of Figure 5.3 shows the course of the radial velocity component as a function of the radius. Overall, the values of the radial velocity were smaller than the values of the tangential velocities for both of the tested impellers and for both operation conditions suggesting that the flow was mainly rotating in the casing. The curves of both impellers clustered together at each of the operation conditions. Similar to the tangential velocities, the radial velocity for BEP operation increased for small radii until a maximum was reached. From this radius onwards the speed decreased. For operation at shut-off conditions the radial velocity component was small, even close to zero. This could be due to the pump operating fully throttled so that the flow could not radially exit the pressure pipe.

The bottom left panel of Figure 5.3 depicts the vorticity over the radius at BEP operation and shut-off conditions. With increasing radius the courses of the vorticity of all impellers increased, peaked, declined and started fluctuating. The courses of the vorticity for operation shut-off condition were lower than at BEP. This was true for both impellers.

Overall, the increase of blade number — from 8 to 12 straight blades — led to a slight increase of the tangential velocity and to slight increase of the vorticity.

5.2.2 Blade Outlet Angle

To evaluate the influence of the blade outlet angle three impellers were tested. The impellers had outlet angles of 40°, 60°, or 130°. The top left panel of Figure 5.4 shows that the tangential velocities increased with increasing blade outlet angle. This was true for both operation conditions. As for the variation in the blade number, the courses of the tangential velocities of all impellers had a reverse U-shaped trend. The top right panel of Figure 5.4 depicts the radial velocities. Again, the courses of radial velocities for BEP operation were a reverse U-shaped. And, again, the radial velocities for operation at shut-off conditions were small, close to zero. All values of the radial velocity were smaller than the values of the tangential velocities for the respective radius and impeller. The bottom left panel of Figure 5.4 plots the vorticity. As for the variation in the blade number, the courses of all impellers and operation points increase, peak, and then decline with increasing radius until they start fluctuating. Again, the vorticity at shut-off operation were lower than at BEP operation.

A comparison of the performance at BEP to the performance at shut-off condition reveals an interesting fact that the maxima of the tangential velocities seem to depend on the operation point. Figure 5.5 shows the tangential velocity for BEP operation and at shut-off conditions for the impellers with various blade outlet angles. The left panel of Figure 5.5 suggests that the tangential velocity for operation at shut-off conditions was higher than it was for BEP operation for an impeller with a blade outlet angle of 40°. Increasing the blade outlet angle to 60° (middle
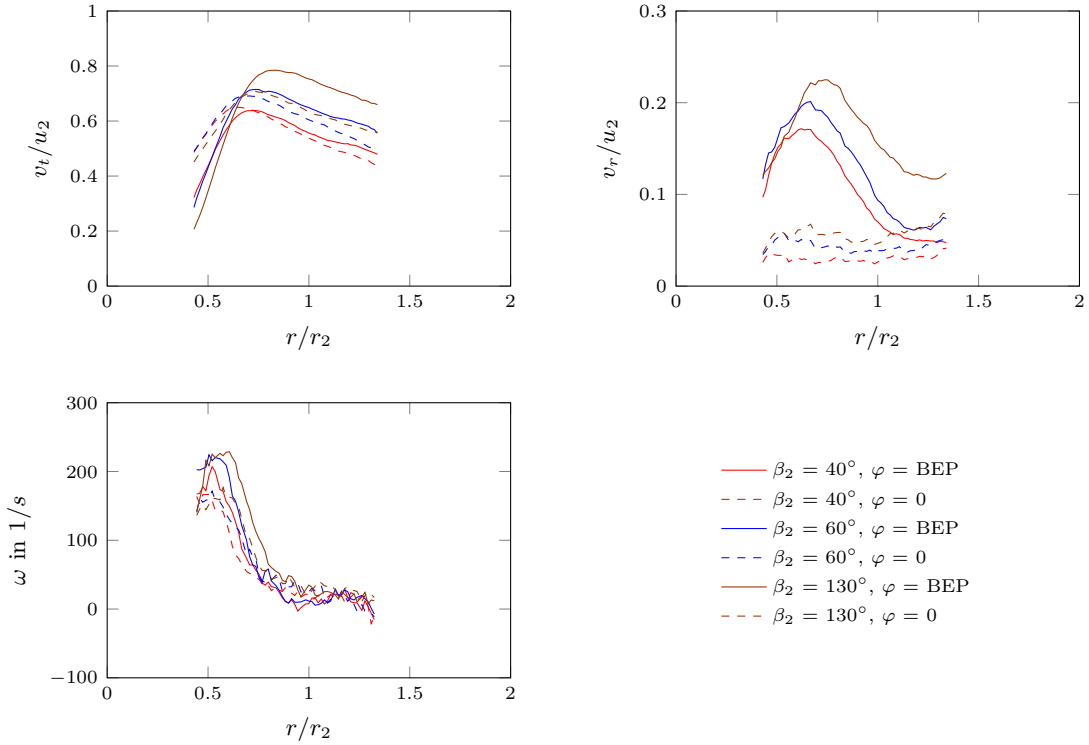

Figure 5.4: Influence of the blade outlet angle on the tangential velocity (top left), the radial velocity (top right), and the vorticity (bottom left) for BEP operation ($\varphi = $ BEP) and for operation at shut-off conditions ($\varphi = 0$).
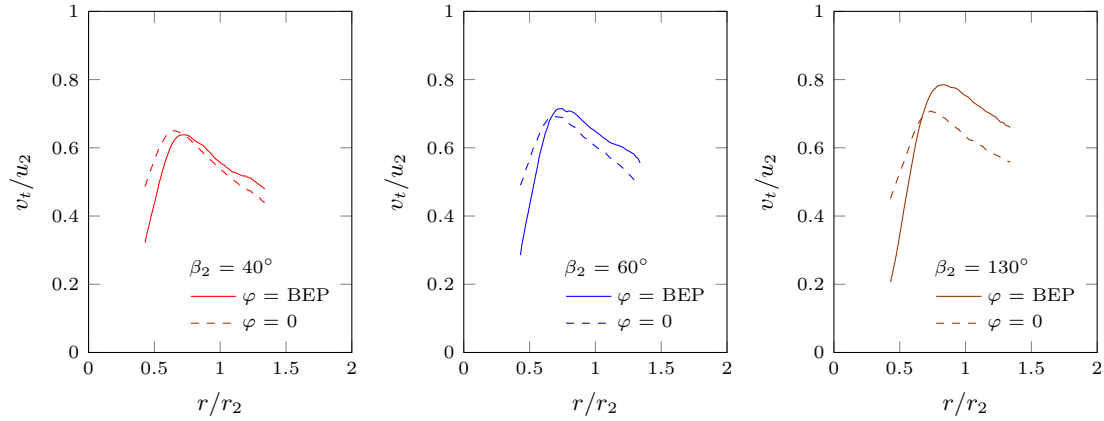
Figure 5.5: Influence of the operation point on the tangential velocity over the normalized radius for a blade outlet angle of 40° (left), 60° (middle), and 130° (right).

panel) and 130° (right panel) led to greater tangential velocities for BEP operation than for operation at shut-off conditions. This means, the tangential velocity values of the operation point depend on the blade outlet angle. However, for all impellers the radial velocity and the vorticity were higher for BEP operation than for operation at shut-off conditions, irrespective of the blade outlet angle. Overall, increasing the blade outlet angle increased the tangential velocity, the radial velocity, and the vorticity.

5.2.3 Winglets

The influence of winglets was evaluated by comparing impellers with 4 curved blades that either had or had not additional winglets. The findings are qualitatively similar to the prior studies. The left panel of Figure 5.6 shows that the tangential velocity was higher for the impeller with winglets compared to the impeller without winglets. The courses of the tangential velocity followed again a reversed U-shaped trend. For both impellers, the peaks of the tangential velocity at shut-off operation were higher and occurred at smaller radii than they did for BEP operation. This might be due to the small outlet angle of 19° of both impellers, suggesting that the tangential velocity values of the operation point depend on the blade outlet angle as for the variation in the blade outlet angle and the impeller with 40° outlet angle.

The top right panel of Figure 5.6 depicts the radial velocity over the radius. The results for BEP operation suggest that for small radii the impeller with winglets reached greater radial velocities than the impeller without winglets did. At a radius of about 0.7 the trends were reversed and the impeller without winglets reached higher velocities. For both impellers, the radial velocity for BEP operation increased in velocity for small radii until a maximum was reached. For operation at shut-off conditions the radial velocity component was small, and it fluctuated close to zero. Again, the radial velocity were smaller than the values of the tangential velocities for the respective radius and impeller.

The bottom left panel of Figure 5.6 plots the course of the vorticity over the radius. As in the other parameter studies, the courses increased, peaked, declined, and then started fluctuating. Overall, the impeller with winglets had higher values of vorticity than the impeller without winglets. BEP operation led to a maximum of vorticity for the impeller without winglets. In contrast, operation at shut-off conditions led to a maximum of vorticity for the impeller with
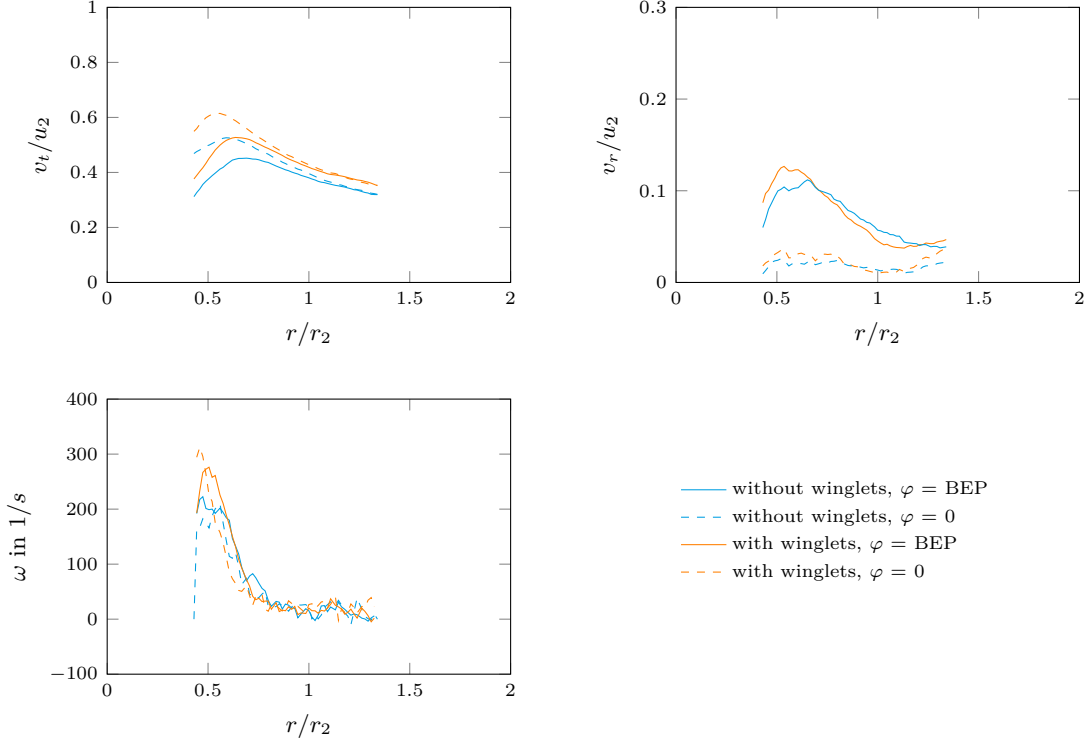
Figure 5.6: Influence of adding winglets on the tangential velocity (top left), the radial velocity (top right), and the vorticity (bottom left) for BEP operation ($\varphi = $ BEP) and for operation at shut-off conditions ($\varphi = 0$).

winglets.

Overall, adding winglets increased the tangential velocity, the radial velocity, and the vorticity.

5.3 Comparison of All Impellers

Figure 5.7 depicts the tangential velocity (top left), the radial velocity (top right), and the vorticity (bottom left) for BEP operation of all tested impellers. Figure 5.8 does the same for operation at shut-off conditions. The comparison of all impellers clearly shows that the different impeller designs led to different tangential velocities (Figure 5.7, top left; Figure 5.8, top left). For all impellers, the tangential velocity increased from small radii up to a maximum and then declined thereafter. Yet, the exact position of the peaks depended on the impeller design (cf. Appendix Figure C7 for an illustration of the not-normalized radius of impellers). Interestingly, the courses of the tangential velocity of all impellers resemble that of a theoretical vortex, such as the Hamel-Oseen vortex (cf. Chapter 2.1).

For BEP operation, the courses of radial velocity of all impellers increased, peaked, and then declined with increasing radius (Figure 5.7, top right). The impeller, which reached the highest tangential velocities also reached the highest radial velocities for BEP operation For operation at shut-off conditions, the radial velocity overall remained small and fluctuated over the radius (Figure 5.8, top right). Again, the courses of the radial velocity of all impellers at BEP operation were similar to the courses of radial velocity of a theoretical vortex, such as the Hamel-Oseen
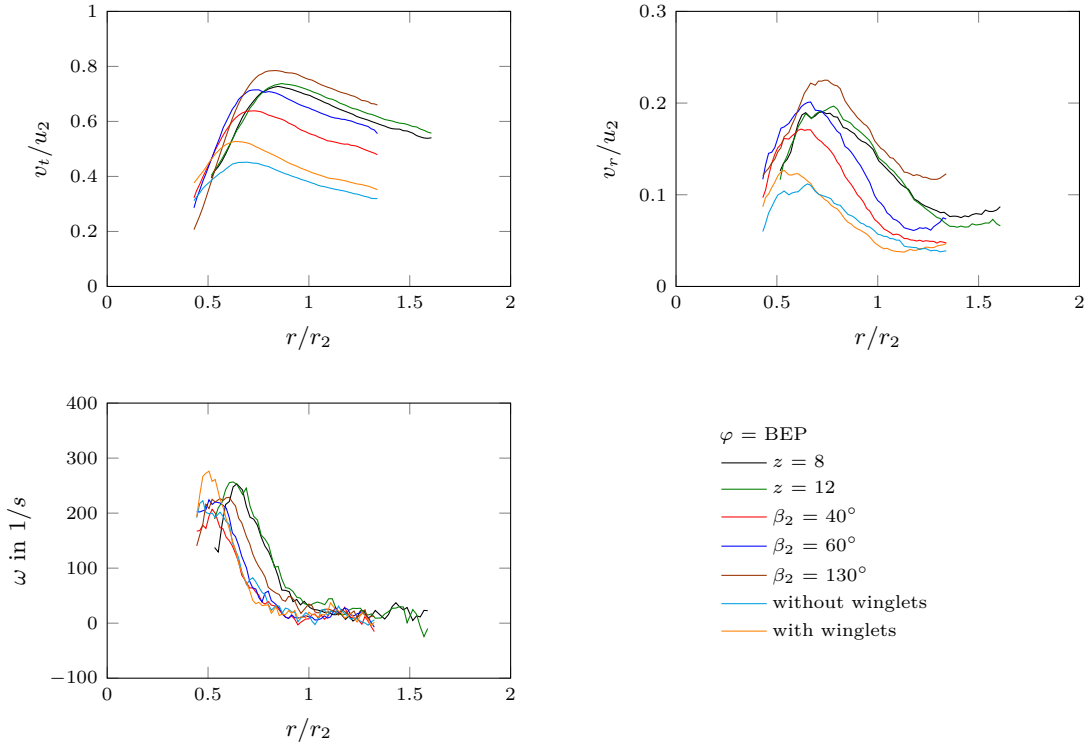
Figure 5.7: Comparison of the tangential velocity (left top), the radial velocity (right top), and the vorticity (bottom left) over the normalized radius for all tested impellers at BEP operation ($\varphi = $ BEP).

vortex.

Over the radius the courses of the vorticity increased, peaked, and then declined until they started fluctuating. This was true for operation at BEP (Figure 5.7, bottom left) and shut-off conditions (Figure 5.8, bottom right). The impeller with 4 blades and the impeller with winglets reached the highest values of vorticity. In contrast to the previous findings, the courses of the vorticity did not correspond to the predictions of a theoretical vortex. A theoretical vortex has its highest vorticity at small radii around 0.

There are several reasons why the observed flow field deviates from a theoretical vortex. For example, the vortex pump under investigation had an axial inflow from the suction pipe. This inflow may have disturbed the flow field. Furthermore, the casing was not symmetrically (as often assumed in theoretical vortices) and fluid continuously exited the casing through the pressure pipe.

5.4 Interim Summery

This chapter analyzed the flow field of a vortex pump in the front gap, between the impeller and the casing. To this end, PIV measurements were conducted and different impeller designs were compared, including variations in the blade number, the blade outlet angle, and the adding of winglets. All impellers were tested for their BEP operation and for their operation at shut-off conditions. The data were post-processed to compare the courses of the tangential velocity, the
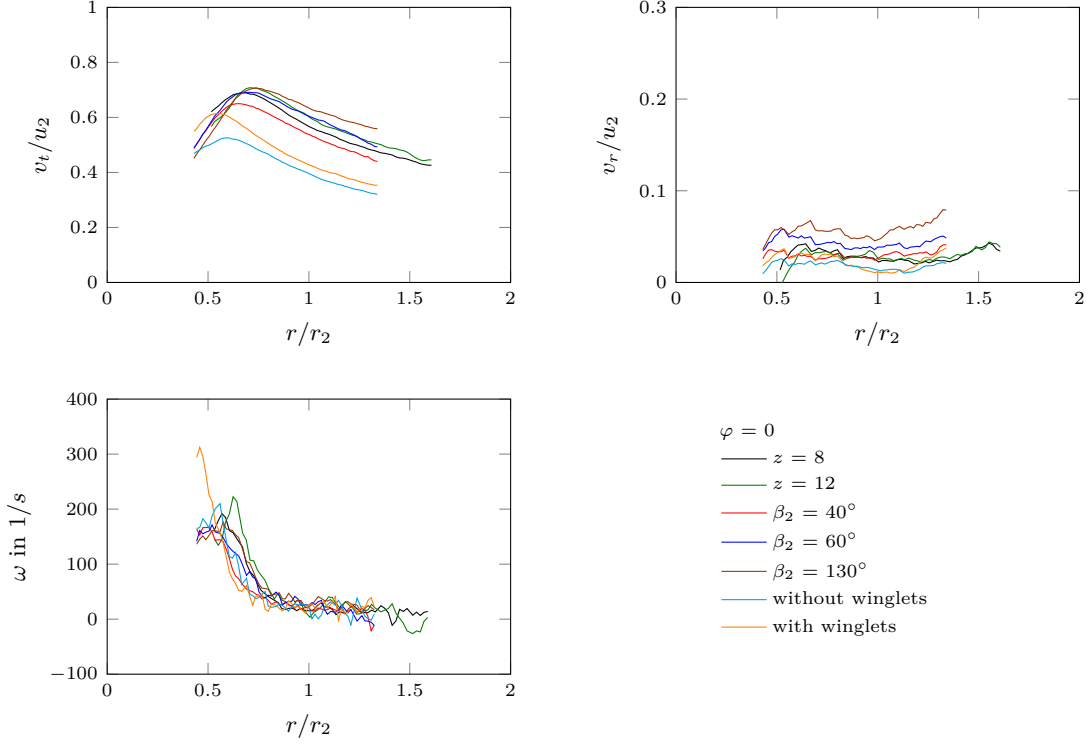
Figure 5.8: Comparison of the tangential velocity (left top), the radial velocity (right top), and the vorticity (bottom left) over the normalized radius for all tested impellers at shut-off operation conditions ($\varphi = 0$).

radial velocity, and the vorticity over the radius. The radius was normalized to the respective outer impeller radius. The tangential velocity and the radial velocity were normalized to their respective circumferential speed of the impeller.

The considered geometric changes to the impellers lead to clear differences in the maxima of the tangential velocity, the radial velocity, and the vorticity. This finding strongly suggests that the design of the impeller can influence the flow structure in the front chamber that again potentially influences the pressure coefficients and the efficiency. To gain direct empirical insights, however, the outflow of the impellers should be experimentally measured to correlate it directly to the pressure coefficients and the efficiency.

Overall, it could be shown that the courses of the tangential velocity of all impellers followed the principal course of the tangential velocity of a theoretical vortex model. Also the radial velocity followed the course of a theoretical vortex although at far smaller values compared to the tangential velocity. The divergence of the tangential and the radial velocities suggests that the flow in the vortex pump is mostly rotating in the casing. If the flow field in a vortex pump corresponds to that of a theoretical vortex, this could be a useless tool for the design process of a vortex pump. Nonetheless, the course of the vorticity of the tested impellers did not correspond to the course of a theoretical vortex model. The findings suggest that a vortex exists but it cannot be described by theoretical vortex model such as the Hamel-Oseen vortex. Thus, definite and formula-based relationships of flow field and related impeller design are not yet grasped.

Moreover, it seems worth inspecting the axial component of the velocity in greater detail.

It would be expected that the axial inflow from the suction side disturbs the vortex formation or might superimpose to the velocities in the casing, thus the courses of the tangential and the radial velocities could resemble that of a theoretical vortex while lacking other features such as the course of vorticity.

Chapter 6

Evaluation of the Clogging Behavior

The previous chapters focused on the behavior and the characteristics of vortex pump operating with clear water. Yet, vortex pumps are mainly applied to transport solids-containing fluids, which have the potential of clogging. In this chapter, therefore, a series of clogging tests were conducted to gain insights into the relationship between geometry parameters and the clogging behavior of vortex pumps when transporting solids-containing fluids. The gained knowledge can be useful for improving the design of vortex pump impellers[1].

6.1 Methods

6.1.1 Test Setup

Figure 6.1 shows a schematic illustration of the test rig that was used for the clogging tests. The test rig consisted of two tanks of similar size. Each tank had a pipe, which was connected to the suction pipe of a vortex pump. Valves allowed switching on or off the tanks. The pressure pipe had a non-return valve to stop the flow from returning to the pump. A throttle valve adjusted the operating point of the pump. A magnetic flow meter measured the flow rate and a differential pressure sensor measured the pressure. Furthermore, a filter was installed upstream of tank 2 so that solids could be filtered before the fluid entered tank 2. Tank 1 did not have a filter. Both tanks were open (open system).

The left panel of Figure 6.2 depicts the vortex pump that was used throughout all tests. The right panel of Figure 6.2 is a cross section view of the pump. The vortex pump had an acrylic, concentric casing. The diameters of the suction and the pressure side were both 80 mm. The drivetrain, including the motor, was mounted on rails to enable a comfortably changing of the impellers and to allow accessing the clogged materials after the tests. Attached to the motor was an incremental encoder to measure the rotational speed. The power consumption of the pump unit, including the motor, was measured too. In addition, time was recorded and a video camera filmed the pumping process to document the clogging in the pump through the front side of the acrylic casing.

Non-woven textiles served as the clogging material. Their dry weight ranged between 3.8 g and 4.1 g with an average size of 30.5 cm by 21.5 cm per textile. Three quantities of textiles

---

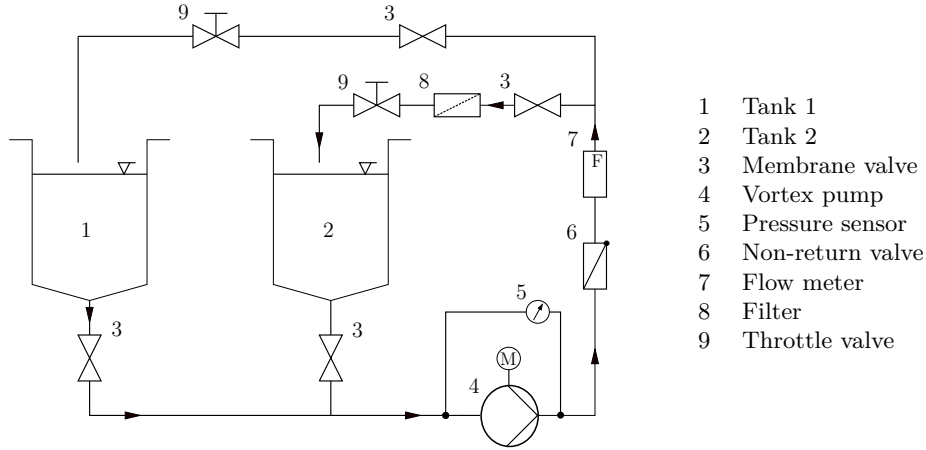[1]Parts of these studies were presented in Gerlach et al. [47] and [48]

Figure 6.1: Schematic illustration of the test rig (adapted from Gerlach et al. [48]).

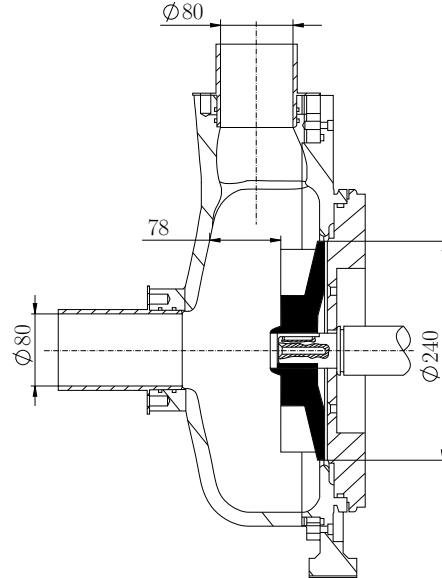|	
1	Tank 1
2	Tank 2
3	Membrane valve
4	Vortex pump
5	Pressure sensor
6	Non-return valve
7	Flow meter
8	Filter
9	Throttle valve

Figure 6.2: The vortex pump used for the tests (left) and its cross section view (right; both taken from Gerlach et al. [48]).

simulated three different degrees of clogging: Either 50 textiles, 100 textiles, and 200 textiles were mixed with 2 m^3 clear water. Thus, the concentration of clogging material in the tests was manipulated by the amount of the textiles. The mixed fluid was then added to tank 1 and the pump was activated so that the textiles-containing fluid was pumped from tank 1 to tank 2 via the filter. The procedure was stopped once tank 1 was empty. After the pumping process all textiles that remained in the pump were removed and classified as not pumped. All textiles that were filtered were classified as pumped.

The study analyzed various changes in the geometry parameters of a vortex pump impeller and it measured their influence on the clogging behavior. The considered parameters included the blade number z, the blade angle β_2, the impeller diameter D_2, and the adding of winglets. The

Table 6.1: Tested parameters of the impeller for the clogging tests.

Assessed Parameter	Compared Values	Defined Geometries
Blade number z	$z = 8$ $z = 12$	$D_2 = 200$ mm, $\beta_1 = \beta_2 = 90°$
Blade outlet angle β_2	$\beta_2 = 40°$ $\beta_2 = 60°$	z = 8, $D_2 = 240$ mm, $\beta_1 = 90°$
Impeller diameter D_2	$D_2 = 200$ mm $D_2 = 205$ mm	$z = 8$ $\beta_1 = \beta_2 = 90°$
Adding winglets	without winglets with winglets	$z = 4$, $D_2 = 240$ mm, $\beta_1 = 44°$, $\beta_2 = 19°$

specific parameters under investigation were chosen because their variation proved relatively promising for improving the performance of a vortex pump under clean water operation (see Chapter 3). Hence, it seems desirable to investigate the extent to which the improvements under clean water operation can be generalized to solids-containing fluids. Table 6.1 lists the variations in the parameters and it describes the associated impellers.

In more details, to investigate the influence of the blade number an impeller with 8 straight blades was compared to an impeller with 12 straight blades. Both impellers had a diameter of 200 mm, an outlet angle of 90°, an inlet angle of 90°, and a blade outlet width of 35.6 mm.

To investigate the influence of the blade outlet angle β_2, two impellers were considered. The first impeller had a blade outlet angle of 40°. The second impeller had a blade outlet angle of 60°. Both impellers had an outside diameter of 240 mm, 8 blades, an inlet angle of 90°, and a blade outlet width of 40.3 mm.

The influence of the diameter was tested via two impellers. The first impeller had a diameter of 200 mm and the second impeller had a diameter of 205 mm. Both impellers had 8 straight blades, that is, an outlet angle of 90° and an inlet angle of 90°. Due to the different diameters and the back shroud design, the blade outlet width of the impeller with the 200 mm diameter was 35.6 mm and the blade outlet width of the impeller with the 205 mm diameter was 36.2 mm.

The influence of winglets was studied by comparing an impeller with winglets to an impeller without winglets. Both impellers had 4 curved blades and a diameter of 240 mm.

Due to the design of the front chamber the different impeller diameters resulted in different axial clearances between the vane tip of the impeller and the front wall of the casing. For impellers with a diameter of 240 mm the axial clearances was 78 mm, for impellers with a diameter of 205 mm the axial clearances was 82 mm, and for impellers with a diameter of 200 mm the axial clearance was 83 mm.

6.1.2 Presentation of the Data

The tested impellers differ in their characteristics for clear water operation. The results are therefore presented by comparing the characteristics values during the clogging tests to the characteristics values during clear water operation. That is, to determine the BEPs the clear water characteristics of each impeller were measured on the same test rig before the clogging material was added. Then, the operation point for the clogging tests was adjusted to the Best Efficiency Point under clear water operation. Hence, all characteristics of the clogging tests are relative to the BEP under clear water operation of the respective impeller. This procedure allowed dimensionless analyses of the changes in the flow coefficient, the pressure coefficient, the power coefficient and the efficiency as a function of the change in the geometry parameters.

In particular, the ratio of the flow coefficient during the clogging tests to the flow coefficient during clear water operation is defined as $\Delta\varphi$ (Formula 6.1):

$$\Delta\varphi = \frac{\varphi_{clogging}}{\varphi_{clear}} \tag{6.1}$$

with $\varphi_{clogging}$ as the average flow coefficient during the clogging test, and φ_{clear} as the average flow coefficient during clear water operation.

Similarly, the ratio of the pressure coefficient $\Delta\psi$ is defined as (Formula 6.2):

$$\Delta\psi = \frac{\psi_{clogging}}{\psi_{clear}} \tag{6.2}$$

with $\psi_{clogging}$ as the average pressure coefficient during the clogging test, and ψ_{clear} as the average pressure coefficient during clear water operation.

The ratio of power coefficient $\Delta\lambda$ is defined as (Formula 6.3):

$$\Delta\lambda = \frac{\lambda_{clogging}}{\lambda_{clear}} \tag{6.3}$$

with $\lambda_{clogging}$ as the average power coefficient during the clogging tests, and λ_{clear} as the average power coefficient during clear water operation.

And the ratio of efficiency $\Delta\eta$ is defined as (Formula 6.4):

$$\Delta\eta = \frac{\eta_{clogging}}{\eta_{clear}} \tag{6.4}$$

with $\eta_{clogging}$ as the average efficiency during the clogging test, and η_{clear} as the average efficiency during clear water operation.

To evaluate how many textiles were pumped, the proportion of the pumped textiles to the total amount of textiles is evaluated by $\Delta textiles$ (Formula 6.5):

$$\Delta textiles = \frac{textiles_{pumped}}{textiles_{total}} \tag{6.5}$$

with $textiles_{pumped}$ as the quantity of actually pumped textiles, and $textiles_{total}$ as the total amount of textiles in the system.

The quantity of pumped textile is determined by the difference between the total amount of added textiles and the textiles that are not pumped (i.e., the textiles that remain in the pump; Formula 6.6):

$$textiles_{pumped} = textiles_{total} - textiles_{notpumped} \tag{6.6}$$

Each test was repeated three times for the geometry configuration and amount of textiles. That is, for each tested parameter there were three tests with 50 textiles, three tests with 100 textiles, and three tests with 200 textiles. Thus, the ratios of $\Delta\varphi$, $\Delta\psi$, $\Delta\lambda$, $\Delta\eta$, and $\Delta textiles$ are averaged across the three tests.

6.2 Results

Table 6.2 lists the BEP values of the flow coefficients, the pressure coefficients, the power coefficients, and the efficiencies under clear water operation, which served as the benchmarks for all further tests. Figure 6.3 depicts the associated clear water characteristics.

Table 6.2: BEP values for clear water operation of all impellers.

Assessed Parameter	Compared Values	φ_{BEP}	ψ_{BEP}	λ_{BEP}	η_{BEP}
Blade number z	$z = 8$	0.051	1.110	0.120	0.47
	$z = 12$	0.062	1.088	0.142	0.48
Blade outlet angle β_2	$\beta_2 = 40°$	0.033	0.865	0.056	0.51
	$\beta_2 = 60°$	0.036	1.054	0.073	0.52
Impeller diameter D_2	$D_2 = 200$ mm	0.051	1.110	0.120	0.47
	$D_2 = 205$ mm	0.053	1.138	0.121	0.49
Adding winglets	without winglets	0.019	0.519	0.028	0.36
	with winglets	0.023	0.592	0.032	0.42
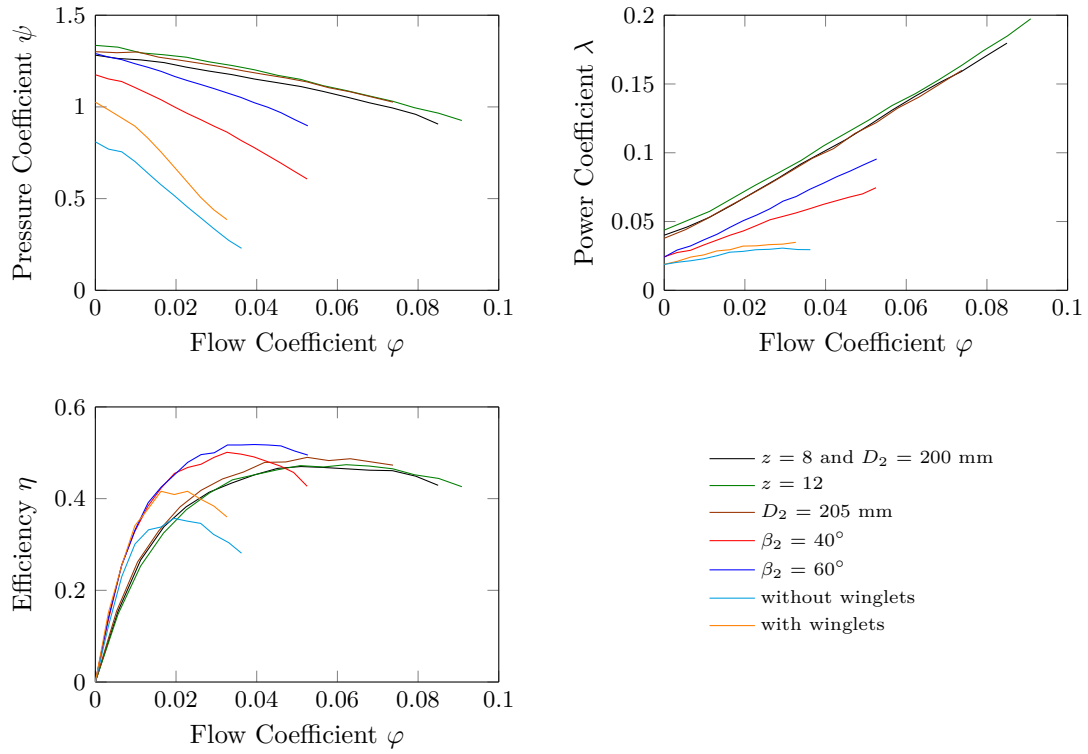
Figure 6.3: Characteristic curves for clear water operation for all impellers.

6.2.1 Blade Number

The influence of blade number was evaluated by comparing an impeller with 8 blades to an impeller with 12 blades. The results of the tests are presented in Figure 6.4, which shows the resulting ratios. The closer these ratios are to 1 the closer the observation to the respective BEP under clear water operation. The 8-bladed impeller almost kept its flow coefficient (top left panel) and its pressure coefficient (top middle) under various degrees of clogging. In contrast, the 12-bladed impeller had lower flow coefficients and lower pressure coefficients under clogging than under clear water operation especially when clogging was strong (i.e., 200 textiles). The power consumption (top right) of both impellers increased with the number of textiles increasing. Altogether, the 8-bladed impeller consumed more power across all clogging conditions than the 12-bladed impeller did, especially when clogging was strong. For both impellers the vortex pump maintained the pumping process under operation of clogging. The efficiency depended on the degree of clogging: the more textiles were added the lower the efficiency (bottom left). The proportion of pumped textiles (bottom middle) was relatively similar for both impellers with the 12-bladed impeller slightly outperforming the 8-bladed impeller. For both impellers, the ratio of pumped textiles increased the more textiles were added to the water. This effect was probably due to all tests using the same volume of 2 m^3 water and thus the concentration varied.

In addition to the measurements, the flow in the casing was observed during the clogging tests. After each test, the clogged textiles were inspected. Table 6.3 illustrates the vortex pump during and after a test with 100 textiles, and it also depicts the not-pumped textiles for an impeller with 8 and an impeller with 12 straight blades. During the tests, the textiles seemed mostly evenly distributed in the casing. However, the textiles accumulated in the area of suction pipe and near the hub of the casing. Such accumulation was observed for all tests, independent of number of textiles. The concentration was especially visible after the tests. The not-pumped textiles were tightly knotted. Single textiles could hardly, if at all, be separated from the accumulation.
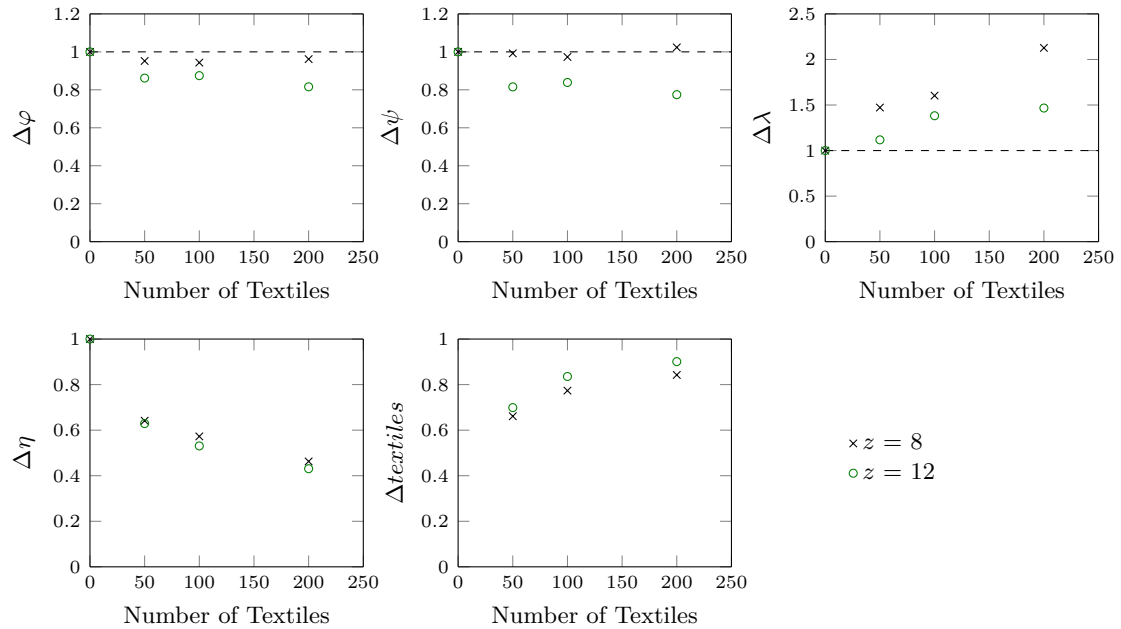

Figure 6.4: Influence of the blade number under various degrees of clogging.

Table 6.3: Exemplary pictures of the textiles (test with 100 textiles and varying blade numbers).

Compared Values	Vortex Pump During the Test	Vortex Pump After the Test	Sample of Not-Pumped Textiles After the Test
$z = 8$			
$z = 12$			

Overall, the impeller with 12 blades thus pumped more textiles and consumed less power than the 8-bladed impeller did. However, the flow coefficient and the pressure coefficient of the 8-bladed impeller outperformed those of the 12-bladed impeller.

6.2.2 Blade Outlet Angle

To investigate the influence of the blade outlet angle an impeller with an outlet angle of 40° was compared to an impeller with an outlet angle of 60°. Figure 6.5 illustrates the associated changes in the ratios. The ratios of the flow coefficients (top left) and of the pressure coefficients (top middle) stayed close to 1, irrespective of the number of textiles, suggesting that the performance under clogging conditions was close to that under clear water operation. Overall, the impeller with a blade outlet angle of 40° reached somewhat better ratios of the flow coefficients and better ratios of the pressure coefficients than the impeller with 60° did. However, the ratios of the power coefficient (top right) increased with the intensity of clogging increasing. The power coefficients were lower for the impeller with the 60° outlet angle. Taken together, this means that the impeller with the 60° outlet angle, and especially the impeller with the 40° outlet angle, consumed more power the more severe the clogging. The ratio of the efficiencies (bottom left) decreased for both impellers the greater the clogging: Increasing the number of textiles led to lower efficiencies. The two impellers were almost indistinguishable in terms of their ratios of efficiencies. The amount of pumped textiles (bottom middle) suggested that the impeller with an outlet angle of 40° overall pumped more textiles than the impeller with 60° did. Again, textiles accumulated in the casing near the suction pipe and near the hub for all tests.

All in all, the results suggest that the impeller with a blade outlet angle of 40° was superior to the impeller with 60° in terms of pumped textiles, flow coefficients, and pressure coefficients.
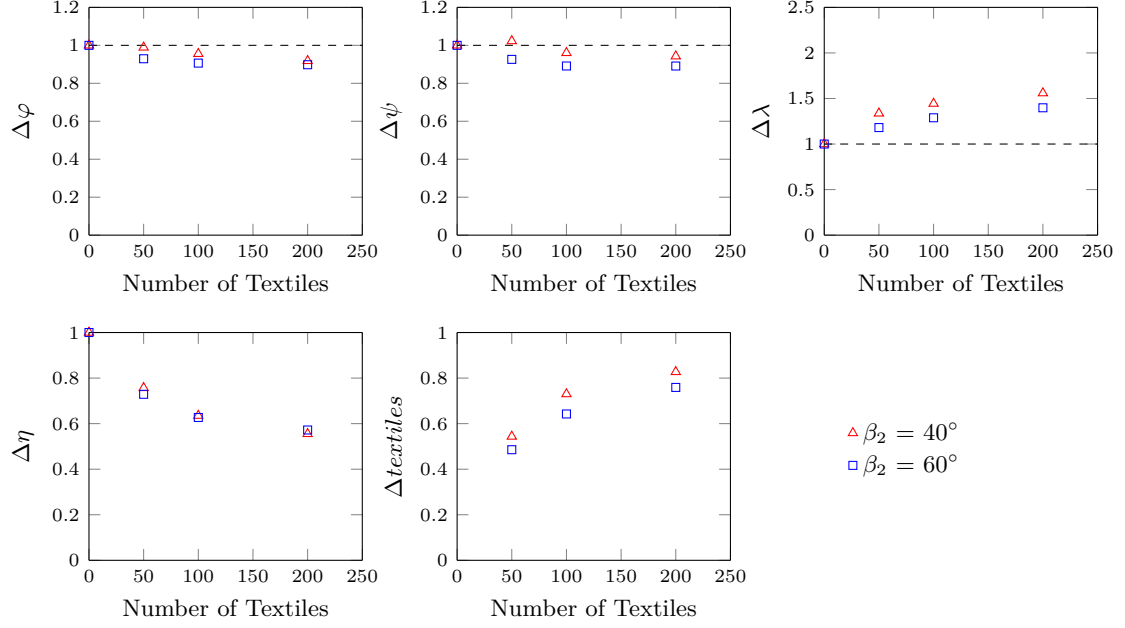
Figure 6.5: Influence of the blade outlet angle under various degrees of clogging.

However, the ratio of the power coefficients of the impeller with an outlet angle of 40° was higher too. This result is in contrast to the result of the influence of the blade number, which suggested that an impeller which pumped more textiles also has lower ratios of the power coefficients.

6.2.3 Impeller Diameter

Next, the influence of the impeller diameter was analyzed by comparing an impeller with a diameter of 200 mm to an impeller with a diameter of 205 mm. Figure 6.4 illustrates the resulting ratios. For both impellers, the flow coefficients (top left) and the pressure coefficients (top middle) during clogging was relatively close to the benchmark of clear water operation. This was especially true for the impeller with a diameter of 200 mm. Power consumption (top right) for both impellers rose with the degree of clogging increasing. This effect especially pronounced for the impeller with a diameter of 200 mm. The decline in efficiency (bottom left) was comparable for both impellers. The impeller with a diameter of 205 mm pumped a slightly greater proportion of textiles than the impeller with a diameter of 200 mm did. Both impellers tended to pump a greater proportion of textiles with increasing number of textiles.

The findings suggest that the impeller with a diameter of 200 mm was superior to the impeller with a diameter of 205 mm in terms of the flow coefficients and the pressure coefficients. However, the ratios of the power coefficients were higher for the impeller with a diameter of 200 mm. The two impellers had comparable ratios of their efficiencies and the proportion of pumped textiles was almost indistinguishable.
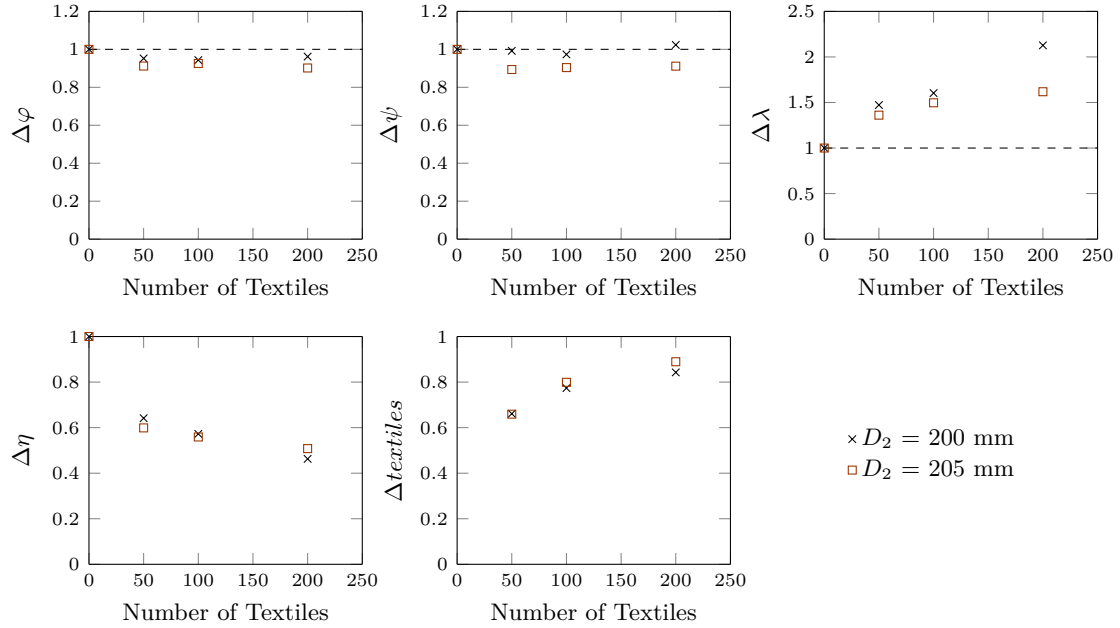
Figure 6.6: Influence of the impeller diameter under various degrees of clogging.

6.2.4 Winglets

Figure 6.7 illustrates the influence of adding winglets on the ratios by comparing an impeller with 4 curved blades to an impeller with 4 curved winglets. The ratios of the flow coefficient (top left) for both impellers remained close to clear water operation. The ratio of pressure coefficient (top middle) was slightly higher for operation under clogging than under clear water operation irrespective of the impeller. For both impellers, the power consumption (top right) was higher for all clogging tests and it increased the more textiles were added. The efficiency (bottom left) decreased over the clogging tests for both impellers. The impeller with 4 curved blades reached values that were closer to clear water operation than the impeller with curved winglets did, which was overall less efficient. Interestingly, both impellers pumped the same proportion of textiles (bottom right), with greater proportions of textiles pumped the more textiles were added.

Overall, the impeller with 4 curved blades was thus superior to the impeller with 4 curved winglets in terms of ratios of flow coefficient, pressure coefficient, and efficiency. The two impellers had a comparable ratio of power coefficient and they pumped about the same proportion of textiles.

6.3 Comparison of All Impellers

All in all, each introduced change in the geometries of the impellers led to both, positive and negative, consequences on the outcome measures. That is, none of the geometric changes dominated all the outcome measures. Hence, which geometric changes in the impeller are ultimately preferable depends on the targeted parameter that one aims to improve. Trade-offs seem inevitable. For example, it was impossible to infer from a change in the flow coefficient, the pressure coefficient, or the power coefficient a change in the proportion of pumped textiles. Overall, the ratios of the efficiencies remained relatively little affected by geometric modifications. Table 6.4
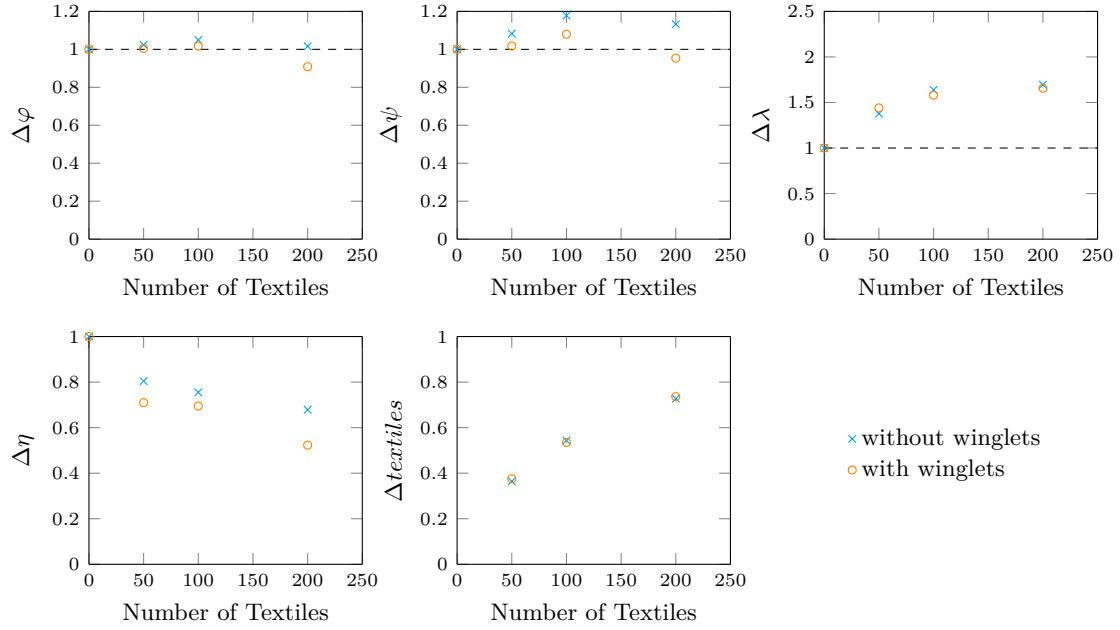
Figure 6.7: Influence of the adding of winglets under various degrees of clogging.

Table 6.4: Tendency of the parameter studies on the performance for operation under clogging.

Assessed Parameter	Compared Values	$\Delta\varphi$	$\Delta\psi$	$\Delta\lambda$	$\Delta\eta$	$\Delta textiles$
Blade number z	$z = 8$	better	better	worse	somewhat better	worse
	$z = 12$	worse	worse	better	somewhat worse	better
Blade outlet angle β_2	$\beta_2 = 40°$	better	better	worse	equal	better
	$\beta_2 = 60°$	worse	worse	better	equal	worse
Impeller diameter D_2	$D_2 = 200$ mm	somewhat better	better	worse	equal	somewhat worse
	$D_2 = 205$ mm	somewhat worse	worse	better	equal	somewhat better
Adding winglets	without winglets	better	better	equal	better	equal
	with winglets	worse	worse	equal	worse	equal

provides an overview on all implications of the test results.

For designers and users alike, it seems most interesting to learn which impeller design performs best (in terms of a performance that is as close to the clear water operation as possible) and

which pumped most of the textiles. To provide such direct comparison of all the impellers Figure 6.8 plots all the ratios over the degrees of clogging by lumping together all impellers into single diagrams. Figure 6.8 illustrates that the impeller with 4 curved blades performed best with regard to the flow coefficient (top left), the pressure coefficient (top right), and the efficiency (middle right) and the impeller with 12 blades performed worst. However, the impeller with 4 curved blades pumped the fewest percentages of textiles and the 12-bladed impeller pumped the most. Thus, the opposite performance of these impellers indicates a negative correlation between the percentage of pumped textiles and their efficiency: The more textiles were pumped the smaller the efficiency.
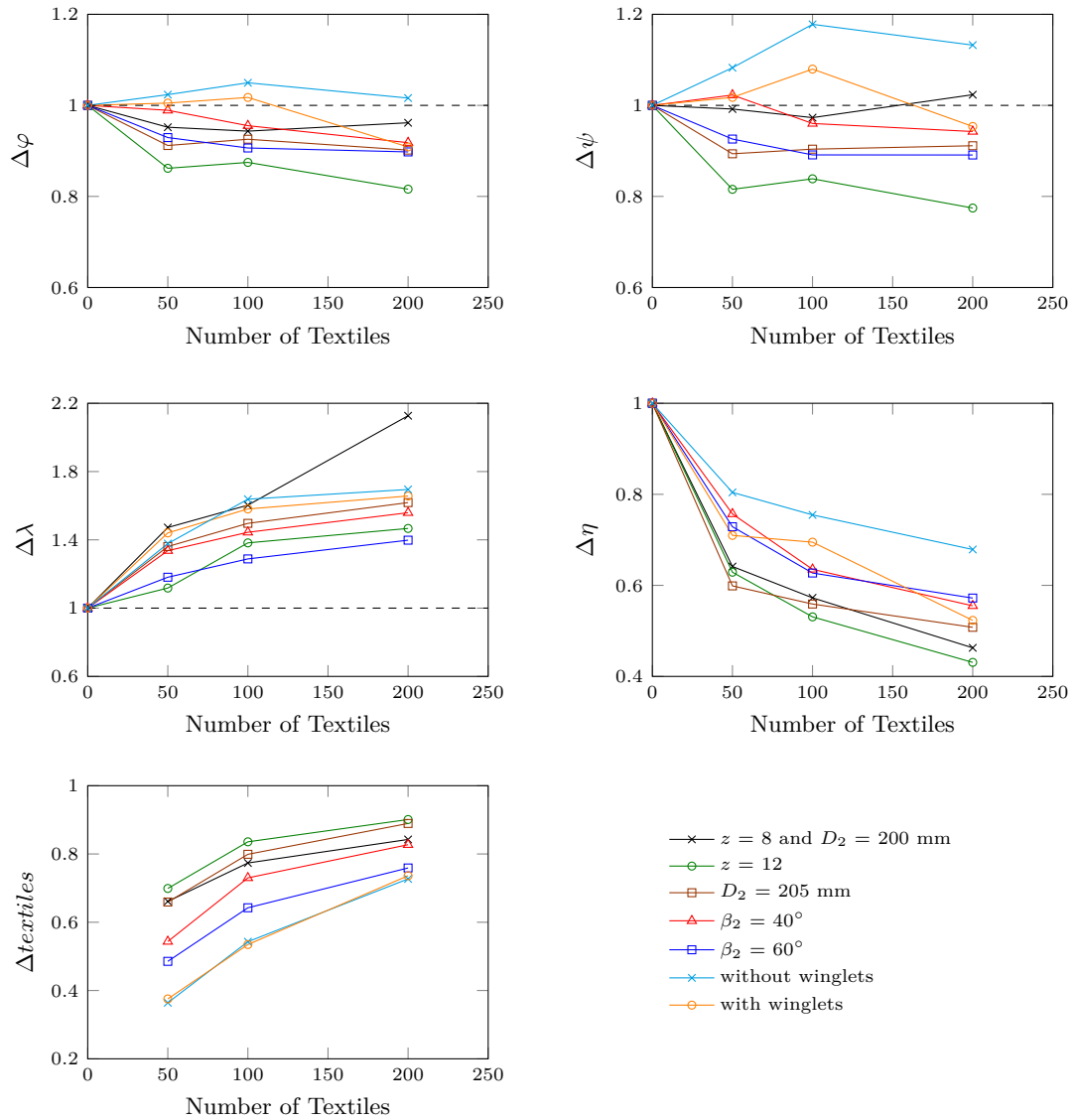

Figure 6.8: Comparison of all tested impellers under various degrees of clogging.

6.4   Limitations

Several limitations of this study and the conclusion that may be drawn from it warrant consideration. Foremost, the specific test design may not be representative or generalize to other application areas of vortex pumps, for example, in terms of the textiles that were used as the clogging material, their amount, their premixing with the defined volume of 2 m^3 of clear water, etc. Further, the specific design of the used vortex pump could have influenced other factors besides the geometry of the impeller itself. That is, the vortex pump had a concentric casing design, which may have caused the textiles to hit the tongue and in this way prevented the textiles from leaving the casing through the pressure pipe. Also, varying the blade number and in the blade outlet angle led to a change of the diameter. To isolate the effect of these parameters it would have been better to compare impellers of the same diameter. However, the impellers with straight blades were tested with a reduced diameter, because their power consumption was already high and the additional power consumption during the clogging tests would have exceeded the performance of the motor (22 kW).

It should be emphasized that the textiles accumulated in the casing, between the hub and the suction pipe. This accumulation was independent of the amount of textiles or the specific impeller under investigation and it needs further clarification.

6.5   Interim Summary

This chapter analyzed the influence of various impeller designs of a vortex pump on its clogging behavior. In particular, variations in the blade outlet angle, the blade number, the impeller diameter, and the adding of winglets were evaluated. To this end, different degrees of clogging were simulated via non-woven textiles, which were mixed with clear water. All tests referred to the BEP of the impeller under clear water operation conditions. All of the impellers managed to maintain the pumping process. For all concentration of clogging material, the flow coefficient and the pressure coefficient remained relatively close to the values of clear water operation and no drastic collapse of these coefficient were observed. Maintaining the pumping process for larger amounts of clogging material, however, was at the cost of the power consumption. A comparison of all tested impellers suggested that a decrease of efficiency during the clogging tests negatively correlated with the proportion of pumped textiles: The more textiles are pumped the more the ratio of efficiency decreases.

An impeller with 12 straight blades pumped most of the textiles but it also lost most of its efficiency under more severe clogging conditions. Such a design is in accordance to the recommendations of the literature (Chapter 2), which are largely based on tests with clear water. The findings of this chapter question the generalizability of these clear water tests to clogging conditions. Moreover, the findings suggest that an impeller with a good performance under clear water conditions can be capable of pumping a large proportion of textiles. However, its operation is at the cost of efficiency. Overall, the clogging behavior in vortex pumps seems insufficiently understood. Hence, more research is needed before sophisticated conclusions about an optimized impeller design for vortex pumps can be drawn.

Chapter 7

Conclusions and Discussion

This dissertation investigated the influence of design parameters on the performance of a vortex pump. It included studies of clear water operation of various impeller designs (Chapter 3), the flow field (Chapter 5), and clogging tests (Chapter 6). Table 7.1 schematically summarizes the influence of the most impactful design parameters on the H-Q-curve, P-Q-curve, and η-Q-curve for clear water operation: Increasing the blade number, increasing the blade outlet angle, increasing the impeller diameter and adding winglets improve the characteristic values.
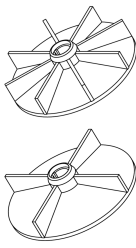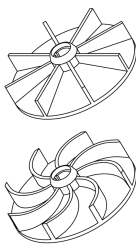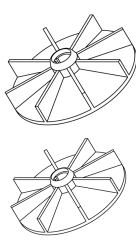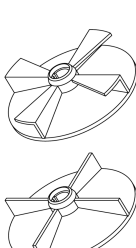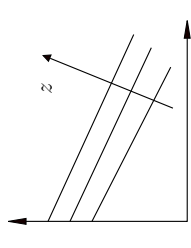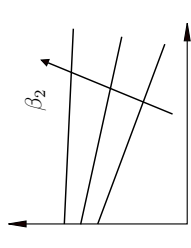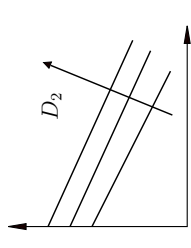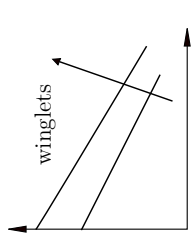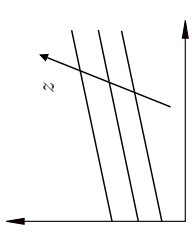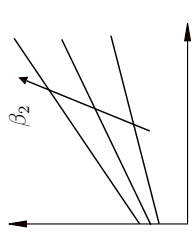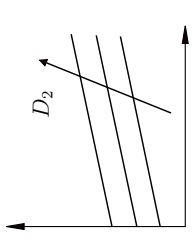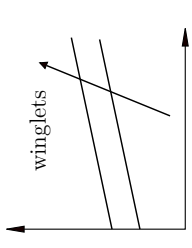
Several findings indicate that the operation principle of a vortex pump is similar to that of a conventional centrifugal pump, in particular to a centrifugal pump with a semi-open impeller: For both pumps, the effect of increasing the impeller diameter and increasing the blade number on the head and efficiency is similar; the blade outlet angle influences the characteristics; the slope of the H-Q-curve depends on the blade outlet angle; straight and forward curved blades can achieve higher efficiency as compared to backward curved blades; adding splitter blades increase the characteristic values; the relation of impeller diameter and rotational speed to the flow rate and the head is equivalent. Even, the best-performing impellers of these tests lie on the Cordier-line suggesting that the characteristic curve of a vortex pump, including the design process of impeller, can be adapted from conventional centrifugal pumps.

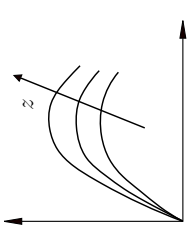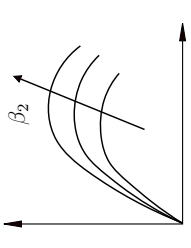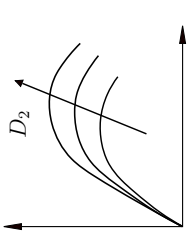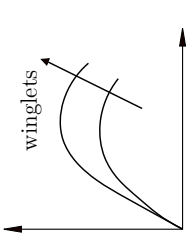Figure 7.1 summarizes the main experimental findings of this dissertation. Depicted are the curves for the pressure coefficient and efficiency for clear water operation as a function of the flow coefficient (top left and top right); the tangential velocities and the radial velocity in the side chamber as a function of the normalized radius (middle left and middle right); and the results of the clogging tests by plotting the ratios of efficiency and the ratios of textiles against the number of textiles (bottom left and bottom right).

Studies of the flow field in the side chamber suggest that a vortex develops for all tested impellers. The existence of a vortex is indicated by the high tangential flow velocity, which is in contrast to the low radial flow velocity. The fluid predominantly rotates in the side chamber contributing little to the transportation of the fluid. Impeller designs that intend to influence the vortex formation imply that the vortex formation should be weakened. Taken together, these findings suggest that a vortex exists but it disturbs the pumping process and it lowers the pressure coefficient and the efficiency of the vortex pump.

Optimizing the vortex pump impeller design to reach high pressure coefficients and high efficiency with low power consumption at the same time would need an impeller design with a high radial velocity and a low tangential velocity. However, radial and tangential velocity seems to be coupled as designs which increased the pressure coefficients and the efficiency led to a high radial velocity but also to a high tangential velocity. Moreover, power consumption rises when

Table 7.1: Summary of the influence of the most impactful design parameters on the clear water characteristics.

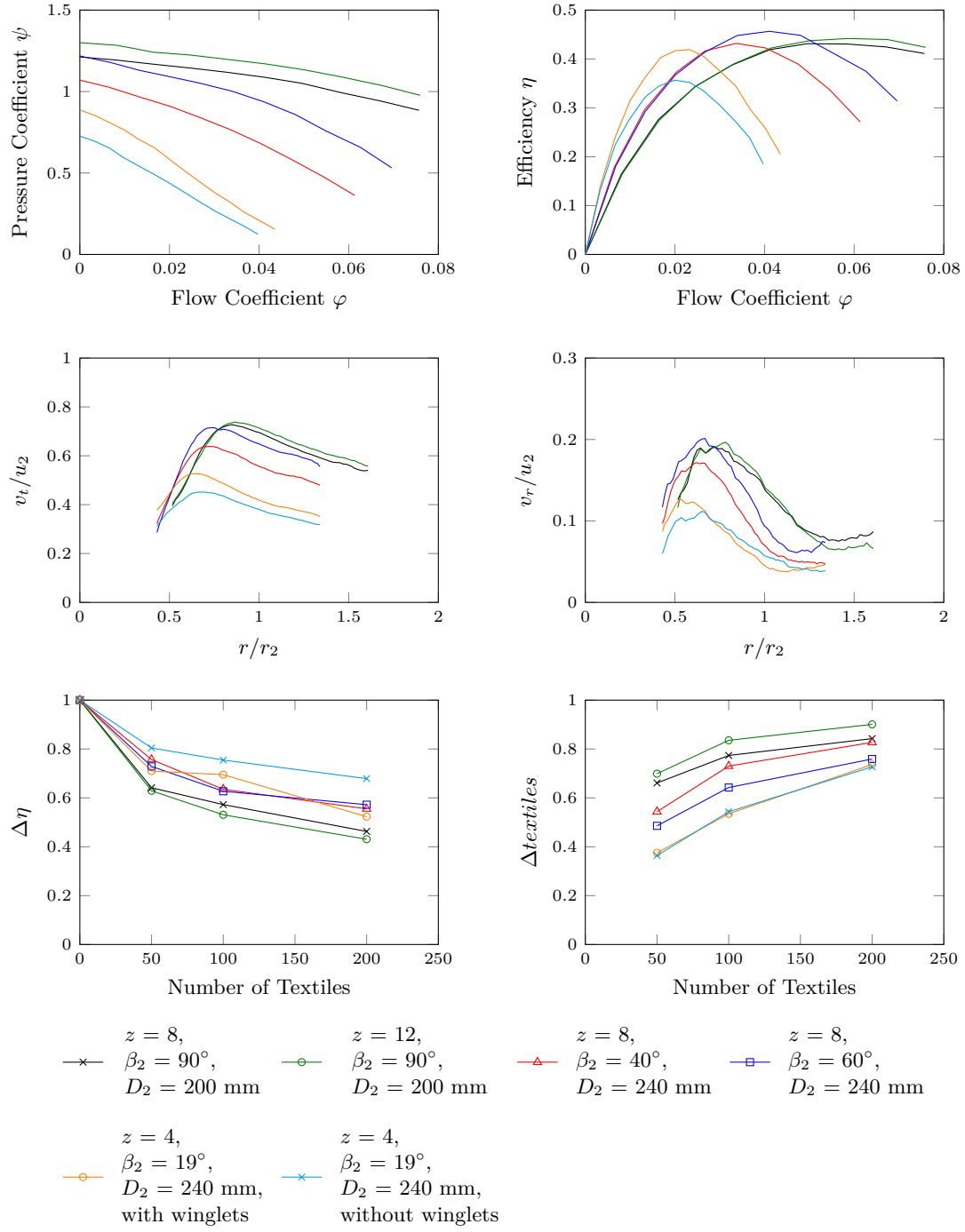| Design Parameter	Blade Number	Blade Outlet Angle	Impeller Diameter	Adding Winglets
Modification	$z \uparrow$	$\beta_2 \uparrow$	$D_2 \uparrow$	winglets $\uparrow$
H-Q-curve	z	β_2	D_2	winglets
P-Q-curve	z	β_2	D_2	winglets
η-Q-curve	z	β_2	D_2	winglets

Figure 7.1: Comparison of impellers with regard to the pressure coefficient (top left), the efficiency (top right), the tangential velocity (middle left), the radial velocity (middle right), the ratio of efficiency (bottom left), and the ratio of textiles (bottom right).

the impeller design improves the pressure coefficient and efficiency. Overall, a limit of achievable efficiency for vortex pumps seems likely: The hydraulic efficiency appears to be capped between 50% and 60%. Even optimized impeller designs substantially lose power through the tangential velocity component of the flow — that is, the vortex. Only reducing the space for the vortex might indeed help preventing the vortex formation. Reducing the space, however, would mean to reduce the gap size between the casing and the impeller. Doing so contradicts the central idea of a vortex pump, namely to keep this passage as large as possible to transport solids-containing fluids without clogging. Hence, the optimization process for a vortex pumps seems to always mean striking a balance between efficiency and applicability.

Further investigations on vortex pumps should aim at gaining more insights on the relation between the vortex pump geometry (impeller and casing) and the resulting flow field. It is striking that the tangential velocity and the radial velocity both resemble the distribution of a theoretical vortex, such as the Hamel-Oseen vortex. However, the comparisons of the vorticity with a theoretical vortex (Chapter 5) suggested that the measured vorticity course was not in agreement with the course of a theoretical vortex. To draw final conclusions it seems worth inspecting small radii of the pump chamber. The axial inflow from the suction pipe might superimpose the velocities in the casing. In this way, the courses of the tangential and the radial velocities could resemble that of a theoretical vortex while lacking other features such as the course of vorticity.

Clogging tests imply that an impeller with a high pressure coefficient and great efficiency for clear water operation indeed pumps most of the clogging material. However, the efficiency of such an impeller significantly decreases under conditions of clogging (Chapter 6). In contrast, an impeller with a low pressure coefficient and low efficiency for clear water operation can keep most of its efficiency under operation of clogging. One reason why the clear water conditions do not generalize to clogging conditions is the tight accumulation of textiles at the impeller hub: Impellers with high pressure coefficients and great efficiency for clear water operation suffered from tighter accumulations of textiles at the impeller hub than the impellers with lower efficiency did. A tight accumulations of textiles leads to a greater power consumption to maintain the pumping process. To fully understand how the tight accumulations of textiles can be avoided it seems worth exploring the area of the hub through more fine-grained experimental investigations. So far, the results suggest that the velocity distribution in the side chamber provokes the tight accumulations of textiles at the hub region: The textiles enter the pump in the area of the hub via the suction pipe. The area near the hub is also the area of side chamber in which the tangential and radial velocities are relatively low. In order to exit the pump, the textiles need to be accelerated in radial direction. However, because the radial velocity in the side chamber is always lower than the tangential velocity the textiles often lack the necessary velocity to leave the casing. Hence, they accumulate in the area of the hub, caught in a rotation. To help solving the clogging accumulation the course of tangential velocity could be directed asymmetrically over the circumference. Partly lowering the peak of the tangential velocity would help that the radial velocity and tangential velocity balance out. Hence, more textiles with less energy and small radial velocity would reach the discharge pipe. A favourable direction for discharging could be implemented by an optimized designs of the geometrical components of the vortex pump, such as an asymmetrical casing design of the front side of the casing (e.g., as it is known from the bull's-eye design of washing machines) or an asymmetrical impeller (e.g., an impeller with an irregular arrangement of the blades or 'missing blade').

The current approaches for designing vortex pump impellers by optimizing their clear water performance is therefore at the cost of their performance under clogging conditions. Clearly, more research is needed to build better-applicable vortex pumps.

Bibliography

[1] A. Gerlach, P.U. Thamsen, S. Wulff, and C. Jacobsen. Design Parameters of Vortex Pumps: A Meta-Analysis of Experimental Studies. *Energies*, 10(1):58, 2017.

[2] V. M. Lubieniecki. Some Performance Characteristics of a Centrifugal Pump with Recessed Impeller. In *Gas Turbine Fluids Eng. Conf. Prod. Show, San Fr. USA, 72-FE-10*, 1972.

[3] G. Grabow and G. Gneipel. Berechnung von Strömungsvorgängen in Freistromradpumpen zur hydraulischen Feststofförderung (Calculation of Flow Processes in Vortex Pumps for Hydraulic Solids Transport). *Maschinenmarkt (Machine Mark.)*, 95(13):152–157, 1989.

[4] K. Rütschi. Die Arbeitsweise von Freistrompumpen (The Operation Principle of Vortex Pumps). *Schweizerische Bauzeitung (Swiss Civ. Eng. Journal)*, 86(32):575–582, 1968.

[5] H. Ohba, Y. Nakashima, K. Shiramoto, K. Shiramoto, and T. Kozima. A Study on Performance and Internal Flow Pattern of a Vortex Pump. In *Bull. JSME*, volume 21, pages 1741–1749, 1978.

[6] M. Aoki. Borutekkusu ponpu ni tsuite (About the Vortex Pump). *Tabo kikai (Turbo Maschine)*, 12(2):80–87, 1984.

[7] R. Zhu, J. Chen, X. Wang, and B. Su. Numerical Simulation and Experimental of Influence of Hem and High-Low Blade on Performance of Vortex Pump. *Liu Ti Ji Xie (Fluid Mach.)*, 40(1):1–5, 2012.

[8] R. Zhu, B. Su, X. Wang, and Y. Yin. Numerical Simulation and Experiment of Influence of Hem on Performance of Vortex Pump. *J. Drain. Irrig. Mach. Eng.*, 28(5):398–401, 2010.

[9] H. Sarvanne. Impeller for a Pump, Especially a Vortex Pump. United States Patent No. 4,676,718, 1987.

[10] M. Aoki. Studies on the Vortex Pump (1st Report, Internal Flow). In *Bull. JSME*, volume 26, pages 387–393, 1983.

[11] V. Hofmann. *Einfluss der Spaltweite auf die Strömung in offenen Laufrädern radialer Bauart (Influence of Gap Width on the Flow in Open Impellers of Radial Type)*. D.eng. thesis, Technische Hochschule Darmstadt, 1992.

[12] H. Ohba, Y. Nakashima, K. Shiramoto, K. Shiramoto, and T. Kojima. A Study on Internal Flow and Performance of a Vortex Pump - Part 2 A Comparison between Analyses and Experimental Results, and a Design Method of Pump. In *Bull. JSME*, volume 26, pages 1007–1013, 1983.

[13] M. Aoki. Studies on the Vortex Pump (3rd Report, Estimation of Pump Performance). In *Bull. JSME*, volume 26, pages 1014–1019, 1983.

[14] J. Wang. Xuan Liu Beng De Xing Neng Shi Yan Yan Jiu (Performance Testing of a Vortex Pump Investigating the Inner Losses). *Drain. Irrig. Mach.*, 8(3):8–15, 1989.

[15] G. P. Schivley and J. L. Dussourd. An Analytical and Experimental Study of a Vortex Pump. *J. Basic Eng.*, 92(4):889–900, 1970.

[16] H. Ohba, Y. Nakashima, and K. Shiramoto. A Study on Internal Flow and Performance of a Vortex Pump - Part 1 Theoretical Analysis. In *Bull. JSME*, volume 26, pages 999–1006, 1983.

[17] Y. Sha and L. Hou. Effect of Impeller Location and Flow Measurement in Volute of a Vortex Pump. *Nong Ye Ji Xie Xue Bao (Agricultural Mech. Journal)*, 41(11):57–62, 2010.

[18] S. Li and J. Feng. The Preliminary Study on Vortex Pump. *J. Beijing Agric. Eng. Univ.*, 7(4):39–46, 1987.

[19] X. Guan, D. Xie, X. Zhang, and L. Xu. Design of Immersible Sludge Pump. *J. Jiangsu Inst. Technol.*, 10(3):26–37, 1989.

[20] J. Wu, Y. Sha, and X. Xu. Experimental Investigation on Variable Speed Performance and Volute Flow of Vortex Pump. *J. Zhejiang Univ. (Engineering Sci.)*, 44(9):1811–1817, 2010.

[21] P.G.Saffman. *Vortex Dynamics*. Cambridge Monographs on Mechanics and Applied Mathematics, 1992.

[22] A. Gerlach, E. Preuss, P.U. Thamsen, and F. Lykholt-Ustrup. Numerical Simulations of the Internal Flow Pattern of a Vortex Pump Compared to the Hamel-Oseen Vortex. *J. Mech. Sci. Technol.*, 31(4):1711–1719, 2017.

[23] F. Morrison. *An Introduction to Fluid Mechanics*. Cambridge University Press, 1st edition, 2013.

[24] J. Daily and D. Harleman. *Fluid Dynamics*. Addison-Wesley Publishing Company, Inc., 2nd edition, 1973.

[25] X. Guan, D. Xie, X. Zhang, and Y. Sha. Xuan Liu Beng Te Xing Ji Sheji Fang Fa Yan Jiu (Design Method Research on a Vortex Pump). *Fluid Eng.*, 18(5):18–23, 1989.

[26] M. Zheng, S. Yuan, and C. Chen. Influence of Structural Parameter of a Vortex Pump on its Performance. *Nong Ye Ji Xie Xue Bao (Transaction Chinese Soc. Agric. Mach.)*, 2(32):46–49, 2000.

[27] Y. Sha, M. Yang, S. Yuan, J. Wang, C. Li, and J. Wen. Experimental Study on Performance and Design Method of a Submarine Sewage Vortex Pump. *Nong Ye Ji Xie Xue Bao (Agricultural Mech. Journal)*, 35(5):82–86, 2004.

[28] Y. Sha, M. Yang, C. Kang, J. Wang, and C. Huilong. Design Method and Characteristic Analysis of Vortex Pump. *Trans. CSAE*, 20(1):124–127, 2004.

[29] Y. Sha, M. Yang, C. Kang, and X. Wang. Design and Performance Experiment of Sewage and Slurry Vortex Pump. *J. Jiangsu Univ. (Natural Sci. Ed.)*, 26(2):153–157, 2005.

[30] D. Jiang, J. Lü, L. Dai, and B. Su. A Numerical Simulation of and Experimental Research on Optimum Efficiency of Vortex Pumps. *Zhong Guo Nong Cun Shui Li Shui Dian (Chinese Agric. Hydraul. Power)*, 4:92–98, 2012.

[31] A. Gerlach, P. U. Thamsen, and F. Lykholt-Ustrup. Experimental Investigation on the Performance of a Vortex Pump using Winglets. In *16th Int. Symp. Transp. Phenom. Dyn. Rotating Mach. Honolulu, Hawai'i, USA*, 2016.

[32] Q. Cheng, Y. Liu, and F. Luo. Xuan Liu Beng Beng Ti De Shi Yan Yan Jiu (Experiments on the Casing of a Vortex Pump). *Drain. Irrig. Mach.*, 11(2):12–15, 1992.

[33] Y. Sha and X. Bai. Xuan Liu Beng Bian Zhouan Su Te Xing Shi Yan Yan Jui (Experimental Investigation on Changing Rotational Speed of a Vortex Pump). *Shui Beng Ji Shu (Water Pump Tech.*, 4:9–12, 2010.

[34] M. Aoki. Studies on the Vortex Pump (2nd Report, Pump Performance). In *Bull. JSME*, volume 26, pages 394–398, 1983.

[35] X. Wang, R. Zhu, B. Su, and Z. Yu. Numerical Simulation and Experiment of Latin Square Design on Non-Overload Vortex Pump. *Nong Ye Ji Xie Xue Bao (Agricultural Mech. Journal)*, 43(1):48–52, 2012.

[36] X. Wang, R. Zhu, Z. Yu, and B. Su. Influences of High-Low Blade on Performance of Vortex Pumps. *Zhong Guo Ji Xie Gong Cheng (Mechanical Eng.)*, 22(17):2030–2033, 2011.

[37] M. Cervinka. Computational Study of Sludge Pump Design with Vortex Impeller. In *18th Int. Conf. Eng. Mech. Svratka, Czech Repub.*, 2012.

[38] A. Steinmann, H. Wurm, and A. Otto. Numerical and Experimental Investigations of the Unsteady Cavitating Flow in a Vortex Pump. In *9th Int. Conf. Hydrodyn. Shanghai, China*, 2010.

[39] C. Pfleiderer and H. Petermann. *Strömungsmaschinen (Turbomachinery)*. Springer Berlin Heidelberg, 1991.

[40] J. F. Gülich. *Kreiselpumpen (Centrifugal Pumps)*. Springer Vieweg, 4th edition, 2013.

[41] M. Ganter. *Experimentelle Untersuchungen des Spaltverlustes radialer Kreiselpumpen mit offenem Laufrad (Experimental Studies of the Gap Loss of Radial Centrifugal Pumps with Open Impeller)*. D.eng. thesis, Technische Universiät Carolo-Wilhelmina zu Braunschweig, 1985.

[42] L. Ni. *Modellierung der Spaltverluste bei halboffenen Pumpenlaufrädern (Modeling the Gap Losses in Semi-Open Pump Impellers)*. Fortschrittberichte VDI, Reihe 7: Strömungstechnik Nr. 269, 1995.

[43] A. Gerlach, P. U. Thamsen, D. Perlitz, F. Lykholt-Ustrup, and S. Rasmussen. The Optimal Vortex Pump Impeller-An Experimental Parameter Study. In *Int. Rotating Equip. Conf. Düsseldorf, Germany*, 2016.

[44] H. Siegloch. *Strömungsmaschinen (Turbomachinery)*. Carl Hanser Verlag München, 4th edition, 2009.

[45] S. Yedidiah. *Centrifugal Pump User's Guidebook*. Chapman & Hall, 1st edition, 1996.

[46] O. Cordier. Ähnlichkeitsbedingungen für Strömungsmaschinen (Similarity Conditions for Turbomachinery). *BWK Bd.6, Nr.10*, 1953.

[47] A Gerlach, S. Wulff, D. Perlitz, F. Lykholt-Ustrup, and P.U. Thamsen. The Optimal Vortex Pump Impeller-An Experimental Study on Clogging Behaviour. In *Proc. 12th Eur. Conf. Turbomach. Fluid Dyn. Thermodyn. Stock. Sweden*, 2017.

[48] A. Gerlach, D. Perlitz, C. B. Jacobsen, F. Lykholt-Ustrup, and P.U. Thamsen. The Clogging Behavior of a Vortex Pump-An Experimental Study on the Influence of Impeller Designs. In *Proc. ASME 2017 Fluids Eng. Div. Summer Meet. Waikoloa, Hawai'i, USA*, 2017.

Nomenclature

Abbreviation

BEP	Best Efficiency Point
PIV	Particle Image Velocimetry

Roman Symbols

D_2	Impeller diameter in m
D_S	Suction pipe diameter in m
D_d	Pressure pipe diameter in m
H	Head in m
M	Torque in Nm
P	Power in W
Q	Flow rate in m^3/s
T	Time in s
b_2	Impeller width in m
b_4	Volute width in m
g	Gravitational acceleration m/s^2
k	Experienced based factor for vortex pumps
n	Rotational speed in 1/s
p	Slip factor
r	Radius in m
r_1	Impeller inner radius in m
r_2	Impeller outer radius in m
s	Covering in m
t	Blade thickness in m
u_1	Circumferential velocity at the leading edge of blade in m/s
u_2	Circumferential velocity at the outlet tip of blade in m/s
v_t	Tangential velocity in m/s
v_r	Radial velocity in m/s
z	Blade number

Greek Symbols

Γ	Circulation in m^2/s
$\Delta\varphi$	Ratio of flow coefficient
$\Delta\psi$	Ratio of pressure coefficient
$\Delta\lambda$	Ratio of power coefficient

$\Delta\eta$	Ratio of efficiency
$\Delta textiles$	Ratio of textiles
β_1	Blade inlet angle in Degree
β_2	Blade outlet angle in Degree
δ	Diameter number
η	Efficiency
κ	Experienced based factor
λ	Power coefficient
ν	Kinematic viscosity in m^2/s
ρ	Density in kg/m^3
σ	Speed number
φ	Flow coefficient
ψ	Pressure coefficient
ψ'	Experienced based factor
ω	Vorticity in 1/s

Subscriptions

clogging	Clogging test
clear	Clear water test
sf	Shock losses free
th, x	Finite number of blades
th, ∞*, x*	Infinite number of blades

78

Appendices

Appendix A

Table A1: Assessed parameters, defined geometries, and related BEP Data of the tested impellers.

Assessed Parameter	Prefix	Compared Values	Defined Geometries	φ_{BEP}	ψ_{BEP}	λ_{BEP}	η_{BEP}
Blade number	z	$z = 8$	$D_2 = 240$ mm	0.048	1.100	0.114	46.6%
		$z = 12$	$\beta_1 = \beta_2 = 90°$	0.049	1.146	0.118	47.3%
		$z = 14$	$b_2 = 40.3$ mm	0.049	1.151	0.119	47.2%
Blade outlet angle	β_2	$\beta_2 = 40°$	$D_2 = 240$ mm	0.034	0.765	0.060	43.2%
		$\beta_2 = 60°$	$z = 8$	0.041	0.937	0.084	45.7%
		$\beta_2 = 90°$	$\beta_1 = 90°$	0.048	1.100	0.114	46.6%
		$\beta_2 = 130°$	$b_2 = 40.3$ mm	0.049	1.159	0.127	45.0%
Impeller diameter	D_2	$D_2 = 240$ mm	$z = 8$ & $z = 12$	0.048	1.100	0.114	46.6%
		$D_2 = 220$ mm	$\beta_1 = \beta_2 = 90°$ $b_2 = 40.3$ mm	0.053	1.064	0.129	43.8%
Impeller width	b_2	$b_2 = 40.3$ mm	$D_2 = 240$ mm	0.020	0.462	0.026	36.2%
		$b_2 = 37.3$ mm	$z = 4$	0.020	0.412	0.024	34.0%
		$b_2 = 34.3$ mm	$\beta_2 = 19°$	0.017	0.410	0.022	31.7%
Impeller inlet diameter	D_S	no inlet	$D_2 = 240$ mm	0.020	0.445	0.025	35.9%
		$D_2/D_S = 3$	$z = 4$	0.020	0.433	0.024	35.4%
		$D_2/D_S = 2$	$\beta_2 = 19°$	0.020	0.381	0.023	33.1%
Adding winglets	-	4 curved winglets	$D_2 = 240$ mm	0.023	0.514	0.029	41.9%
		4 curved blades	$\beta_2 = 19°$	0.020	0.439	0.025	35.7%
Length of winglets	-	no winglets	$D_2 = 240$ mm	0.041	0.974	0.098	40.9%
		1/4 length	$z = 4$	0.041	1.033	0.099	43.1%
		1/2 length	$\beta_1 = \beta_2 = 90°$	0.034	0.980	0.083	39.8%

Table A1: (continued).

| Assessed Parameter	Prefix	Compared Values	Defined Geometries	φ_{BEP}	ψ_{BEP}	λ_{BEP}	η_{BEP}
Orientation of winglets	-	no winglets	$D_2 = 240$ mm	0.041	0.974	0.098	40.9%
		suction side	$z = 4$	0.041	1.033	0.099	43.1%
		pressure side	$\beta_1 = \beta_2 = 90°$	0.041	0.964	0.096	41.0%
		both sides	$b_2 = 40.3$ mm	0.041	1.004	0.097	42.4%
Splitter blades	-	4 blades	$D_2 = 240$ mm	0.041	0.970	0.097	40.8%
		4 splitter blades	$z = 4 - 8$	0.049	1.074	0.115	45.9%
		8 blades	$\beta_1 = \beta_2 = 90°$	0.049	1.120	0.114	48.2%
Pan-like impeller	-	semi-open	$D_2 = 240$ mm	0.041	0.970	0.097	40.8%
		pan-like	$z = 4, \beta_2 = 90°$	0.034	0.822	0.077	36.5%
Vortex-strengthening design	-	4 blades	$D_2 = 240$ mm	0.041	0.970	0.097	40.8%
		VS-No1	$z = 4$	0.041	0.790	0.090	36.0%
		VS-No2	$\beta_1 = \beta_2 = 90°$	0.041	0.659	0.088	30.7%
Vortex-weakening design	-	4 blades	$D_2 = 240$ mm	0.041	0.970	0.097	40.8%
		VW-No1	$z = 4$	0.042	1.050	0.099	44.0%
		VW-No2	$\beta_1 = \beta_2 = 90°$	0.049	1.028	0.111	45.3%
Rotational speed	n	50 Hz	$D_2 = 240$ mm	0.023	0.514	0.029	41.9%
		35 Hz	$z = 4, \beta_1 = 44°$	0.019	0.606	0.030	38.4%
		25 Hz	$\beta_2 = 19°$	0.020	0.585	0.035	33.1%

Appendix B
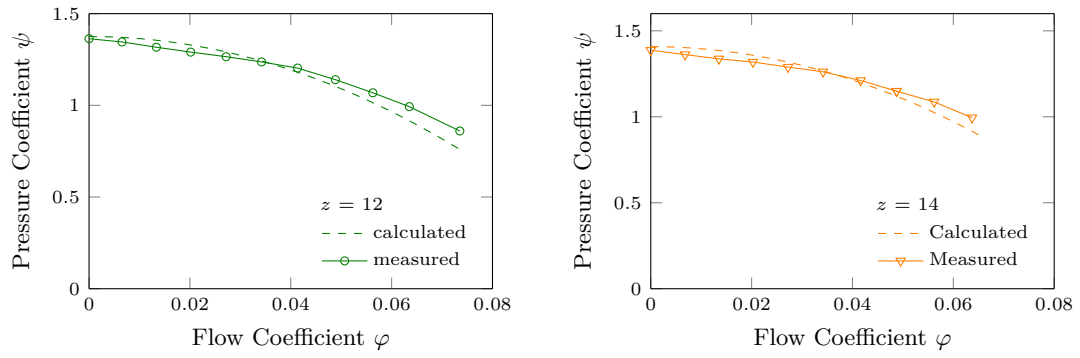
Figure B1: Comparison of the calculated with the measured throttle curves for impellers with 12 straight blades (left) and with 14 straight blades (right).

Appendix C

Table C1: Operation data of tested impellers of the flow field measurements.

Assessed Parameter	Tested Values	φ_{BEP}	ψ_{BEP}	λ_{BEP}	η_{BEP}	$\psi_{\varphi=0}$
Blade number z	z = 8	0.033	1.008	0.077	0.43	1.213
	z = 12	0.058	1.042	0.138	0.44	1.255
Blade outlet angle β_2	$\beta_2 = 40°$	0.034	0.754	0.060	0.42	1.053
	$\beta_2 = 60°$	0.041	0.937	0.085	0.45	1.206
	$\beta_2 = 130°$	0.049	1.155	0.127	0.44	1.291
Adding winglets	without winglets	0.020	0.439	0.024	0.36	0.730
	with winglets	0.020	0.582	0.028	0.42	0.886
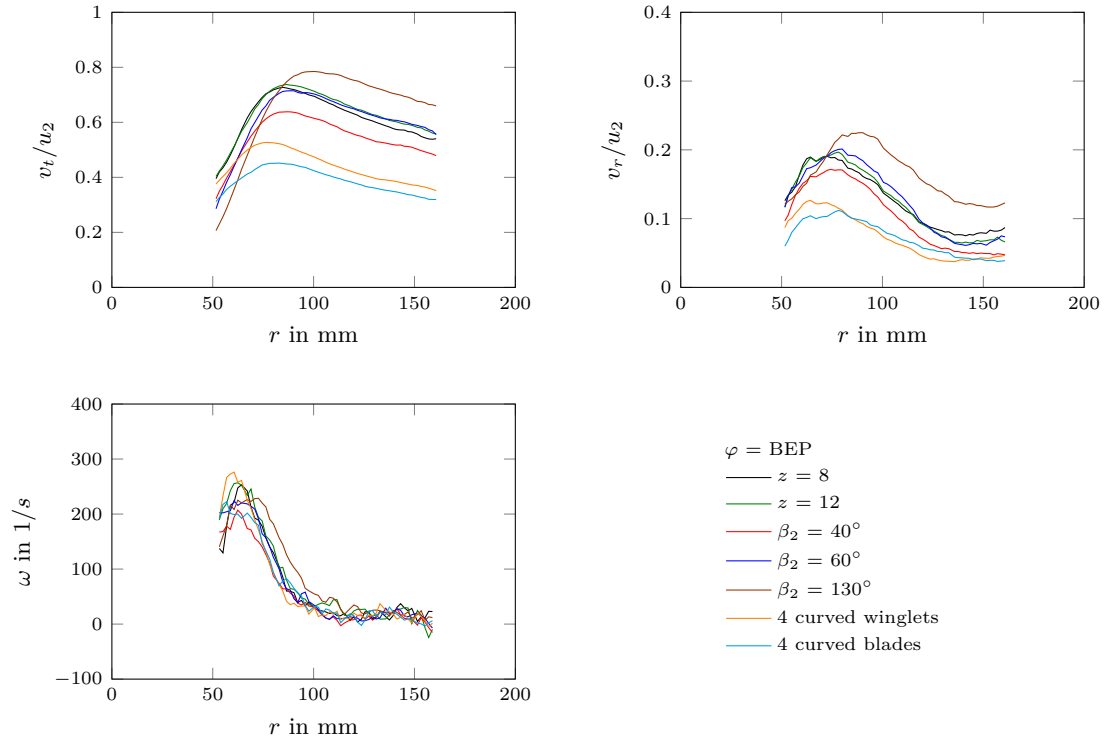
Figure C1: Comparison of tangential velocity (left top), radial velocity (right top), and vorticity (bottom left) over the not normalized radius for all tested impellers at operation at BEP $\varphi = \text{BEP}$.

Appendix D

Additionally to the 'short tests' described in Chapter 6, a second type of clogging test was performed. This test will be referred as to as the 'long tests' (for details, see Gerlach et al. [47]). Similar to the short test, the long test involved mixing either 50, 100 or 200 textiles with 2 m3 of clear water in tank 1. However, the textile-containing fluid was then pumped in circle for one hour so that it re-entered tank 1. After one hour elapsed, the textiles were pumped to tank 2 and the not-pumped textiles were assessed by measuring their dry weight. The long test was conducted once for each amount of textiles (i.e., one test per 50, 100, and 200 textiles). During the tests, the flow rate, the head, the rotation speed and the power consumption were measured. Again, the casing was filmed to report the clogging process. The following figures (Figures D1 to D7) compare the short tests with the long tests. All in all, the long tests suggested qualitatively similar trends as the short tests.
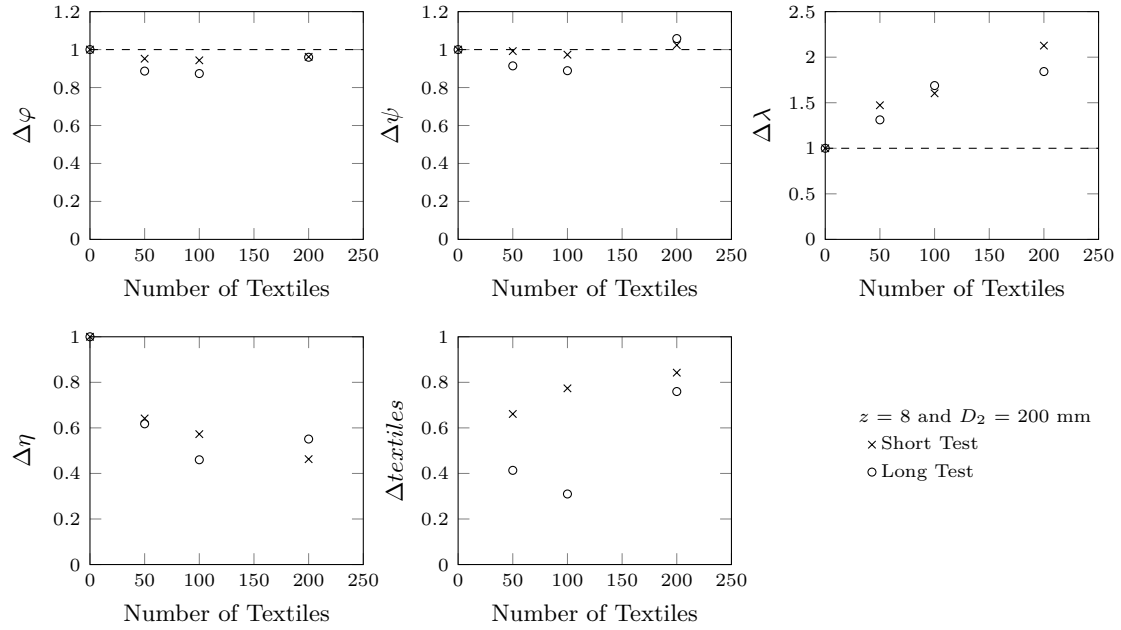
Figure D1: Comparison of the short test with the long test for an impeller with 8 straight blades and a diameter of 200 mm.
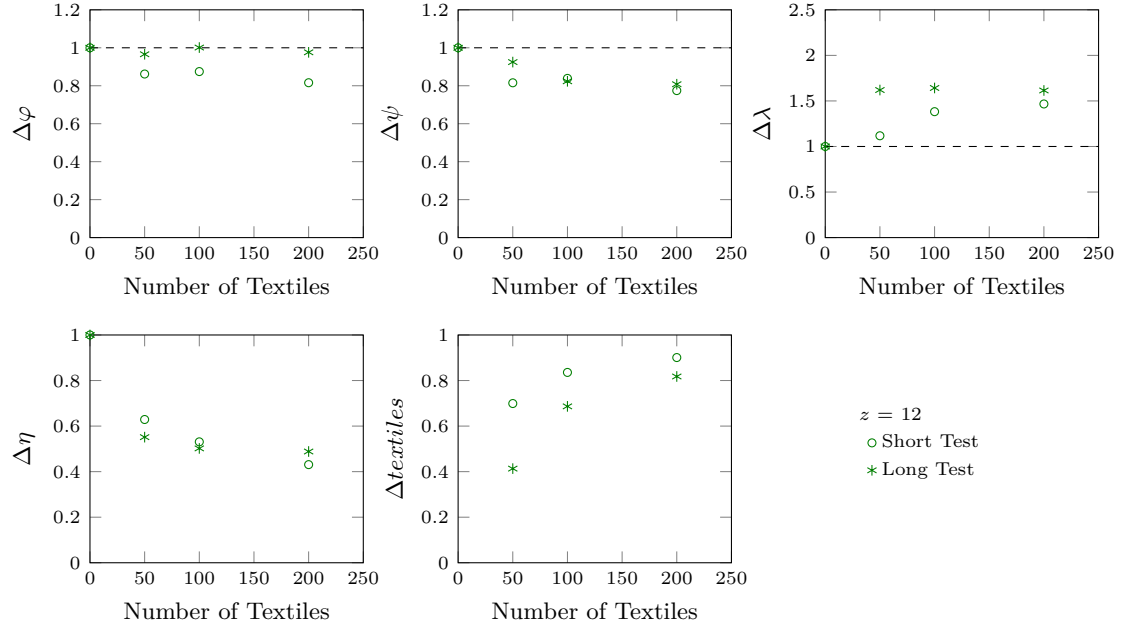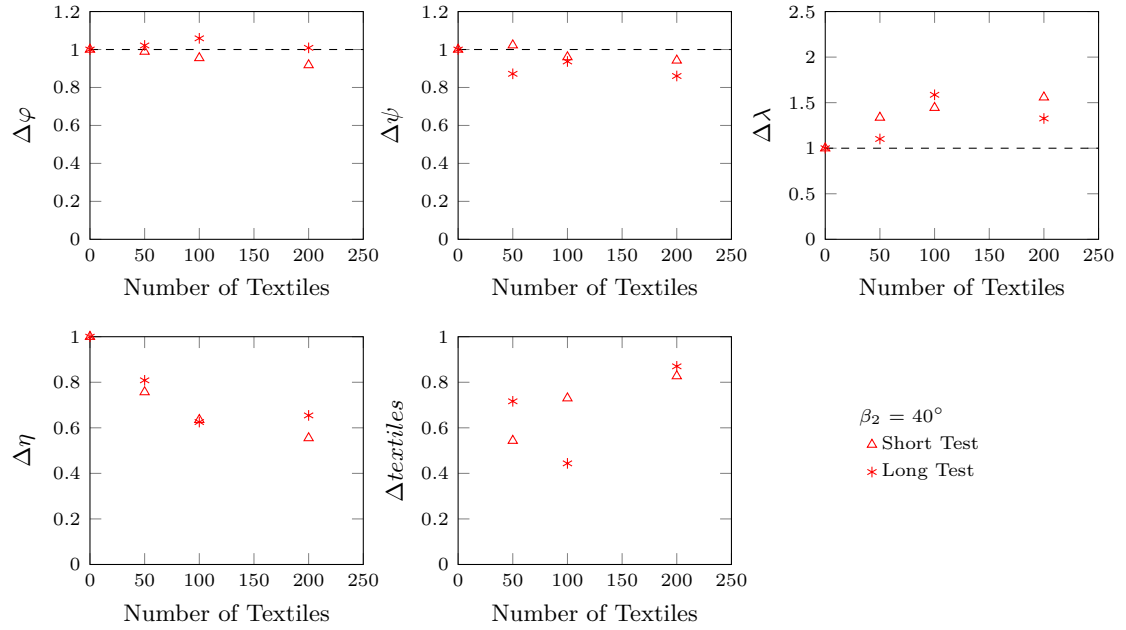
Figure D2: Comparison of the short test with the long test for an impeller with 12 straight blades.

Figure D3: Comparison of the short test with the long test for an impeller with a 40° blade outlet angle.
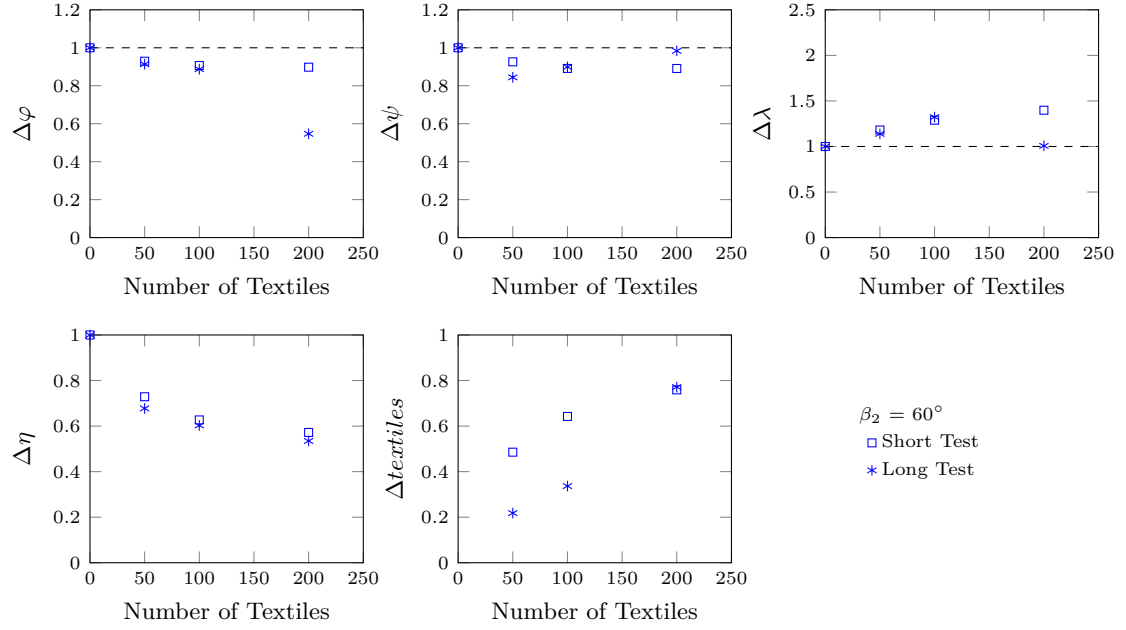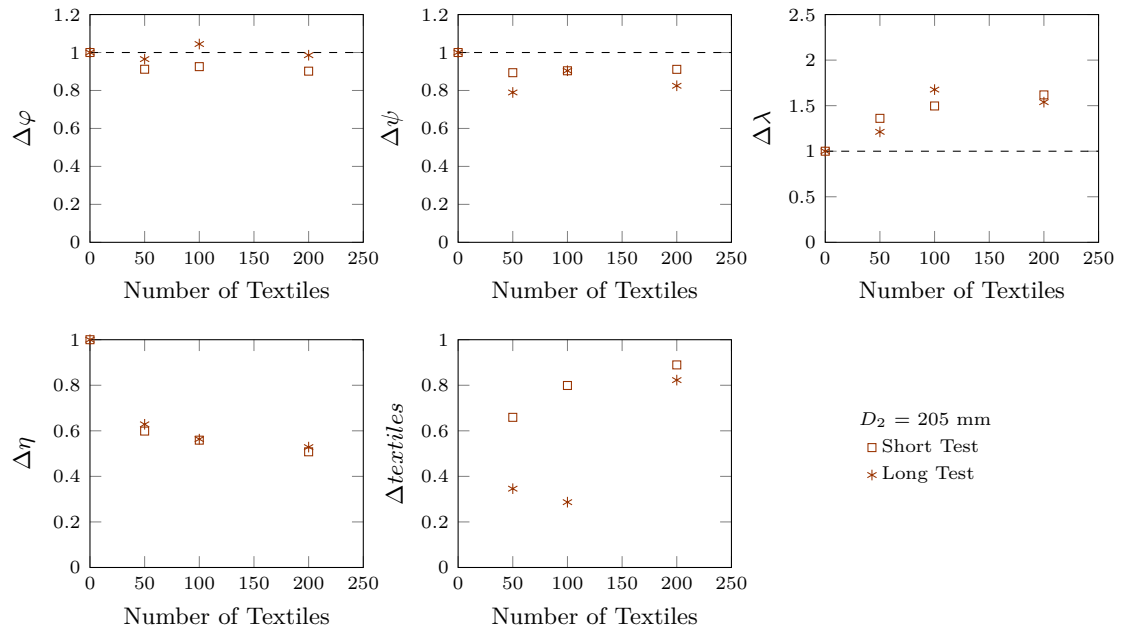
Figure D4: Comparison of the short test with the long test for an impeller with a 60° blade outlet angle.

Figure D5: Comparison of the short test with the long test for the impeller with a diameter of 205 mm.
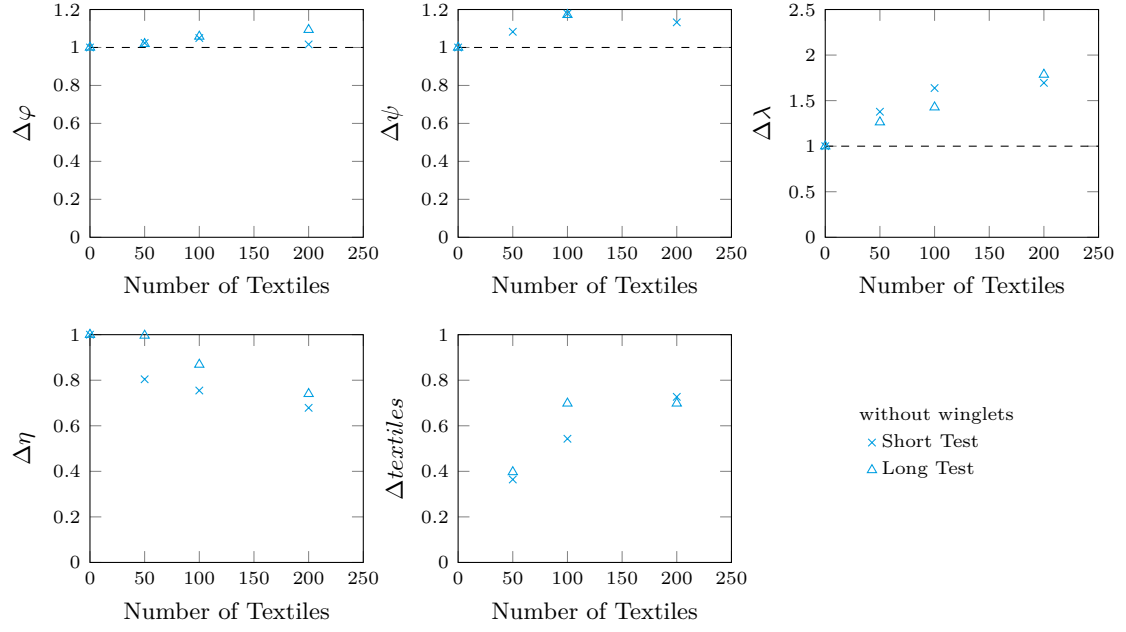
Figure D6: Comparison of the short test with the long test for an impeller with 4 curved blades without winglets.
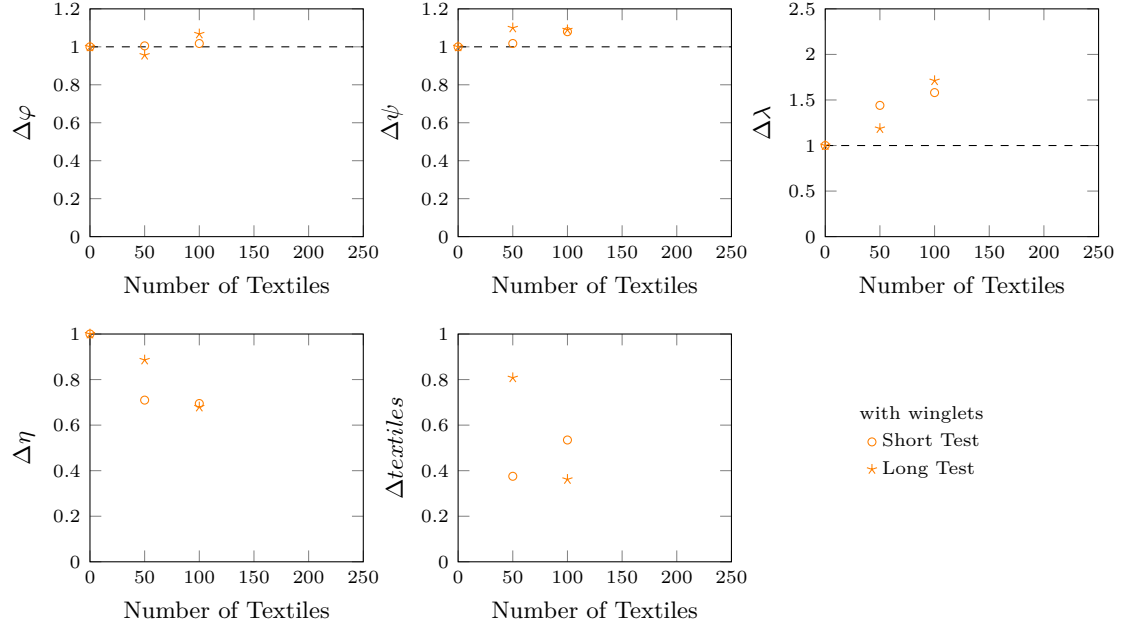

Figure D7: Comparison of the short test with the long test for an impeller with 4 curved winglets.
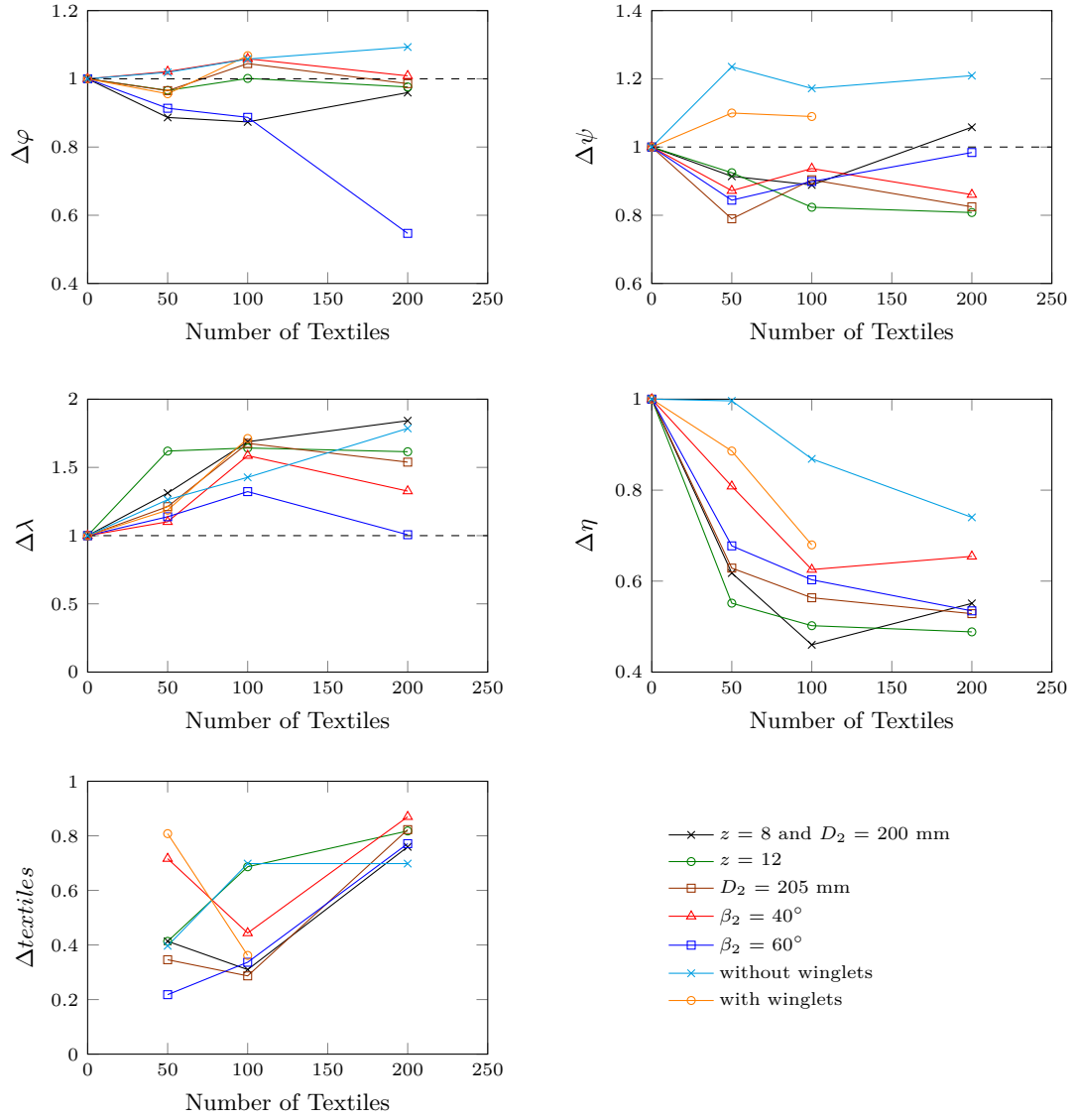
Figure D8: Comparison of all tested impellers for the long test.